Circulation and transformation of Atlantic and Arctic water masses in climate models

Helene Reinertsen Langehaug

Thesis for the degree of philosophiae doctor
at the University of Bergen

Circulation and transformation of Atlantic and Arctic water masses in climate models

Helene Reinertsen Langehaug

Geophysical Institute
University of Bergen

Nansen Environmental
and Remote Sensing Center

Bjerknes Centre
for Climate Research

Thesis for the degree of philosophiae doctor
at the University of Bergen

September 2011

In loving memory of mom and dad

Thank you

Contents

Preface

In the summer of 2008 the ideas of this research work were initiated, and since then these ideas have been explored to form an article-based thesis. This thesis is composed of a synopsis and a collection of papers, and is in partial fulfillment the requirement for the degree philosophiae doctor (PhD) in physical oceanography at the Geophysical Institute, University of Bergen, Norway.

The synopsis consists of two chapters. The first chapter describes the scientific background for the research that has been performed. The second chapter gives the motivation for the collected research works, the main objectives, summaries of the individual papers, and then finally the main conclusions and future perspectives.

The following four chapters consist of the collection of papers that are to be submitted to, in revision for, or published in international peer reviewed journals. The first three papers are analyses of multi-century climate model simulations and form the main body of the thesis. The last paper is an example of an observational study using traditional methodology from observational oceanography. This methodology has partly been applied for the model simulations in the second and third paper.

- **Paper I.** Langehaug H. R., P. B. Rhines, T. Eldevik, J. Mignot, and K. Lohmann, 2011: Water mass transformation and the North Atlantic Current in three multi-century climate model simulations. Manuscript to be submitted, *Journal of Geophysical Research*.
- **Paper II.** Langehaug, H. R., I. Medhaug, T. Eldevik, and O. H. Otterå, 2011: Arctic/Atlantic exchanges via the Subpolar Gyre. In revision, *Journal of Climate*.
- **Paper III.** Medhaug, I., H. R. Langehaug, T. Eldevik, T. Furevik, and M. Bentsen, 2011: Mechanisms for decadal scale variability in a simulated Atlantic Meridional Overturning Circulation, *Climate Dynamics*, doi:10.1007/s00382-011-1124-z
- **Paper IV.** Langehaug, H. R. and E. Falck, 2011: Changes in the properties and distribution of the intermediate and deep waters in the Fram Strait. Revised manuscript resubmitted, *Progress in Oceanography*.

This study was funded by the Research Council of Norway through the International Polar Year project: Bipolar Atlantic Thermohaline Circulation (BIAC).

Acknowledgements

The last three years have been a time that I have enjoyed with great pleasure. And for this, there are many persons to thank. First of all, I would like to thank my key supervisor throughout the project.

Tor, I'm grateful for your indispensable and constant support; that means from the very first day to the very last day. Your continuous ability to see challenges in a broad, and therefore much more interesting, perspective has truly been enlightening and encouraging. Thank you, Tor, for always taking your time and for being a good friend. Great thanks goes to my supervisor, Peter, for letting me stay in Seattle the late summer and fall of 2010. This was an exciting time both in research and in meeting new people and places. Thank you, Peter, for being such an inspiration. Your way of describing the ocean gives life and color to the research.

Many thanks to Iselin for great collaboration and friendship. Working with someone in the same situation is sometimes a much better help than any other. I remember your research visit in Seattle with very much fun, and particularly our sharing enthusiasm in coffee and breweries. Thanks also to my supervisors Odd Helge and Helge. Odd Helge, I very much appreciates your help in teaching me how to use a climate model and not least, for letting me go crazy with water mass analysis on your model simulation. Helge, it has been a privilege to have an oracle to ask for large-scale questions. I also want to express my gratitude to my co-authors Eva, Mats, Tore, Juliette, and Katja for good discussions and collaboration with the papers.

Thanks to my dear family for your constant optimism in my work (although not understanding what I really do). A warm thank you to my sister Julie and my grandparents for always being there. Also, a cheerful thanks to good friends. I hope there will be many more cheers in the future. A special thanks goes to Kristina and Natalia; thank your for the hours with social work out, helping me not to grow (physically) in the office chair in the last couple of months. Thanks too, to the administration at the Nansen Center for meeting me every morning with a smiling "Good Morning". Then finally, but not least important, I would like to thank my dearest love and favorite friend, Stig-Arild. Thank you for bearing with me in this time when thick books have seen to be more central than anything else. Thank you for your never-ending support, but most vital, for reminding me of the wonderful life outside the books.

Helene R. Langehaug
Bergen, September 2011

Abstract

Ocean heat transport and associated heat loss to the atmosphere contributes significantly to the anomalously mild climate of northwestern Europe and its variability. In this thesis, the circulation and transformation of water masses in the northern North Atlantic and the Nordic Seas have been assessed and explored in state-of-the-art climate models. A most important aspect of model evaluation is to identify the degree of realism in model climatology and variability, e.g., for model improvement or in order to assess the potential for decadal-scale climate prediction. A main approach for assessing simulated ocean circulations herein is water mass analysis as routinely applied in observational oceanography. Air-sea exchange and water mass transformation at northern high latitudes are accordingly related to the Atlantic Meridional Overturning Circulation (AMOC). The variable overturning of the Bergen Climate Model (BCM) – the core model system in this thesis – is found to reflect decadal variability in dense water formation in the Labrador Sea and in the oceanic heat transport into the Nordic Seas, the overall constraint on the northernmost water mass transformation. The simulated AMOC is strongly interconnected with the horizontal Subpolar Gyre circulation. Decadal variability of BCM's Subpolar Gyre, as its AMOC, can partly be explained as a response to distinct patterns of atmospheric variability. The intercomparison of BCM with two other climate models finds the model pathways for the North Atlantic Current and the model sea-ice covers to differ substantially, and hence their oceanic poleward transport of heat, their air-sea exchange, and consequent northern water mass transformation to be very different.

Chapter 1

Background

This chapter is divided into three sections. The first two sections describe the oceanic and atmospheric circulation in the North Atlantic region, whereas the last section introduces and verifies tools that can be used to investigate the long-term mean and decadal variability of ocean circulation.

The focus of this thesis is the oceanic circulation, and the first section therefore provides a description of the heat and salt transported by different oceanic currents in the North Atlantic Ocean. The section starts with the poleward flowing Gulf Stream originating in the Subtropics off the coast of North America and ends with the southward flowing deep and cold current formed in the northern seas.

Air-sea exchanges at northern high latitudes convert warm and saline surface water to colder and fresher water, and the second section therefore presents the three dominant modes of atmospheric variability in the North Atlantic region. The first mode is the well-known North Atlantic Oscillation. To investigate the oceanic circulation, as well as the influence of air-sea exchanges on the oceanic circulation, the concept of water mass analysis is used. Different water masses, in analogy with air masses, can be distinguished by their properties, like temperature and salinity. When isolated from the atmosphere, water masses in the deep ocean retain their properties to a high degree. Close to the ocean surface, water masses are in constant transformation due to air-sea exchange of heat and fresh water. This requires tailored analysis tools, and this is described in the last section.

Throughout the thesis, the oceanic circulation and water mass transformation are assessed in state-of-the-art climate models, with the Bergen Climate Model as the core model system. The last section therefore presents some quantification and evaluation of possibilities and limitations by using such models.

1.1 The Atlantic Thermohaline Circulation

The temperature of the deep subtropical Atlantic Ocean was for the first time measured in 1751, and the result was unexpected. The deep water was surprisingly cold compared to the surface water. In 1797 Sir Benjamin Thompson suggested this to be caused by cold and deep ocean currents that propagate from the poles to the equator. Extensive investigations later on showed that in fact about 80% of the world ocean is colder than 5°C. This was the early beginning of understanding the circulation of mass, heat, and salt within the world ocean, of which the Atlantic Thermohaline Circulation is one important contributor. Adapted from Warren (1981).

The transformation of warm and saline to cold and less saline water masses at northern high latitudes is an essential part of the Atlantic Thermohaline Circulation (THC; Rudels 1995; Wunsch 2002), and contributes to the large-scale global ocean circulation (Broecker 1997; Talley 2008). Subtropical Water is carried poleward (red arrows in Fig. 1.1) and large amounts of heat are lost from the ocean as the surface water interacts with colder air masses (McCartney and Talley 1982; Brambilla et al. 2008). The oceanic heat loss contributes to the anomalously mild winters in northwestern Europe (Rahmstorf et al. 2002; Drange et al. 2005; Rhines et al. 2008).

Investigations of the circulation and identification of water masses at the northern high latitudes started already in the second half of the 19th century. The comprehensive and detailed surveys by Helland-Hansen and Nansen (1909) represented for a long time the status of knowledge regarding the circulation and hydrography of the Nordic Seas (Fig. 1.2; Blindheim and Østerhus 2005). Helland-Hansen (1916) further introduced the *TS*-diagram that has become one of the most valuable oceanographic tools in classifying different water types, for instance the above mentioned warm and saline Atlantic-derived water. The Atlantic-derived water is transformed to denser water by cooling at northern high latitudes, and the resulting water masses can be identified in the *TS*-diagram. Nansen (1906) was the first to observe the Greenland Sea Deep Water, and some years later he also observed dense overflows in the Denmark Strait and at the Iceland-Faroe Ridge (Nansen 1912; Fig. 1.2). He did, however, assume that the overflows were not a source for the deep water in the North Atlantic Ocean south of the Greenland-Scotland Ridge. Later studies have shown that these dense overflows are a major contributor to the cold and deep returning branch of the THC (blue arrows in Fig. 1.1; Dickson and Brown 1994; Olsen et al. 2008; Medhaug et al. 2011).

The dense water formation at northern high latitudes has been investigated in a number of studies, both observational and model studies (Mauritzen 1996; Bentsen et al. 2004; Jungclaus et al. 2005; Isachsen et al. 2007). The dense water products from the Nordic Seas and the Labrador and Irminger seas (Fig. 1.2) are readily identified in the deep North Atlantic Ocean as they propagate southward (Smethie and Fine 2001; Yashayaev 2007a; LeBel et al. 2008). The southward propagation of these dense water products is driven by a balance between gravity and rotation, steered by bathymetry, and hence, relatively small-scale topographic features are essential in setting the pathway of the deep flow (Xu et al. 2010). On their way towards the tropics the

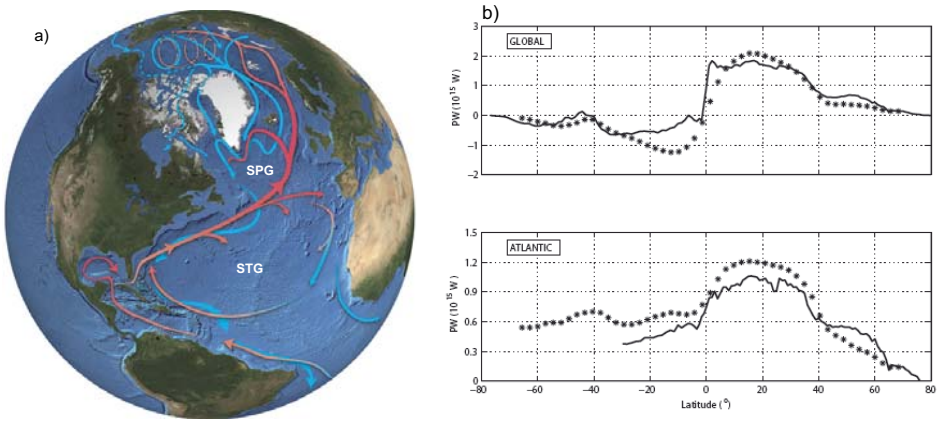

Figure 1.1: a) Warm-to-cold water transformation in the North Atlantic and the Arctic Mediterranean illustrated by red (warm) and blue (cold) arrows. The dominant horizontal circulation is represented by the Subtropical Gyre (STG) and the Subpolar Gyre (SPG). Courtesy: Woods Hole Oceanographic Institution. b) Simulated northward heat transports (PW) for the global and Atlantic oceans by the Bergen Climate Model. Asterisk symbols denote observational estimates based on Trenberth and Caron (2001). From Otterå et al. (2009).

deep water gradually mix with warmer water, thereby slowly rising in the water column (Munk and Wunsch 1998; Kuhlbrodt et al. 2007). The deep water from the northern North Atlantic continue to spread throughout the Atlantic Ocean and is carried to the neighboring oceans by the Antarctic Circumpolar Current (Gordon 1986; Talley 2008), with upwelling of North Atlantic derived deep water in the Southern Ocean and partly in the Indian and Pacific oceans (Schmitz 1995; Kuhlbrodt et al. 2007). The rising branches of the THC are widely distributed over the ocean basins and less known compared to the more geographically confined sinking regions of the THC at northern high latitudes (Kuhlbrodt et al. 2007). Parts of the North Atlantic derived deep water outcrop close to the Antarctic continent, transform to denser water by cooling and brine rejection, and return to the Atlantic Ocean as bottom water (Speer et al. 2000).

The Atlantic Ocean circulation is forced and influenced by several factors: winds, cooling at high latitudes, heating in the tropics, the hydrological cycle, internal waves, and tides (Wunsch 2002; Kuhlbrodt et al. 2007). The THC refers in general to the circulation associated with water mass transformation (Schmitz 1995), where the transformation does not necessarily lead to density changes of the water masses. For instance, a water mass can be converted from warm and saline to cold and fresh, and still remain the same density. The thermohaline driven circulation, which is in part driven by density differences, is difficult to separate from the wind driven circulation, due to the fact that the ocean is not a linear system (Sandstrom 1908; Gill 1982). For instance, buoyancy forcing depends on wind speed. The net effect of all forcing is included in the zonally averaged volume transport, which is defined as the two-dimensional (latitude-depth) Atlantic Meridional Overturning Circulation (AMOC). AMOC is frequently used to quantify the circulation in the Atlantic Ocean.

A two-dimensional "conveyor belt" circulation (Broecker 1987) is commonly used as a simplification and an illustration of the Atlantic ocean circulation, where the densification of water at high latitudes has been one of the most frequently postulated drivers of the ocean circulation. The densest water is formed in the Southern Ocean, whereas slightly less dense water is produced at the northern high latitudes. However, the dense water formation is not an energy source for the overturning circulation, since convective mixing acts to lower the center of mass and therefore reduces the potential energy. The dense water formation has, in light of this, been suggested to be a modifier of the strength and shape of the AMOC (Kuhlbrodt et al. 2007). Although the strength and location of the dense water formation can be very model-dependent, a range of model studies shows a strong influence on the overturning when the dense water formation is reduced at northern high latitudes (e.g., Manabe and Stouffer 1993; Otterå et al. 2004). On the other hand, several recent observation-based studies have challenged the traditional conveyor-belt model with dense water formation in highly localized regions such as the Greenland Sea (Fig. 1.2; Lozier 2010), and increased attention is currently being paid to eddies (Dengler et al. 2006; Bower et al. 2009), wind forcing (Biastoch et al. 2008), horizontal circulation in the northern North Atlantic (Hátún et al. 2005), and gradual water mass transformation along the rim of the ocean basins at northern high latitudes (Mauritzen 1996; Rudels et al. 1999; Eldevik et al. 2009).

The oceanic and atmospheric circulations transport vast amounts of heat poleward, thereby reducing the meridional temperature gradients set up by the differential solar heating between low and high latitudes. The atmospheric contribution to poleward heat transport is larger than the oceanic contribution at all latitudes, except between 0° and 17°N. Within this region the oceanic heat transport has a maximum value of about 2 PW (1 PW=10^{15} W; Fig. 1.1), while the atmospheric transport peaks at 43°N and near 40°S with about 5 PW (Trenberth and Caron 2001).

The meridional transport of heat by the oceans is an important factor in the ability of models to simulate a realistic climate. The heat transport is estimated to 1.3 PW at 25°N, and 0.6 PW across a section stretching from about Newfoundland to Ireland (Ganachaud and Wunsch 2000). The difference in the heat transport between these two sections, 0.7 PW, must be released to the atmosphere to balance the heat budget of the subtropical ocean. In the time-varying climate, heat divergence can also contribute to an increase in the storage of heat in the subtropical ocean. Further north, at the boundary between the subtropical and subpolar North Atlantic Ocean, the heat transport is estimated to 0.6 PW (Ganachaud and Wunsch 2000), while the transport is estimated to 0.3 PW across the Greenland-Scotland Ridge (Østerhus et al. 2005). The heat divergence of 0.3 PW is less than half of the heat divergence in the subtropical ocean. The heat loss within the Nordic Seas is estimated to 0.2 PW (Simonsen and Haugan 1996; Segtnan et al. 2011). The meridional distribution of the heat transport from Trenberth and Caron (2001) is shown in Fig. 1.1, and the heat transport from a multi-century simulation with the Bergen Climate Model is comparable to the observation-based estimates.

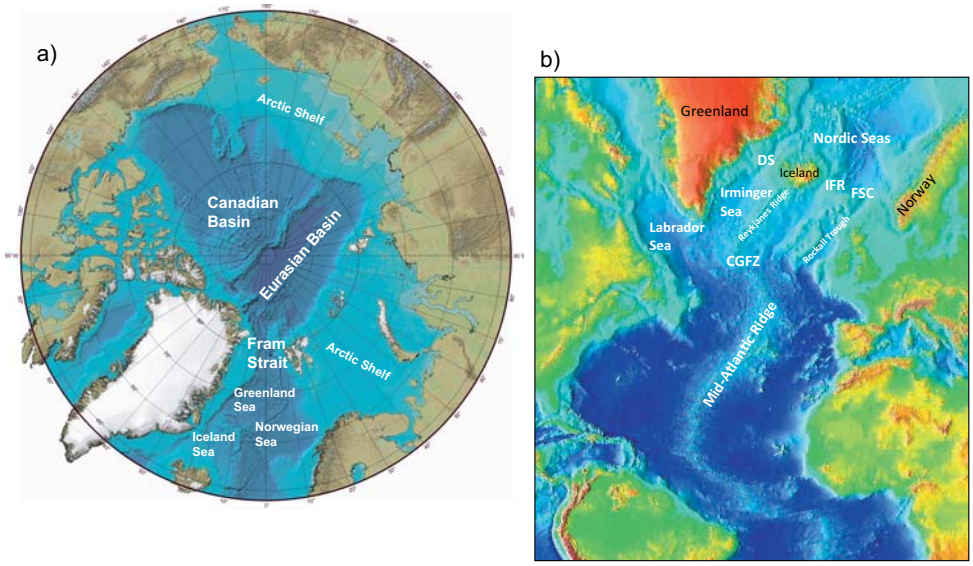

Figure 1.2: a) Bathymetry of the Arctic Ocean (Eurasian and Canadian basins and the Arctic Shelves) and the Nordic Seas (Greenland Sea, Norwegian Sea, and Iceland Sea), comprising the Arctic Mediterranean, first named by Krümmel (1879). Courtesy: The International Bathymetric Chart of the Arctic Ocean. b) Bathymetry of the southern Nordic Seas and the North Atlantic Ocean. Abbreviations are: Denmark Strait (DS); Iceland-Faroe Ridge (IFR); Faroe-Shetland Channel (FSC); Charlie-Gibbs Fracture Zone (CGFZ). Courtesy: National Oceanic and Atmospheric Administration.

The THC is often explained in terms of cooling, heating, and transport of heat, but also changes in freshwater input can change the THC. The air-sea exchanges can explain the cooling of the Atlantic-derived water, but the air-sea exchanges alone cannot explain the changes in the salinity of the Atlantic-derived water (Mauritzen 1996). Precipitation, river run-off, low-salinity Pacific water entering the Arctic Mediterranean via the Bering Strait, and sea ice melt water are sources of freshwater to the ocean. Freshwater input to the ocean decreases the density of the surface water. The Atlantic-derived water is influenced by sea ice melt in the marginal ice zones in the Arctic Ocean, the western part of the Nordic Seas, and in the Labrador Sea. The most important source of freshwater is river run-off from the large Russian rivers (Aagaard and Carmack 1989). The upper layer of the Arctic Ocean is dominated by low-salinity water, insulating the warmer Atlantic-derived water below from the cold atmosphere. However, dense water formation on the vast Arctic shelves occurs due to salinity increase when seawater freezes (Aagaard et al. 1985; Rudels et al. 1999). Therefore, there are two main products of the water mass transformation at northern high latitudes; the denser product due to cooling of Atlantic-derived water and brine release due ice freezing, and the lighter product due to mixing between Atlantic-derived water and freshwater added to the Arctic Mediterranean (Rudels et al. 1999; Isachsen et al. 2007; Rudels 2010). The water mass transformation in the Arctic Ocean is mainly governed by freshwater input, whereas the water mass transformation in the Nordic Seas is mainly determined by

heat loss from the ocean (Isachsen et al. 2007). The two processes can be associated with two distinct loops; a vertical overturning loop providing dense water to the deep ocean of the North Atlantic and a horizontal loop supplying freshwater to the surface ocean of the North Atlantic (Dickson et al. 2007; Rudels 2010). The East Greenland Current and the Labrador Current carry the fresh component at surface in the western part of both the Nordic Seas and the subpolar North Atlantic, respectively (Aagaard and Carmack 1989; Chapman and Beardsley 1989).

Another source of variability in the freshwater content of the Arctic Ocean is found to be the inflow of Atlantic-derived water to the Arctic Ocean (Häkkinen and Proshutinsky 2004). Hence, the variability in salinity of the low-salinity boundary currents could potentially reflect changes in the inflow of Atlantic-derived water. Several large salinity anomalies – Great Salinity Anomalies (GSAs) – have been observed in the North Atlantic (Dickson et al. 1988; Belkin et al. 1998; Häkkinen 2002). These GSAs have the potential to alter the dense water formation and circulation in the Labrador and Irminger seas. Based on model studies, Haak et al. (2003) suggest that the GSAs in the 1970s, 1980s, and 1990s might be caused by anomalous large freshwater export through the Fram Strait, and also through the Canadian Archipelago in the 1990s. Hence, it is likely that the GSAs do not originate locally. The GSAs have only a minor impact on the THC according to Haak et al. (2003), although contrary to the results in Häkkinen (1999).

Several climate model studies have investigated the role of freshwater on the THC by releasing large amounts of freshwater in the Nordic Seas or the subpolar North Atlantic Ocean (e.g., Vellinga and Wood 2002; Otterå et al. 2004; Stouffer et al. 2006). In this manner the northern water mass transformation was artificially suppressed, leading to a decrease in the poleward transport of heat and salt in the climate models. This resulted in a lowering of the sea surface temperature in the North Atlantic Ocean and a cooling over Europe of 1-3°C a few decades after the shutdown of the dense water formation. Changes in the sea surface temperature in the North Atlantic Ocean on multi-decadal scale are believed to influence the European climate, where the sea surface temperature has been suggested to be related to the variability of the THC (e.g., Sutton and Hudson 2005). A recent model study finds that the two dominant periods on multi-decadal scale in the sea surface temperature of the North Atlantic Ocean has different origin (Frankcombe and Dijkstra 2011). The shortest period has its origin in the upper ocean of the North Atlantic and propagates northwards, whereas the longer period has its origin in the Arctic and propagates southwards. However, the mechanisms governing the sea surface temperature in the North Atlantic Ocean on longer time scales are still not well resolved by climate models (Medhaug and Furevik 2011). In addition, it is unclear if and how the surface air temperature over Europe responds to anomalies in the sea surface temperature in the North Atlantic Ocean (Latif et al. 2006).

In this thesis the main objective has been to identify and quantify the northern water mass transformation and ocean circulation in the North Atlantic and the Nordic Seas as simulated in climate models. To assess the models' realism, the model results have been compared with

available observations for the last 50 years. In light of these analyses, the purpose has been to obtain a better understanding of climate models' North Atlantic climate variability and to which degree the simulated variability is likely to occur in real nature.

1.1.1 North Atlantic Current and its northern transformation

The western boundary current in the North Atlantic Ocean starts off at Florida Keys, as the Florida Current. Downstream of Cape Hatteras (35°N) this current continues as the well-known Gulf Stream and diverges from the coastline, following the continental slope (Fig. 1.3; Iselin 1936). This boundary current forms the western part of the Subtropical Gyre (Fig. 1.1). Parts of the Gulf Stream turn southeast to contribute to the Canary Current and recirculate in the Subtropical Gyre. When the Gulf Stream reaches the Grand Banks off Newfoundland it separates into several branches (Krauss 1986). One branch curves north around Grand Banks and eventually turns east between 50° and 52°N at the so-called "Northwest Corner" (e.g., Arhan 1990). This branch continues northeast towards the Nordic Seas and is called the North Atlantic Current (NAC), constituting the southeastern branch of the Subpolar Gyre (Fig. 1.1). This current breaks into the Irminger Current and the Norwegian Atlantic Current as it continues toward the Labrador and Irminger seas in west and into the Nordic Seas in east, respectively.

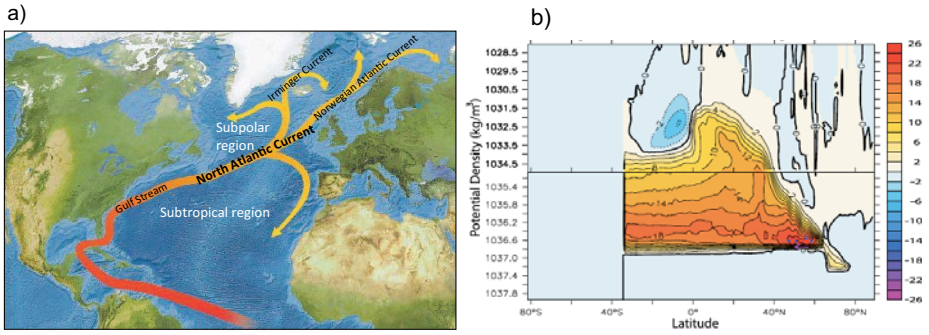

Figure 1.3: a) The Gulf Stream in the subtropical region continues as the North Atlantic Current in the subpolar region, where it bifurcates into the Irminger Current, and the Norwegian Atlantic Current in the Nordic Seas. b) Zonal integrated streamfunction (Sv) in the Atlantic in potential density (σ_2) space (from Zhang 2010).

The NAC is being transformed as it travels the subpolar region and the Arctic Mediterranean (red arrows in Fig. 1.1). The thermohaline changes of the Atlantic-derived water is partly density compensated, but overall the water densifies on its route toward northern high latitudes, i.e., the buoyancy loss from heat loss generally dominates the gain from freshwater input. The densification of the northward flowing water is evident from the zonally averaged streamfunction in latitude-density space (Fig. 1.3), as opposed to the zonally averaged streamfunction in latitude-depth space (e.g., Mauritzen and Hakkinen 1999; Willebrandt et al. 2001; Bailey et al. 2005; Zhang 2010).

In the northeastern North Atlantic the NAC is associated with transformation of warm and saline Subtropical Water to colder and fresher Subpolar Mode Water. Subpolar Mode Water is characterized by thick layers of uniform water above the pycnocline, formed by intense convective mixing during winter (McCartney and Talley 1982; Brambilla and Talley 2008). It has been suggested that the Subtropical Water becomes denser as it circulates cyclonically in the Subpolar Gyre (McCartney and Talley 1982). A revised circulation scheme suggests several meridionally aligned branches of the NAC, where each branch is associated with its own density class of Subpolar Mode Water (Talley 1999; Péreze-Brunius et al. 2004; Brambilla et al. 2008). Brambilla et al. (2008) point to the importance of the bifurcation of NAC, which determines the regions of water mass transformation. For instance, if a model simulates branches that only extend into the Nordic Seas, then there will be little or no formation of Subpolar Mode Water and Labrador Sea Water in the Labrador and Irminger seas. In observations, Labrador Sea Water is found at the high end of the density range of Subpolar Mode Water. Labrador Sea Water is formed by deep convection in the Labrador and Irminger seas mainly due to cold Arctic winds blowing over the sea surface (Pickart et al. 2003). The deep convection in the Labrador Sea is usually associated with a positive phase of the North Atlantic Oscillation (Curry et al. 1998; Yashayaev 2007a; van Aken et al. 2011), the leading pattern of the atmospheric winter circulation in the North Atlantic region (see section 1.2 for more details).

Observations in the northeastern North Atlantic show pronounced decadal variability in the properties of the upper ocean (e.g., Holliday et al. 2008). For this reason, several studies have investigated the causes of thermohaline anomalies in this region (Sarafanov et al. 2008; Häkkinen et al. 2011). These anomalies can be attributed to changes in purely advective signals from the subtropics, changes in local atmospheric forcing, or a combination. Häkkinen et al. (2011) investigated the exchange between the subpolar and subtropical Atlantic, where they found that warm and saline water reach the northern high latitudes in specific periods. The recent appearance of warm and saline water in the northeastern North Atlantic (late 1990s - 2000s), as well as in the Nordic Seas and Arctic Ocean, is such an event, and the early 20th century warming (1930s-1950s) another. These findings indicate decadal variability in the properties of the Subtropical Water reaching the subpolar region and the Nordic Seas. Another study finds that the properties of the inflow to the Nordic Seas are largely influenced by the strength and extent of the Subpolar Gyre (Hátún et al. 2005). More specifically, an increase in the Subpolar Gyre strength is generally associated with an increase in the horizontal extent of the Subpolar Gyre, which will provide the inflow with a larger amount of relatively fresh and cold Subpolar water. In the opposite case, when the Subpolar Gyre strength weakens, a larger amount of relatively warm and saline Subtropical Water is free to propagate to the Nordic Seas. Häkkinen et al. (2011) suggest that this gyre mechanism described by Hátún et al. (2005) is driven by the second dominant pattern of the total variability of the wind stress curl in the North Atlantic. When both the subpolar and subtropical gyre relaxes due to the wind forcing, the subpolar gyre contracts whereas the subtropical gyre expands. These changes give a gateway for the Subtropical Water to propagate to the northern high latitudes (Häkkinen et al. 2011).

The Atlantic-derived water enters the Nordic Seas across the Greenland-Scotland Ridge, and is carried further north by the Norwegian Atlantic Current (Fig. 1.3; NwAC). The warmest and most saline water is located at the easternmost part of the ridge. Parts of the NwAC reach the Arctic Ocean via the Barents Sea and the Fram Strait (red arrows around Svalbard in Fig. 1.1), while large parts recirculate in the Nordic Seas. The parts that enter the Arctic Ocean subducts under the cold halocline, and circulates as a cyclonic boundary current along the vast ocean basins. Eventually the Atlantic-derived water completes a loop within the Arctic Ocean and exits the Arctic Ocean via the Fram Strait. The parts of the NwAC that recirculates the Nordic Seas gradually densifies and becomes the main contributor to the dense water spilling over the Greenland-Scotland Ridge; Overflow Water (Mauritzen 1996; Rudels et al. 1999; Eldevik et al. 2009). A recent study has found that the overflow in the Denmark Strait not only consists of water carried by the East Greenland Current, but also of water feed to the strait by the newly discovered North Icelandic Jet (Jónsson and Valdimarsson 2004; Våge et al. 2011). It is suggested that this current is part of a smaller overturning loop within the Iceland Sea; Atlantic-derived water is transported northward by the Irminger Current and dense water is carried southward by the North Icelandic Jet to the deepest part of the Denmark Strait (Våge et al. 2011).

As described earlier, the Atlantic-derived water is also transformed into a fresher and lighter component on its route in the Arctic Mediterranean from freshwater input. Relatively warm and saline Atlantic-derived water enters the Nordic Seas and the Arctic Ocean, whereas cold and fresh surface Polar Water is carried southward with the East Greenland Current and Labrador Current in the western part of the Nordic Seas and subpolar region, respectively. The Polar Water carried by these boundary currents is an important factor in the pre-conditioning of deep water formation in the respective basins. Realistic simulation of these currents, as well as the sources to the low-salinity water such as river-runoff and ice processes, is a challenge in course resolution climate models. This has been shown often to result in a too saline Labrador Sea (Bailey et al. 2005), which is also the case in the Bergen Climate Model.

From a conveyor belt (Broecker 1987) perspective, there seems to be a straightforward relationship between the transformed Atlantic-derived water and the sinking branch of AMOC. For instance, regions of dense water formation at high-latitude seas have often been thought to correspond to regions of downward mass flux (e.g., Schmitz and McCartney 1993). Nevertheless, dense water formation and downwelling are fundamentally different processes, where regions of dense water formation do not need to correspond with regions of net downwelling (Marotzke and Scott 1999). In an ocean governed by geostrophy, Spall and Pickart (2001) show that an unrealistic strong horizontal flow is required to allow interior sinking. This is because horizontal flow divergence is only related to changes in the Coriolis parameter, which varies little in convective mixing regions, and is thus not sufficient for sinking. On the other hand, close to boundaries, as well as steep topography, geostrophic balance breaks down, and gives rise to sinking (Spall and Pickart 2001). Straneo (2006) proposes an idealized model for a convective basin to relate dense water formation (a diapycnal mass flux) with overturning circulation

(a vertical mass flux). She finds that the overturning circulation takes place in the boundary current and not in the interior region of the basin, where dense water formation is occurring. The boundary current plays an essential role in the exchange of light and dense water with the interior region.

1.1.2 Deep Western Boundary Current

The dense products of the transformed Atlantic-derived water are the main sources to the Deep Western Boundary Current (DWBC). These products are the Nordic Seas Overflow Water and the Labrador Sea Water, commonly named as North Atlantic Deep Water (NADW), where the Labrador Sea Water flows above the Overflow Water (Fig. 1.4). The amount of Overflow Water flowing across the Greenland-Scotland Ridge is about 6 Sv (Hansen and Østerhus 2000; Olsen et al. 2008), and including the entrainment of Subpolar Mode Water as the overflow descends the ridge, the overflow has been estimated to contribute about 2/3 of the NADW (Dickson and Brown, 1994).

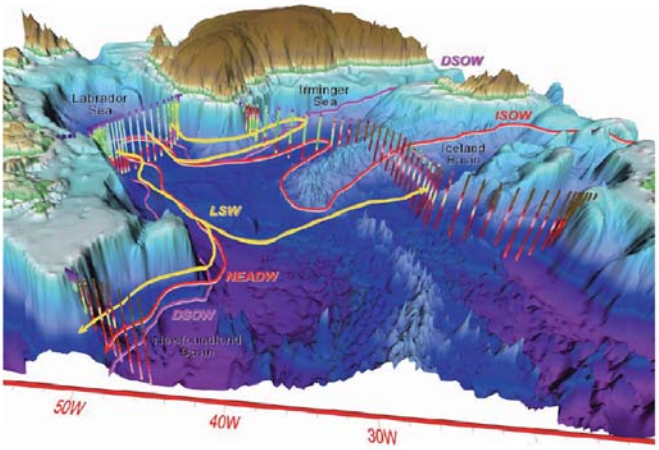

Figure 1.4: Dense water products from the transformation at northern high latitudes: Labrador Sea Water (LSW), Denmark Strait Overflow Water (DSOW), and Iceland Scotland Overflow Water (ISOW), constituting the Deep Western Boundary Current. Northeast Atlantic Deep Water (NEADW) originates from the ISOW. From Yashayaev (2007b).

As the Overflow Water descends the Greenland-Scotland Ridge, it transforms to lighter water due to the entrainment of Subpolar Mode Water (Brambilla et al. 2008). The overflow is restricted to flow through the Denmark Strait (sill depth of 600 m) and the Faroe-Shetland Channel (1000 m), as well as over the shallower Iceland-Faroe Ridge (500 m). Most of the overflow from the Faroe-Shetland Channel continues into the Faroe Bank Channel, while only a smaller fraction continues over the Wyville-Thompson Ridge and into the Rockall Trough (Fig. 1.2). The southward propagation of the transformed overflow in the North Atlantic basin

is largely steered by the bathymetry (Xu et al. 2010). The deep water from the Denmark Strait flows along the western continental slope, while the overflow from the Iceland-Scotland Ridge flows along the eastern flank of the Reykjanes Ridge (Fig. 1.2). Eventually the latter flows into the Labrador and Irminger seas via gaps in the Reykjanes Ridge and through the Charlie Gibbs Fracture Zone (Fig. 1.2 and 1.4). At the Charlie Gibbs Fracture Zone the deep flow passes immediately below the eastward flowing North Atlantic Current, causing interaction between the two currents.

The deep water components meet in the Labrador and Irminger seas, and together they form the DWBC (Schott et al. 2004; Dengler et al. 2006). The overflow from the Denmark Strait flows southward along the bottom, while the overflow from the Iceland-Scotland Ridge is sandwiched between the former and the Labrador Sea Water (Fig. 1.4). This is the deep limb of the AMOC (Smethie and Fine 2001). There are decadal and multi-decadal variations in the Labrador Sea Water (van Aken et al. 2011), but the sources and variability of the DWBC are still not clearly understood (Bacon and Saunders 2010). For instance, a recent study has underlined that eddies are important in the southward propagation of the deep water masses (Lozier 2010), forming a more diffusive pathway in the interior part of the western North Atlantic basin than the narrow DWBC (Bower et al. 2009). Climate models are not able to simulate eddies and will therefore not resolve the eddy related part of the DWBC. On the other hand, Rhein et al. (2011) emphasize the importance of the narrow DWBC. In their study the strongest variability in the western basin of the subpolar North Atlantic is related to the front between the cold DWBC and the warmer NAC.

Although their contribution to the DWBC are debated, additional deep water components are produced in the Arctic Mediterranean: Dense water formation by open ocean convection in the Greenland Sea (Nansen 1906), which has weakened since the late 1970s (Rhein 1991; Schlosser et al. 1991; Budéus and Ronski 2009). The water mass transformation in this region was earlier believed to be the main source for the dense water spilling over the Greenland-Scotland Ridge (Aagaard et al. 1985). Another deep water component is obtained from cooling and brine-release at the Arctic Shelves (Fig. 1.2), forming High Salinity Shelf Water; bottom water on the vast shelves of the Arctic Ocean (Aagaard et al. 1985). The High Salinity Shelf Water gradually fills the very deep basins of the Arctic Ocean (Rudels et al. 1999): the Canadian and Eurasian Basin (Fig. 1.2), which exceed depths of 4000 m. The relative warm and saline deep water from these basins pass through the Fram Strait, with a sill depth of 2600 m, and influence the relatively cold and fresh deep water in the Nordic Seas. These water masses are found at depths below the sill depth of the Greenland-Scotland Ridge. However, on longer time scales these water masses might contribute to the variability of the overflow. For instance, the deep water of the Eurasian Basin has a residence time of about 75 years, while the bottom water in the Canadian Basin has a residence time of about 300 years (McDonald et al. 2005). On the other hand, warmer and fresher intermediate water formed in the Arctic Ocean and the Nordic Seas have been found to contribute to the overflow in the Denmark Strait in specific years (Jeansson et al. 2008).

1.2 North Atlantic atmospheric regimes

The atmosphere and the ocean interact through winds, and heat and freshwater exchanges. The response time of the ocean to changes in the atmosphere is slower than that of the atmosphere to changes in the ocean. This difference in the response time is mainly due to the much larger mass of the ocean, and hence, much larger heat capacity (e.g., Gill 1982). Therefore the ocean will respond to the long-term integrated atmospheric variability. The large heat capacity of the ocean also implies that the ocean is capable of storing and transporting a large percentage of the Earth's heat. The three dominant modes of the atmospheric variability in the North Atlantic are the North Atlantic Oscillation, the East Atlantic Pattern, and the Scandinavian Pattern (Wallace and Gutzler 1981; Barnston and Livezey 1987; Hurrel 1995). The North Atlantic Oscillation and East Atlantic Pattern typically account for 30% and 15% of the total sea level pressure variance (Hurrell et al. 2003).

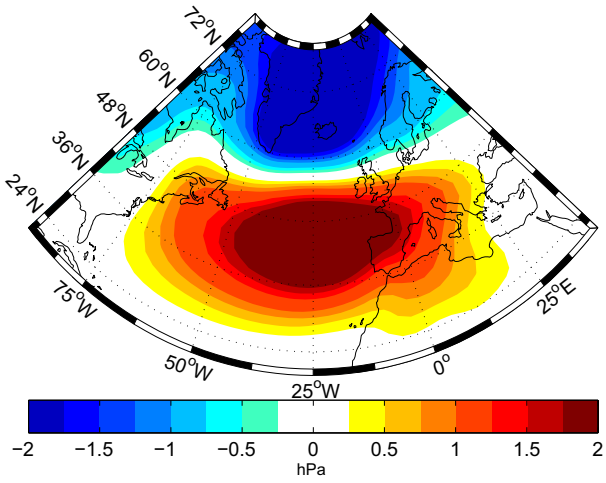

Figure 1.5: Positive phase of the North Atlantic Oscillation in the Bergen Climate Model. This is the first empirical orthogonal function of the variance in the winter mean sea level pressure field for the North Atlantic sector.

The North Atlantic Oscillation (NAO; Fig. 1.5) has a large impact on the weather and climate in the North Atlantic region. When the NAO is in its positive phase, there is a strong high-pressure center in the subtropical Atlantic and a strong low-pressure center in the vicinity of Iceland. This re-organization of atmospheric mass leads to changes in the wind pattern. The Westerlies become strengthened and brings warm and moist air from the tropics to the extra-tropics in a northeastward storm track, leading to reduced sea ice cover in the Nordic Seas. Also, the strength of the NAC has been found to reflect the integrated NAO variability (Curry and McCartney 2001; Visbeck et al. 2003). For instance, an increase in the NAC corresponds

to an integrated positive NAO forcing - an analogue to the strengthened Westerlies during a positive phase of NAO. The extension of the NAC into the Nordic Seas appears to be related more to the wind-stress curl than the NAO (Orvik and Skagseth 2003). West of Greenland, in the Labrador Sea, the wind direction is more southward in a positive NAO phase, leading to lower temperatures in this region (cold polar air is carried by the winds). During positive NAO phases, Europe experiences warmer and wetter winters, while Greenland and Northern Canada are subject to cold and dry winters (Hurrell 1995; Hurrell and Deser 2009).

When the NAO is in a negative phase, the pressure gradient between the subtropical Atlantic high and Icelandic low is reduced, weakening the Westerlies and the storm track will have a more eastward direction. The warm and moist air from the tropics will therefore arrive in the Mediterranean region. Warmer winds over the Labrador Sea give higher temperatures in this region. Hence, during negative phases, the Northern Europe is cold and dry, while Greenland experiences relatively mild winters (Hurrell 1995; Hurrell and Deser 2009). The phases of the NAO is expressed by the NAO index, which is a measure of the atmospheric mass loading over the Atlantic sector. The index is commonly quantified as the surface pressure difference between Iceland and Azores (i.e., between the Icelandic low and the Azores high; Hurrel et al. 1995), or the principal component obtained from an empirical orthogonal function analysis of the sea level pressure in the North Atlantic (Barnston and Livezey 1987; Hurrel 1995) or the Northern Hemisphere (Thompson and Wallace 1998). The mechanisms that account for the variability and trends in the NAO are still not entirely understood (Hurrell et al. 2003).

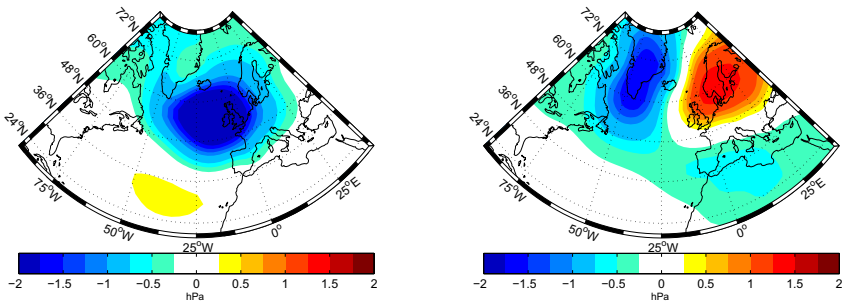

Figure 1.6: Positive phase of the East Atlantic Pattern (left) and Scandinavian Pattern (right) in the Bergen Climate Model. These are the second and third empirical orthogonal function of the variance in the winter mean sea level pressure field for the North Atlantic sector, respectively.

The East Atlantic Pattern (EAP; Fig. 1.6) also indicates changes in the strength and position of the Westerlies (Woollings et al. 2010). The EAP consists of a north-south dipole of a low- and high-pressure center, respectively. The centers of action in the EAP are displaced southeastward compared to the NAO, but this does not indicate that the EAP is simply a southward-shifted NAO. A positive phase of the EAP is associated with a northward shift of the Westerlies and

stronger zonal winds, providing warmer weather in Europe and more (less) precipitation over northern (southern) Europe (http://www.cpc.ncep.noaa.gov).

The Scandinavian Pattern (SP; Fig. 1.6) has its center of action over Scandinavia. During positive phases of SP, there are positive pressure anomalies over Scandinavia, occasionally associated with strong blocking high-pressure systems and therefore called the "Blocking" regime (Hurrell and Deser 2009). Likewise, during negative phases of SP, there are negative pressure anomalies over this region. A positive phase of SP is related with lower temperatures than normal in western Europe, with less precipitation over Scandinavia and more precipitation over central and southern Europe (http://www.cpc.ncep.noaa.gov).

1.3 Tools to understand oceanic circulation and variability

1.3.1 Concepts of water mass analysis

Different water masses can be identified and classified by their *TS*-properties (Helland-Hansen 1916), and visualized in a temperature-salinity (*TS*) diagram (Fig. 1.7a). A homogeneous water mass is manifested as a single point and is defined in the theory of water masses as a water type. A water type typically represents a water mass in its formation region, from where it gradually mixes with other water masses and thereby modifies its properties (Tomczak 1999).

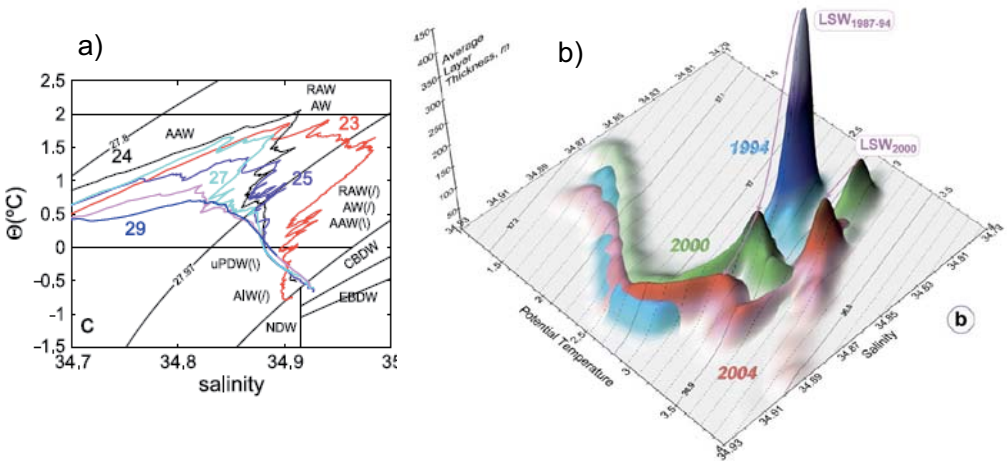

Figure 1.7: a) TS-diagram showing the relationship between potential temperature and salinity for Atlantic and Arctic derived water masses in a section just north of the Fram Strait (Rudels et al. 2005) and b) Volumetric TS-diagram showing the relationship between potential temperature, salinity, and layer thickness for Labrador Sea Water (LSW) for different years (Yashayaev 2007a).

In the upper layer of the ocean the surface water is constantly changing, i.e., new water masses are formed due to air-sea-ice exchanges. Four physical processes are known to form new water masses: subduction, convection, subsurface mixing, and advection when considering parts of the world ocean (Tomczak 1999). Both subduction and convection are driven by air-sea exchanges. The annual surface forcing causes the mixed layer to expand and shrink in the course of a year, causing the mixed layer to exchange mass and other properties with the interior ocean and thereby to ventilate the latter. The subduction of water from the mixed layer to the thermocline is found to take place in late winter (Stommel 1979). Convection means vertical mixing in the water column due to hydrostatic instability (Marshall and Schott 1999): The atmosphere cools the ocean surface, creating a body of water that is denser than its surroundings, thereby causing it to sink into the ocean interior, separating it from the atmosphere. Simultaneously, lighter water rises between the dense plumes. E.g., Labrador Sea Water is formed by open-ocean convection in the Labrador and Irminger seas (Curry et al. 1998; Pickart et al. 2003).

In the deeper parts of the ocean water masses are isolated from the atmosphere, and can therefore more easily maintain their properties. The water masses typically spread from their formation region and decay slowly through mixing with other water masses. The basis of water mass analysis in the deep ocean is that variations in a water mass in its formation region are small compared to variations among different water masses (Tomczak 2000). The spreading and evolvement of water masses can be analyzed by the use of *TS*-diagrams (Fig. 1.7a). The *TS*-diagrams give information on the properties of the water masses, but it does not provide information about the relative volume of the water masses. The layer thickness of a water mass, defined as the vertical distance between two isopycnals, is one way to obtain an estimate of relative volumes. By combining the layer thickness, temperature, and salinity of a specific region, different water masses and their relative abundance become evident (Fig. 1.7b). This is what is called a volumetric *TS*-diagram; the most important development in water mass analysis after Helland-Hansen's contribution in 1916 (Worthington 1981).

Instead of the layer thickness, the volume transport through a section can also be applied to give information about the amount of the different water masses. In model simulations this is easy to achieve, by sorting the volume transport in each grid cell into the temperature and salinity bins of the *TS*-diagram. The circulation and transformation of the different water masses of the ocean can be enlightened by analyzing volumetric *TS*-diagrams for several vertical sections downstream of the formation regions, and will reveal circulations pattern on how heat and salt are distributed in the oceans (Gulev et al. 2003; Bailey et al., 2005).

Estimation of water mass transformation

Water mass transformation due to heat- and freshwater fluxes can be estimated and a method was introduced by Walin (1982), who related the heat flux to the thermal circulation of the ocean. Speer and Tziperman (1992) expanded this methodology to include also the contribution from freshwater fluxes, and presented a formula that converts the integrated heat and

freshwater flux in water mass outcrop regions to diapycnal transport. This is the surface-forced water mass transformation. Walin (1982) introduced his method for a steady state, while Speer and Tziperman (1992) performed analyses for a time-varying climate, and hence time varying outcrop regions. Observation-based annual mean water mass transformation in the subpolar North Atlantic is shown in Fig. 1.8. Brambilla et al. (2008) calculated monthly water mass transformation from heat- and freshwater fluxes in outcrop regions, and from this obtained the annual mean water mass transformation.

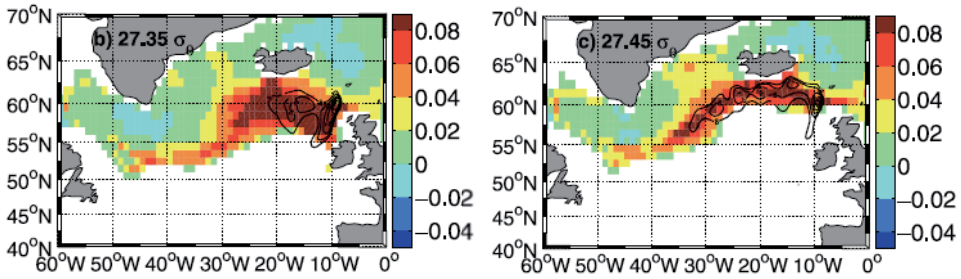

Figure 1.8: Observation-based regional distribution of surface-forced water mass transformation across the isopycnals indicated in the figures. This provides a valuable benchmark for assessing the surface-forced water mass transformation in climate models. From Brambilla et al. (2008).

Another source for water mass transformation, besides the surface density fluxes, is interior mixing. Walin (1982) recognized the interior mixing, but this part was neglected in his relation of the heat flux and thermal circulation. Garrett et al. (1995) revealed a non-linear relationship between surface-forced water mass transformation and interior mixing. Later, Nurser et al. (1999) investigated in detail the effect of different types of interior mixing on water mass transformation in the Atlantic Ocean. They found that surface forcing acts to increase density differences, whereas interior mixing acts to reduce density differences. Without interior mixing, the ocean would gradually be filled with denser water, and a steady state would not be possible. In the tropics, the interior mixing is essential for the water mass transformation, while at northern high latitudes the surface density fluxes are the dominant source for water mass transformation (Nurser et al. 1999). However, diapycnal mixing is an essential process in the transformation of the overflow as it cascades down the southern flank of the Greenland-Scotland Ridge (Dickson and Brown 1994; Medhaug et al. 2011).

Water mass transformation can be linked to meridional overturning circulation in latitude-density space (Speer 1997). The latter quantifies zonally averaged water mass transformation due to both surface density fluxes and interior mixing. Marsh (2000) and Marsh et al. (2000) use a modified form of the Walin (1982) method: the water mass transformation at a reference latitude is related to all air-sea exchange north of that latitude. The interior mixing is neglected, and the light-to-dense overturning becomes a function solely of surface density fluxes. More recent model studies have investigated the relationship between the surface forced transforma-

tion and the maximum of the AMOC at different latitudes (Grist et al. 2009; Josey et al. 2009). Josey et al. (2009) find that the integrated surface forced transformation has a significant relationship with the lagged maximum value of the AMOC between 35-65^{o}N.

1.3.2 Numerical coupled climate models

Climate models are built to explore and improve the understanding of the climate system with its different components, air – sea – land – ice, and their interaction. Fully coupled climate models can simulate climates for the past, present, and future, and are valuable tools for investigating variability on decadal to multidecadal time scales (e.g., Delworth and Mann 2000; Cooper and Gordon 2002; Randall et al. 2007). In combination with instrumental observations and reconstructed paleo climate, climate models can help to understand the underlying mechanisms behind the variability (e.g., Cooper and Gordon 2002; Jungclaus et al. 2010). Instrumental and paleo data are, nevertheless, either restricted to a few decades or are incomplete, for instance, with respect to spatial coverage. In addition, it is difficult and expensive to monitor the three-dimensional space and time varying climate, such as for instance the strength and shape of AMOC (e.g., Cunningham et al. 2007; Drijfhout and Hazeleger 2007). In these cases, climate models are highly valuable tools in the understanding of climate dynamics associated with large-scale mechanisms on decadal to multidecadal time scales.

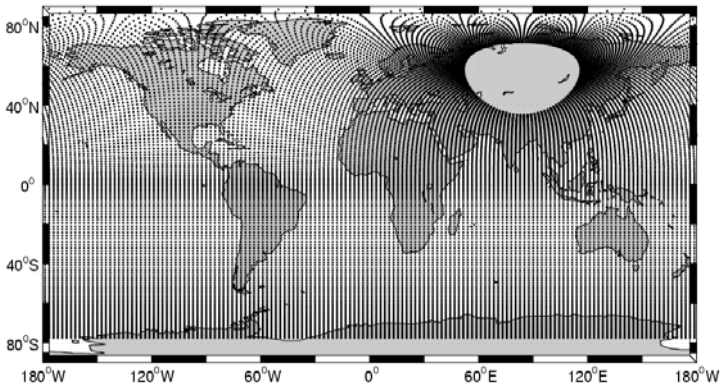

Figure 1.9: The horizontal grid distribution (2.4° x 2.4°) for the ocean component in the Bergen Climate Model. From Furevik et al. (2003).

Climate models are generally intended to simulate the global climate over long time, and require therefore high computational cost. For that reason, these models have rather coarse spatial resolution (Fig. 1.9). There are several known deficits in climate model simulations. For instance, these models are non-eddy permitting and they poorly resolve processes over small-scale topography, as well as small-scale boundary currents (e.g., Bailey et al. 2005; de Jong et al. 2009). One specific example is the overflow processes, such as entrainment of ambient Atlantic-derived

water into the descending overflows. These processes are generally operating on sub-grid scales (Legg et al. 2009). Sub-grid scale processes are processes that are not resolved by the model grid and are therefore not explicitly simulated (Haidvogel and Beckmann 1999). The effects of these processes must therefore be specified at the grid scale of the model, i.e., *parameterized* (Hartmann 1994). The inclusion of the effects sub-grid scale processes is thus based on the state of the simulated climate. For instance, when there is hydrostatic instability, determined from the simulated density at different levels, the water column changes according to the parameterization. In the Bergen Climate Model the deep convection is parameterized by an instant re-stratification of the water column, and thickening of denser layers (Medhaug et al. 2011). The way sub-grid scale processes are parameterized can play a crucial role in climate models (Hartmann 1994; Legg et al. 2009). However, because of an incomplete understanding of numerous physical processes in the natural climate, climate model simulations are expected to be affected by our approximations and parameterizations.

Furthermore, some small-scale processes are not present at all in climate models. For instance, the coastal current and the East Greenland Current play an important role in controlling the freshwater distribution to the western North Atlantic, and they receive part of their freshwater from meltwater runoff from Greenland and calving of icebergs (Sutherland and Pickart 2008). Such processes are generally not presented in the generation of climate models used in the Fourth Assessment Report of the Intergovernmental Panel on Climate Change (IPCC), since no ice sheet model is incorporated in the climate models in the last assessment (Randall et al. 2007). Another example is the Greenland Tip Jet; a sub-synoptic meteorological feature that enhances surface fluxes in the vicinity of Cape Farewell (Sproson et al. 2010). The unresolved processes becomes evident when climate models are used to investigate the climate of a specific region rather than the more global climate (e.g., Bailey et al. 2005; de Jong et al. 2009).

It is common to assess the model performance by comparing model climatology with existing observations (e.g., Otterå et al. 2009; de Jong et al. 2009). Observations are typically snap-shots of present-day climate or from specific time periods. These short time periods can therefore be biased by a specific type of forcing, such as the negative phase of the North Atlantic Oscillation in the late 1960s (Häkkinen et al. 2011). On the other hand, model simulations for pre-industrial or present-day climate are run for several decades, and are thus free to follow their own climates. Hence, differences between the observations and the model data might be expected. It is therefore similarly important that the structure of, for instance, simulated and observed sea surface temperature are comparable rather than the absolute magnitude of the temperature. A complimentary way of assessing the performance of climate models is model-model intercomparison. Such intercomparisons highlights similarities and differences among models, helping to pinpoint aspects that need to be improved and to increase creditability of robust and persistent features across different model formulations (e.g., Lambert and Boer 2001; Gregory et al. 2005; Medhaug and Furevik 2011). Intercomparison studies help to constrain climate variability on decadal and multidecadal times scales and are therefore important with respect to future decadal predictions.

Chapter 2

This study

2.1 Motivation and Objectives

The water mass transformation of Subtropical Water to Polar Water and intermediate and deep water in the North Atlantic Ocean and Nordic Seas influences the European Climate and the large-scale ocean circulation. Therefore, it is essential to investigate the ability of climate models to simulate the ocean circulation and water mass transformation in this region (cf. Chapter 1). This assessment of climate models is also useful for future climate predictions. The most important variables to assess in the ocean are temperature and salinity. These have been key in observational studies as long as the ocean has been measured. There is a difference in how observational oceanography and climate modeling approach the ocean circulation and variability. In observational oceanography the data are very often restricted to specific time periods, or is only snapshots of nature. Ocean temperature and salinity are used together with velocity to distinguish between different water masses and to determine their circulation. In climate modeling long time series of several decades or centuries are available. Therefore, the model data is often analyzed by use of statistical methods. For example, by computing the dominant modes of variability, energy spectra of specific variables, or long-term correlations. However, it would be beneficial for both communities to merge this gap by applying methods consistent with observational oceanography on climate model simulations, as several studies have attempted (Gulev et al. 2003; Bailey et al. 2005).

There is a range of climate models which vary in their performance in simulating the climate, depending partly on the configuration of the model, such as the vertical coordinate and the resolution of the horizontal grid. The grid configuration of the Bergen Climate Model (BCM; Furevik et al. 2003) is focused on the North Atlantic region, and several aspects of the ocean circulation in this region are found to be well represented in a multi-century simulation by this model (Otterå et al. 2009). The ocean component of BCM is defined on isopycnal coordinates, which makes it well suited to explore the "life story" of water masses; their formation, propagation, and decay as they travel the ocean, compared to the more traditional depth coordinate models (Bleck et al. 1992; Willebrandt et al. 2001). In this thesis the BCM have been com-

pared with multi-century simulations from the depth coordinate models of the Institute Pierre Simon Laplace Coupled Model (IPSLCM4; Marti et al. 2010; Servonnat et al. 2010) and the Max Planck Institute for Meteorology Earth System Model (MPI-M ESM; Jungclaus et al. 2010). Model intercomparison studies are important to identify mechanisms that are robust, for instance, which mechanisms that set the main regions of light-to-dense water mass transformation at northern high latitudes.

The mechanisms controlling the long-term variability of the water mass transformation and the horizontal and vertical circulation of the North Atlantic Ocean are of particular interest, since these constrain the northward oceanic heat transport. Climate variability on time scales longer than a few decades is generally not possible to investigate directly from observations. Multi-century simulations by climate models are therefore highly valuable in the investigations of decadal and multi-decadal scale variability. These simulations can be used to establish relationships between key processes in the subpolar North Atlantic Ocean. Example on this could be atmospheric and oceanic variability in the Nordic Seas and the Labrador Sea, and their relation to the strength of the horizontal (Subpolar Gyre) and vertical (Atlantic Meridional Overturning Circulation) ocean circulation.

The objectives for this study are:

- Measure the skill of the ocean component in BCM to reproduce the main water masses and their associated currents in the North Atlantic Ocean, using methodology routinely applied to observations (examples are given in Paper IV). Results are given in Paper I, II and III.
- Estimate and compare the water mass transformation and variability associated with Subpolar Mode Water in three multi-century climate model simulations from BCM, IPSLCM4, and MPI-M ESM. The simulations are provided by the EU project *Thermohaline Overturning - at Risk?, THOR*). Results are given in Paper I.
- Identify key processes for the ocean circulation at the northern high latitudes in BCM, such as the formation of Nordic Seas Overflow Water and Labrador Sea Water. Quantify the decadal relationship between the intermediate and deep water components and the strength of the Subpolar Gyre and Atlantic Meridional Overturning Circulation. This objective form the main deliverable in the IPY project *Bipolar Atlantic Thermohaline Circulation, BIAC*, which this study has been part of. Results are given in Paper II and III.

The essence of these objectives is: How is the northern light-to-dense water transformation related to the large-scale ocean circulation in the North Atlantic, as manifested in state-of-the-art climate models?

2.2 Presentation of the papers

Paper I, II, and III are presented in an order consistent with the Atlantic THC (cf. Chapter 1), starting with the Subtropical Water and ending with the North Atlantic Deep Water. Finally, a summary of Paper IV is given. This study shows examples of the water mass analyses commonly used in observational oceanography, which are applied on the multi-century simulation from the Bergen Climate Model herein.

Paper I. Water mass transformation and the North Atlantic Current in three multi-century climate model simulations

1) What are the similarities and differences in the northern water mass transformation in three climate models?

2) Which factors can explain the decadal variability of the water mass transformation in the northeastern North Atlantic?

Warm and saline Subtropical Water carried by the North Atlantic Current undergoes substantial transformation on its way to higher latitudes since heat is released from ocean to atmosphere. The regional distribution of surface-forced water mass transformation is assessed in three different multi-century climate model simulations, where we have focused on the eastern subpolar North Atlantic Ocean. In the diagnosis used here, originally introduced by Walin (1982), transformation in water mass outcrop areas is estimated from heat and freshwater fluxes. In all models the integrated heat flux in the eastern subpolar region has a larger contribution than the freshwater flux to the water mass transformation. However, there are significant differences in the strength and distribution of the heat and freshwater fluxes among the models. In two of the models the western subpolar region has a larger buoyancy gain due to freshwater input than buoyancy loss due to heat loss. The differences in surface-forced water mass transformation can largely be attributed to the position of the North Atlantic Current and sea ice extent, which differ among the models.

A strengthening of the Atlantic Meridional Overturning Circulation (AMOC) in latitude-density space is associated with an increase in the volume transport of the densest layers, and a lagged increase in surface-forced water mass transformation in the eastern subpolar region 7-8 years later in two of the models. In the third model there is no significant correlation between AMOC and the water mass transformation. The same model has an unrealistic freshwater input in the southern subpolar region and a North Atlantic Current that subducts beneath this fresh surface layer. The methodology applied in this study, based on surface fluxes and hydrography, has shown to be a useful tool in assessing surface-forced water mass transformation in climate models.

Paper II. Arctic/Atlantic exchanges via the Subpolar Gyre

1) How are the main water masses in the subpolar North Atlantic Ocean represented in the Bergen Climate Model?

2) Which factors can explain the decadal variability of Subpolar Gyre strength?

This study investigates the decadal variability of the subpolar North Atlantic Ocean in a 600 years pre-industrial simulation of the Bergen Climate Model. The paper is divided into two main parts. The first part describes the model performance in the subpolar region, by assessing the model's ability to simulate the main water masses and the associated circulation. Identifying the main water masses entering and exiting the subpolar region, the Arctic/Atlantic exchanges, reveals the main water mass transformation occurring in the subpolar region. Subtropical Water enters the subpolar region from the south and transforms to denser water that flows further north into the Nordic Seas or re-circulate in the western subpolar region. The water carried by the latter branch transform to dense Labrador Sea Water in the Labrador and Irminger seas, which eventually reach Grand Banks. Dense Overflow Water enters the subpolar region from the north and transform to a lighter deep water component due to entrainment of Atlantic Water and continues then southward. The model resembles reality rather well, particularly in the water mass exchange at the Greenland-Scotland Ridge. However, the model has difficulties in reproducing the westward flow of overflow-derived water through the Charlie Gibbs Fracture Zone. This is likely to be the reason for the weaker Deep Western Boundary Current in this model, compared to what is found in observation-based studies.

The second part of the paper identifies key processes in the subpolar region that potentially can explain parts of the decadal variability of the Subpolar Gyre strength. This investigation reveals that a combination of the overflow from the Nordic Seas, the formation of Labrador Sea Water, and the East Atlantic Pattern can explain 44% the decadal variability of the Subpolar Gyre strength. The latter predictor is strongly related to the wind stress in the subpolar region. The Nordic Seas overflow reflects the strength of the water mass transformation within the Nordic Seas, while the amount of Labrador Sea Water is found to be linked to the most dominant atmospheric pattern in the North Atlantic region - the North Atlantic Oscillation.

Paper III. Mechanisms for decadal scale variability in a simulated Atlantic Meridional Overturning Circulation

1) Which factors can explain the decadal variability of the Atlantic Meridional Overturning Circulation?

2) What are the relative contributions of Overflow and Labrador Sea Water to the North Atlantic Deep Water?

This study analyses the behavior of the Atlantic Meridional Overturning Circulation in a 600 years pre-industrial simulation of the Bergen Climate Model. The overturning is well simulated in terms of magnitude and low frequency variations. A detailed diagnosis of the local air-sea exchanges at northern high latitudes is performed to understand the model's formation of key water masses in the large-scale ocean circulation in the North Atlantic. An increase in the deep convection in the Labrador Sea and the northeastern Nordic Seas is associated with a positive and negative phase of the North Atlantic Oscillation, respectively. However, the amount of dense water spilling over the Greenland-Scotland Ridge and into the deep North Atlantic Ocean is related to the Scandinavian Pattern. A negative phase of this pattern is associated with increased northerly winds over the Nordic Seas, strengthening the Nordic Seas overflow. The decadal variability of the deep convection in the Labrador Sea and the poleward heat transport at the Greenland-Scotland Ridge are significantly correlated with the lagged strength of Atlantic Meridional Overturning Circulation.

The products of the convective activity in the Labrador Sea and the water mass transformation in the Nordic Seas are the major sources to the lower limb of the overturning circulation. The Nordic Seas overflow, including the entrainment of Atlantic Water in the vicinity of the Greenland-Scotland Ridge, and the Labrador Sea Water contribute with 2/3 and 1/3, respectively, to the North Atlantic Deep Water. This water mass distribution is similar to observation-based estimates.

Paper IV. Changes in the properties and distribution of the intermediate and deep waters in the Fram Strait

1) What are the main intermediate and deep water masses in the Fram Strait and how has the water mass distribution changed during the last three decades?

2) What are the temperature and salinity changes of these water masses during the study period?

Possible changes in the properties and distribution of the intermediate and deep water masses passing through the Fram Strait have been studied for the period from 1982 to 2008. With a sill depth of approximate 2600 m, the Fram Strait is the only deep connection between the Arctic Ocean and rest of the world ocean. The exchange of mass, heat, and salt are therefore of particular interest in this region. Relatively cold and fresh deep water originate from the Norwegian Sea and Greenland Sea in the Nordic Seas, while relatively warm and saline originate from the deep the Canadian Basin and Eurasian Basin in the Arctic Ocean. These water masses are carried by the two dominating currents in the Fram Strait; the West Spitsbergen Current and the East Greenland Current in the eastern and western part of the strait, respectively. The Fram Strait is characterized by strong mixing, largely owed to the irregular bathymetry and the deep sill depth allowing a large variety of water masses to pass the strait.

Vertical zonal transects of potential temperature and salinity revealed changes in the location and spatial extent of the different water masses, while a classical *TS*-analysis gave information on how the properties of the different water masses have changed. The deep water from the Norwegian Sea became warmer (about 0.10°C) during the study period, due to increased influence of deep water from the Eurasian Basin, and the presence of very cold water (temperature below -1.1°C) disappeared after 1997. A diagnosis of the layer thickness of intermediate water shows that the amount of intermediate water has increased in the Fram Strait during the study period.

2.3 Summary and Conclusions

In this thesis the ocean circulation and light-to-dense water mass transformation in the North Atlantic and the Nordic Seas have been investigated in state-of-the-art climate models. While Paper I focuses on the upper water masses in the eastern subpolar region, Paper II focuses more on the deeper water masses in the western subpolar region. The upper eastern part represents the overall source water mass, Subtropical Water, and the deep western part represents mainly the products of the northern water mass transformation. The water mass exchange at the Greenland-Scotland Ridge reflects the water mass transformation within the Arctic Mediterranean. The main factor in transforming the Subtropical Water is the heat loss from the ocean to the atmosphere. The connection between the eastern and western subpolar region is the Subpolar Gyre, the depth-integrated horizontal circulation. While Paper II identifies factors that contribute to the decadal variability of the Subpolar Gyre, Paper III identify factors that contribute to the decadal variability of the Atlantic Meridional Overturning Circulation (AMOC). AMOC is the zonally integrated circulation, which includes the poleward transport of the source waters and the southward transport of the products of the northern water mass transformation, and hence the Subpolar Gyre circulation.

The main conclusions in this thesis are the following (cf. objectives in Section 2.1):

- The Bergen Climate Model has in general realistic ocean transports and water mass distribution in the subpolar North Atlantic Ocean according to observations. However, there are challenges with the sea ice extent and freshwater input in the Nordic Seas and the Labrador Sea, which results in Polar Water and Labrador Sea Water that are more saline than found in observations. Another challenge is the flow over small-scale topography, such as the geographical distribution of the Nordic Seas overflow at the Greenland-Scotland Ridge. The simulated relative amount of Overflow Water east and west of Iceland differs from observations. See Paper I, II, and III.

- There are large differences in the distribution and strength of heat and freshwater fluxes at northern high latitudes among climate models. These differences are related to the models' pathway of the North Atlantic Current and sea ice extent. Although diverging climates, the structure of their AMOC and mechanisms on decadal time scale appear to an extent to be similar among the models. See Paper I.

- The decadal variability in the strength of the Subpolar Gyre and AMOC is related to air-sea exchanges, mainly heat and momentum fluxes, in the subpolar region and the Nordic Seas. A strengthening of the Subpolar Gyre is lead by an increase in the deep water components (Labrador Sea Water and Nordic Seas Overflow), and is followed by an increase in the strength of AMOC. Anomalies in the amount of deep water, such as layer thickness anomalies, can be followed as they propagate southward in the deep North Atlantic Ocean and are robust signals throughout the Bergen Climate Model multi-century simulation. See Paper II and III.

Recommendations and Future perspectives

In this thesis, water mass analysis has been the common denominator for assessing the oceanic circulation in climate models. Applying volumetric *TS*-diagrams on model data has shown to be a valuable tool in understanding water mass transformation and on tracking water masses that are isolated from the sea surface (e.g., Paper II and III).

A particularly suitable location for water mass analysis is the Greenland-Scotland Ridge. The transformation from warm and saline to colder and fresher water masses within the Nordic Seas is reflected in the water mass exchanges across the ridge. The method is rather simple to implement when using climate models, since it only requires temperature, salinity, and velocity from a specific section. When using observational data (e.g., Paper IV), these field variables are more difficult to achieve, generally because of the lack of velocity observations. However, the temperature and salinity of the ocean are relatively well sampled, and therefore provides a robust test bed for assessment of simulated temperature and salinity. An advantage when using climate models is therefore the inclusion of the relative volume of different water masses. Importantly, the water mass analysis provides a direct visualization of water masses since water masses largely follow density surfaces, which to great accuracy are functions of temperature and salinity.

Tracking of water masses at and near the ocean surface is a challenge, since the surface water constantly changes its properties when in contact with the atmosphere. To circumvent this difficulty, we introduce the established theory introduced by Walin (1982), relating air-sea exchanges to oceanic flow of water masses across surfaces of constant density (e.g., Paper I). This methodology is, again, rather simple to implement when using model data. The water mass transformation across density surfaces is then estimated from heat- and freshwater fluxes at the surface, in addition to the sea surface temperature and salinity fields. It is demonstrated in Paper

I that this way of assessing the water mass transformation at northern high latitudes is a valuable tool in comparison with the frequently analyzed and diagnosed AMOC.

The North Atlantic Climate variability is often related to the (lagged) temporal variations in AMOC. However, AMOC is only a measure of the zonal mean volume fluxes, it does not tell where water mass transformation and heat loss are taking place. As Paper I demonstrates, the pathway of the North Atlantic Current and the associated heat loss can be located in different regions in different climate models even tough their AMOCs have similar structure. The actual location of the heat loss from the ocean to the atmosphere is likely of some importance for the European Climate. A central question in this regard is whether the bulk of simulated water mass transformation occurs in the northeastern North Atlantic or the Nordic Seas. The analysis in Paper I points to the importance of additional analysis (such as the approach of Walin) to the AMOC diagnosis to gain additional knowledge about the distribution of the northern water mass transformation, and hence the possible influence on European Climate.

To improve climate models, it is essential to understand how the models operate and to assess their performance with respect both to instrumental data and reconstructed paleo climate. A continuous evaluation of the performance and nature of climate models will allow us to quantify uncertainties in climate models and to identify which mechanisms are robust and which are not. It is important to be aware of where and at which time scales the climate models are representative and reliable, and where they are less skillful. By addressing these questions one will gain in understanding on how the climate models operate, and knowledge of how to improve the models. The natural variability of the North Atlantic Ocean and Nordic Seas must be constrained if the future coming climate prediction is to be proficient for the North Atlantic region.

Some suggestions for further assessment and exploration of climate models are:

- This thesis is mainly focused on the effects of heat loss at northern high latitudes; the light-to-dense water mass transformation. How is the freshwater input at northern high latitudes simulated in climate models and how important is this effect on the water mass transformation compared to the heat loss?

- A continued assessment of the water mass distribution and circulation in the Bergen Climate Model by *TS*-volumetric plots for key sections in the world ocean could form an "Atlas of the Bergen Climate Model water masses".

- Further exploration of the Subpolar Gyre dynamics, including the exchanges between the Subpolar Gyre and Subtropical Gyre. In recent observation-based studies, a link is found between the strength of the gyres and changes in the salinity and temperature of the Atlantic Water in the vicinity of the Greenland-Scotland Ridge. Periods with weak gyre circulation is associated with positive temperature and salinity anomalies, propagating from the Subtropical gyre towards the Arctic Ocean (Häkkinen et al. 2011).

References

Aagaard, K., and E. C. Carmack, 1989: The Role of Sea Ice and Other Fresh Water in the Arctic Circulation. *J. Geophys. Res.*, 94(C10):14485-14498.

Aagaard, K., J. H. Swift, E. C. Carmack, 1985: Thermohaline circulation in the Arctic Mediterranean Seas. *J. Geophys. Res.*, 90(C5):4833-4846.

Arhan, M., 1990: The North Atlantic Current and Subarctic Intermediate Water. *J. Mar. Res.*, 48:109-144.

Bacon, S., and P. M. Saunders, 2010: The Deep Western Boundary Current at Cape Farewell: Results from a Moored Current Meter Array. *J. Phys. Oceanogr.*, 40:815-829, doi: 10.1175/2009JPO4091.1.

Bailey, D. A., P. B. Rhines, and S. Häkkinen, 2005: Formation and pathways of North Atlantic Deep Water in a coupled ice-ocean model of the Arctic-North Atlantic Oceans. *Climate Dyn.*, 25:497-516, doi: 10.1007/s00382-005-0050-3.

Barnston, A. G., and R. E. Livezey, 1987: Classification, seasonality and persistence of low-frequency atmospheric circulation patterns. *Mon. Wea. Rev.*, 115:1083-1126.

Belkin, I. M., S. Levitus, J. Antonov, and S.-A. Malmberg, 1998: Great Salinity Anomalies in the North Atlantic. *Prog. Oceanogr.*, 41:1-68.

Bentsen M., H. Drange, T. Furevik, and T. Zhou, 2004: Simulated variability of the Atlantic meridional overturning circulation. *Clim. Dyn.*, 22:701-720. doi:10.1007/s00382-004-0397-x

Biastoch A., C. W. Böning, J. Getzlaff, J. M. Molines, G. Madec, 2008: Causes of interannual-decadal variability in the meridional overturning circulation of the mid-latitude North Atlantic Ocean. *J. Clim.*, 21:6599-6615. doi: 10.1175/2008JCLI2404.1

Bleck R., C. Rooth, D. Hu, and L. T. Smith, 1992: Salinity-driven thermocline transients in a wind- and thermohaline-forced isopycnic coordinate model of the North Atlantic. *J. Phys. Oceanogr.*, 22:1486-1505.

Blindheim, J., and S. Østerhus, 2005: The Nordic Seas, Main Oceanographic Features, in AGU Geophysical Monograph Series, pages 11-38, American Geophysical Union, Washington, DC.

Bower, A. S., M. S. Lozier, S. F. Gary, and C. W. Böning, 2009: Interior pathways of the North Atlantic Meridional Overturning Circulation. *Nature*, 459:243-247.

Brambilla, E., and L. D. Talley, 2008: Subpolar mode water in the northeastern Atlantic: 1. Averaged properties and mean circulation. *J. Geophys. Res.*, 113, C04025, doi: 10.1029/2006JC004062.

Brambilla, E., L. D. Talley, and P. E. Robbins, 2008: Subpolar Mode Water in the northeastern Atlantic: 2. Origin and transformation. *J. Geophys. Res.*, 113, C04026, doi: 10.1029/2006JC004063.

Broecker, W. S., 1987: The biggest chill. *Natural History*, 96:74-82.

Broecker, W. S., 1997: Thermohaline circulation, the Achilles heel of our climate system: Will man-made CO2 upset the current balance? *Science*, 278:1582-1588.

Budéus, G., and S. Ronski, 2009: An Integral View of the Hydrographic Development in the Greenland Sea Over a Decade. *The Open Oceanography Journal*, 3:8-39.

Chapman, D. C., and R. C. Beardsley, 1989: On the origin of shelf water in the Middle Atlantic Bight. *J. Phys. Oceanogr.*, 19:384-391.

Cooper, C., and C. Gordon, 2002: North Atlantic oceanic decadal variability in the Hadley Centre coupled model. *J. Clim.*, 15:45-72.

Cunningham, S. A., and Coauthors, 2007: Temporal variability for the Atlantic Meridional Overturning Circulation at 26.5N. *Science*, 317:935-937, doi:10.1126/science.1141304.

Curry, R. G., and M. S. McCartney, 2001: Ocean gyre circulation changes associated with the North Atlantic oscillation. *J. Phys. Oceanogr.*, 31(12):3374-3400.

Curry, R. G., M. S. McCartney, and T. Joyce, 1998: Oceanic transport of subpolar climate signals to mid-depth subtropical waters. *Nature*, 391:575-577.

de Jong, F., S. S. Drijfhout, W. Hazeleger, H. M. van Aken, and C. A. Severijns, 2009: Simulations of hydrographic properties in the north western North Atlantic Ocean in Coupled Climate Models. *J. Clim.*, 22(7):1767-1786, doi: 10.1175/2008JCLI2448.1.

Delworth, T. L., and M. E. Mann, 2000: Observed and simulated multidecadal variability in the Northern Hemisphere. *Clim. Dyn.*, 16:661-676.

Dengler, M., J. Fischer, F. A. Schott, and R. Zantopp, 2006: Deep Labrador Current and its variability in 1996-2005. *Geophys. Res. Lett.*, 33, L21S06, doi: 10.1029/2006GL026702.

Dickson, R. J., and J. Brown, 1994: The production of North Atlantic Deep Water: sources, rates and pathways. *J. Geophys. Res.*, 99(C6):12319-12341.

Dickson, R. R., J. Meincke, S.-A. Malmberg, and A. J. Lee, 1988: The "great salinity anomaly" in the northern North Atlantic, 1968-1982. *Prog. Oceanogr.*, 20:103-151.

Dickson, R., B. Rudels, S. Dye, M. Karcher, J. Meincke, and I. Yashayaev, 2007: Current estimates of freshwater flux through Arctic and subarctic seas. *Prog. Oceanogr.*, 73:210-230, doi:10.1016/j.pocean.2006.12.003.

Drange, H., and Coauthors, 2005: The Nordic Seas: An Overview. In AGU Geophysical Monograph Series, pp. 1-10, American Geophysical Union, Washington, DC.

Drijfhout, S. S., and W. Hazeleger, 2007: Detecting Atlantic MOC changes in an ensemble of climate change simulations. *J. Clim.*, 20:1571-1582.

Eldevik, T., J. E. Ø. Nilsen, D. Iovino, K. A. Olsson, A. B. Sandø, and H. Drange, 2009: Observed sources and variability of Nordic seas overflow. *Nat. Geosci.*, 2:406-410, doi: 10.1038/ngeo518.

Frankcombe, L. M., and H. A. Dijkstra, 2011: The role of Atlantic-Arctic exchange in North Atlantic multidecadal climate variability. *Geophys. Res. Lett.*, 38, L16603, doi:10.1029/2011GL048158.

Furevik, T., M. Bentsen, H. Drange, I. K. T. Kindem, N. G. Kvamstø, and A. Sorteberg, 2003: Description and validation of the Bergen Climate Model: ARPEGE coupled with MICOM. *Climate Dyn.*, 21:27-51, doi: 10.1007/s00382-003-0317-5.

Ganachaud, A., and C. Wunsch, 2000: Improved estimates of global ocean circulation, heat transport and mixing from hydrographic data. *Nature*, 408:453-457.

Garrett, C., K. Speer, and E. Tragou, 1995: The relationship between water mass formation and surface buoyancy flux, with application to Phillips' Red Sea model. *J. Phys. Oceanogr.*, 25:1696-1705.

Gill, A. E., 1982: Atmosphere-Ocean Dynamics, 662 pp, Elsevier, New York.

Gordon, A. L., 1986: Interocean exchange of thermocline water. *J. Geophys. Res.*, 91:5037-5046.

Gregory, J. M., and Coauthors, 2005: A model intercomparison of changes in the Atlantic thermohaline circulation in response to increasing atmospheric CO2 concentration. *Geophys. Res. Lett.*, 32, L12703, doi:10.1029/ 2005GL023209.

Grist, J. P., R. Marsh, and S. A. Josey, 2009: On the Relationship between the North Atlantic Meridional Overturning Circulation and the Surface-Forced Overturning Streamfunction. *J. Clim.*, 22:4989-5002, doi: 10.1175/2009JCLI2574.1.

Gulev, S. K., B. Barnier, H. Knochel, J.-M. Molines, M. Cottet, 2003: Water mass transformation in the North Atlantic and its impact on the meridional circulation: insights from on ocean model forced by NCEP/NCAR reanalysis surface fluxes. *J. Clim.*, 16:3085-3110.

Haak, H., J. Jungclaus, U. Mikolajewicz, and M. Latif, 2003: Formation and propagation of great salinity anomalies. *Geophys. Res. Lett.*, 30(9), 1473, doi:10.1029/2003GL017065.

Haidvogel, D. B., and A. Beckmann, 1999: Numerical ocean circulation modeling, Imperial College Press, London.

Häkkinen, S., 1999: A Simulation of Thermohaline Effects of a Great Saliniy Anomaly. *J. Clim.*, 12:1781-1795.

Häkkinen, S., 2002: Freshening of the Labrador Sea surface waters in the 1990s: Another great salinity anomaly? *Geophys. Res. Lett.*, 29(24), 2232, doi:10.1029/2002GL015243.

Häkkinen, S., and A. Proshutinsky, 2004: Freshwater content variability in the Arctic Ocean. *J. Geophys. Res.*, 109, C03051, doi:10.1029/2003JC001940.

Häkkinen, S., P. B. Rhines, and D. L. Worthen, 2011: Warm and saline events embedded in the meridional circulation of the northern North Atlantic. *J. Geophys. Res.*, 116, C03006, doi: 10.1029/2010JC006275.

Hansen, B., and S. Østerhus, 2000: North Atlantic-Nordic Seas exchanges. *Prog. Oceanogr.*, 45:109-208.

Hartmann, D. L., 1994: Global Physical Climatology, Vol. 56, International Geophysics Series, Academic Press, London.

Hátún, H., A. B. Sandø, H. Drange, B. Hansen, and H. Valdimarsson, 2005: Influence of the Atlantic Subpolar Gyre on the Thermohaline Circulation. *Science*, 309:1841-1844, doi: 10.1126/science.1114777.

Helland-Hansen, B., 1916. Nogen hydrografiske metoder. Forhandlinger ved de skandinaviske Naturforskeres 16de møte, Kristiania, pp. 357-359. (in Norwegian)

Helland-Hansen, B., and F. Nansen, 1909: The Norwegian Sea, its physical oceanography based upon the Norwegian Researches 1900-1904. Report on Norwegian and Marine Investigations, 2, 390 pp.

Holliday, N. P., and Coauthors, 2008: Reversal of the 1960s to 1990s freshening trend in the northeast North Atlantic and Nordic Seas. *Geophys. Res. Lett.*, 35, L03614, doi: 10.1029/2007GL032675.

Hurrell, J. W., 1995: Decadal trends in the North Atlantic Oscillation: Regional temperatures and precipitation. *Science*, 269 (5224):676-679.

Hurrell, J. W. and C. Deser, 2009: North Atlantic climate variability: The role of the North Atlantic Oscillation. *J. Mar. Syst.*, 78(1):28-41.

Hurrell, J. W., Y. Kushnir, G. Ottersen, and M. Visbeck, 2003: An overview of the North Atlantic Oscillation, in AGU Geophysical Monograph Series 134, pages 1-35, American Geophysical Union, Washington, DC.

Isachsen, P. E., C. Mauritzen, and H. Svendsen, 2007: Dense water formation in the Nordic Seas diagnosed from sea surface buoyancy fluxes. *Deep-Sea Res. I*, 54:22-41.

Iselin, C. O'D., 1936: A study of the circulation of the western North Atlantic. *Papers in Physical Oceanography and Meteorology*, 4, 101 pp.

Jeansson, E., S. Jutterström, B. Rudels, L. G. Anderson, K. A. Olsson, E. P. Jones, W. M. Smethie, J. H. Swift, 2008: Sources to the East Greenland Current and its contribution to the Denmark Strait Overflow. *Prog. Oceanogr.*, 78:12-28.

Jónsson, S., and H. Valdimarsson, 2004: A new path for the Denmark Strait overflow water from the Iceland Sea to Denmark Strait. *Geophys. Res. Lett.*, 31, L03305.

Josey, S. A., J. P. Grist, and R. Marsh, 2009: Estimates of meridional overturning circulation variability in the North Atlantic from surface density flux fields. *J. Geophys. Res.*, 114, C09022, doi: 10.1029/2008JC005230.

Jungclaus, J. H., H. Haak, M. Latif, and U. Mikolajewicz, 2005: Arctic-North Atlantic interactions and multidecadal variability of the meridional overturning circulation. *J. Clim.*, 18:4013-4031.

Jungclaus, J. H., and Coauthors, 2010: Climate and carbon-cycle variability over the last millennium. *Climate of the Past*, 6:723-737.
Krauss, W., 1986: The North Atlantic Current. *J. Geophys. Res.*, 91:5061-5074.

Krümmel, O., 1879: Versuch einer vergleichenden morphologie der meeresreume, Verlag von Duncker & Humbolt, Leipzig, p. 110.

Kuhlbrodt, T., A. Griesel, M. Montoya, A. Levermann, M. Hofmann, and S. Rahmstorf, 2007: On the driving processes of the atlantic meridional overturning circulation. *Rev. Geophys.*, 45:RG2001.

Lambert, S. J., and G. J. Boer, 2001: CMIP1 evaluation and intercomparison of coupled climate models. *Climate Dynamics*, 17:83-106.

Latif, M., M. Collins, H. Pohlmann, and N. Keenlyside, 2006: A review of predictability studies of Atlantic sector climate on decadal time scales. *J. Clim.*, 19:5971-5987.

LeBel, D. A., and Coauthors, 2008: The formation rate of North Atlantic Deep Water and Eighteen Degree Water calculated from CFC-11 inventories observed during WOCE. *Deep-Sea Res. I*, 55:891-910, doi: 10.1016/j.dsr.2008.003.009.

Legg, S., and Coauthors, 2009: Improving oceanic overflow representation in climate models: The Gravity Current Entrainment Climate Process Team, *Bull. Am. Meteorol. Soc.*, 90:657-670, doi: 10.1175/2008BAMS2667.1.

Lozier, M. S., 2010: Deconstructing the Conveyor Belt. *Science*, 328:1507-1511, doi: 10.1126/science.1189250.

Macdonald, R. W., T. Harner, J. Fyfe, 2005: Recent climate change in the Arctic and its impact on contaminant pathways and interpretation of temporal trend data. *Sci. Total Environ.*, 342: 5-86. doi: 10.1016/j.scitotenv.2004.12.059.

Manabe, S., R. J. Stouffer, 1993: Century-scale effects of increased atmospheric CO2 on the ocean-atmosphere system. *Nature*, 364:215-218.

Marotzke, J., and J. R. Scott, 1999: Convective mixing and the thermohaline circulation. *J. Phys. Oceanogr.*, 29:2962-2970.

Marsh, R., 2000: Recent variability of the North Atlantic thermohaline circulation inferred from surface heat and freshwater fluxes. *J. Clim.*, 13:3239-3260.

Marsh, R., A. J. G. Nurser, A. P. Megann, and A. L. New, 2000: Water mass transformation in the Southern Ocean of a global isopycnal coordinate GCM. *J. Phys. Oceanogr.*, 30:1013-1045.

Marshall, J. and F. Schott, 1999: Open-ocean convection: observations, theory and models. *Rev. Geophysics*, 37(1):1-64.

Marti, O., and Coauthors, 2010: Key features of the IPSL ocean atmosphere model and its sensitivity to atmospheric resolution. *Clim. Dyn.*, 34:1-26.

Mauritzen, C., 1996: Production of dense overflow waters feeding the North Atlantic across the Greenland-Scotland Ridge, Part I: Evidence for a revised circulation scheme. *Deep-Sea Res. I*, 43:769-806.

Mauritzen, C., S. Häkkinen, 1999: On the relationship between dense water formation and the "Meridional Overturning Cell" in the North Atlantic Ocean. *Deep-Sea Res. I*, 46:877-894.

McCartney, M. S., and L. D. Talley, 1982: The Subpolar Mode Water of the North Atlantic. *J. Phys. Oceanogr.*, 12: 1169-1188.

Medhaug, I., T. Furevik, 2011: North Atlantic 20th century multidecadal variability in coupled climate models: sea surface temperature and ocean overturning circulation. *Ocean Sci.*, 7:389-404. doi: 10.5194/os-7-398-2011.

Medhaug, I., H. R. Langehaug, T. Eldevik, T. Furevik, and M. Bentsen, 2011: Mechanisms for decadal scale variability in a simulated Atlantic meridional overturning circulation. *Clim. Dyn.*, doi: 10.1007/s00382-011-1124-z.

Munk, W., and C. Wunsch, 1998: Abyssal recipes II: energetics of tidal and wind mixing. *Deep-Sea Res. I*, 45:1977-2010.

Nansen, F., 1906: Northern waters. Videnskabs-Selskabets Skrifter, I. Matematisk-Naturvidenskabelig Klasse, 3, 145 pp.

Nansen, F., 1912: Das Bodenwasser und die Abkuhlung des Meeres. Internationale Revue der Gesamten Hydrobiologie und Hydrographie, 5(1), 1-42.

Nurser, A. J. G., R. Marsh, and R. Williams, 1999: Diagnosing water mass formation from air-sea fluxes and surface mixing. *J. Phys. Oceanogr.*, 29:1468-1487.

Olsen, S. M., B. Hansen, D. Quadfasel, and S. Østerhus, 2008: Observed and modeled stability of overflow across the Greenland-Scotland ridge. *Nature*, 455:519-522, doi: 10.1038/nature07302.

Orvik, K. A., and Ø. Skagseth, 2003: The impact of the wind stress curl in the North Atlantic on the Atlantic inflow to the Norwegian Sea toward the Arctic. *Geophys. Res. Lett.*, 30(17), 1884, doi: 10.1029/2003GL017932, 2003.

Østerhus, S., W. R. Turrell, S. Jónsson, B. Hansen, 2005: Measured volume, heat and salt fluxes from the Atlantic to the Arctic Mediterranean. *Geophys. Res. Lett.*, 32:L07603. doi: 10.1029/2004GL022188.

Otterå, O. H., M. Bentsen, I. Bethke, and N. G. Kvamstø, 2009: Simulated pre-industrial climate in Bergen Climate Model (version 2): model description and large-scale circulation features. *Geosci. Mod. Dev.*, 2:197-212.

Otterå, O. H., H. Drange, M. Bentsen, N. G. Kvamstø, and D. Jiang, 2004: Transient response of the Atlantic Meridional Overturning Circulation to enhanced freshwater input to the Nordic Seas-Arctic Ocean in the Bergen Climate Model. *Tellus*, 56A: 342-361.

Pérez-Brunius, P., T. Rossby, and D. R. Watts, 2004: Transformation of the warm waters of the North Atlantic from a geostrophic streamfunction perspective. *J. Phys. Oceanogr.*, 34:2238-2256.

Pickart, R. S., M. A. Spall, M. H. Ribergaard, G. W. K. Moore, and R. F. Milliff, 2003: Deep convection in the Irminger Sea forced by the Greenland tip jet. *Nature*, 424:152-156.

Rahmstorf, S., 2002: Ocean circulation and climate during the past 120,000 years, *Nature*, 419:207-214.

Randall, D. A., and Coauthors, 2007: Climate Models and Their Evaluation. In: Climate Change 2007: The Physical Science Basis. Contribution of Working Group I to the Fourth Assessment Report of the Intergovernmental Panel on Climate Change [Solomon, S., D. Qin, M. Manning, Z. Chen, M. Marquis, K. B. Averyt, M. Tignor, and H. L. Miller (eds.)]. Cambridge University Press, Cambridge, United Kingdom and New York, NY, USA.

Rhein, M., 1991: Ventilation rates of the Greenland and Norwegian Seas derived from distributions of the chlorofluoromethanes F11 and F12. *Deep-Sea Res.*, 38: 485-503.

Rhein, M., and Coauthors, 2011: Deep water formation, the subpolar gyre, and the meridional overturning circulation in the subpolar North Atlantic. *Deep-Sea Res. II*, doi: 10.1016/j.dsr2.2010.10.061.

Rhines, P., S. Häkkinen, and S. A. Josey, 2008: Is oceanic heat transport significant in the climate system? In Arctic-Subarctic Ocean Fluxes: Defining the role of the Northern Seas in Climate, Dickson, B., Meincke, J., and Rhines, P., editors, 87-109. Springer Verlag.

Rudels, B., 1995. The thermohaline circulation in the Arctic Ocean and in the Greenland Sea. *Philos. Trans. R. Soc. Lond.*, A352:287-299.

Rudels, B., 2010: Constraints on exchanges in the Arctic Mediterranean - do they exist and can they be of use? *Tellus*, 62A, 109-122.

Rudels, B., H. J. Friedrich, and D. Quadfasel, 1999: The Arctic Circumpolar Boundary Current. *Deep-Sea Res. II*, 46:1023-1062.

Rudels, B., G. Björk, J. Nilsson, P. Winsor, I. Lake, C. Nohr, 2005: The interaction between waters from the Arctic Ocean and the Nordic Seas north of Fram Strait and along the East Greenland Current: results from the Arctic Ocean-02 Oden expedition. *J. Marine Syst.*, 55:1-30.

Sandström, J. W., 1908: Dynamische Versuche mit Meerwasser, *Ann. Hydrogr. Mar. Meteorol.*, 36:6-23.

Sarafanov, A., A. Falina, A. Sokov, and A. Demidov, 2008: Intense warming and salinification of intermediate waters of southern origin in the eastern subpolar North Atlantic in the 1990s to mid-2000s. *J. Geophys. Res.*, 113, C12022, doi: 10.1029/2008JC004975.

Servonnat, J., P. Yiou, M. Khodri, D. Swingedouw, and S. Denvil, 2010: Influence of solar variability, CO2 and orbital forcing during the last millennium in the IPSLCM4 model. *Climate of the Past*, 6:445-460.

Schlosser, P., G. Bönisch, M. Rhein, R. Bayer, 1991: Reduction of deepwater formation in the Greenland Sea during the 1980s: Evidence from tracer data. *Science*, 251:1054-1056.

Schmitz, W. J. Jr., 1995: On the interbasin-scale thermohaline circulation. *Rev. Geophys.*, 33:151-173.

Schmitz, W. J. Jr., and M. S. McCartney, 1993: On the North Atlantic circulation. *Rev. Geophys.*, 31(1):29-49.

Schott, F. A., R. Zantopp, L. Stramma, M. Dengler, J. Fischer, and M. Wibaux, 2004: Circulation and deep-water export at the western exit of the subpolar North Atlantic. *J. Phys. Oceanogr.*, 34:817-843.

Segtnan, O. H. A., T. Furevik, and A. D. Jenkins, 2011: Heat and freshwater budgets of the Nordic Seas computed from atmospheric reanalysis and ocean observations. *J. Geophys. Res.*, doi:10.1029/2011JC006939, in press.

Simonsen, K., P. M. Haugan, 1996: Heat budgets of the Arctic Mediterranean and sea surface heat flux parameterizations for the Nordic Seas. *J. Geophys. Res.*, 101(C3):6553-6576.

Smethie W. M., and R. A. Fine, 2001: Rates of North Atlantic Deep Water formation calculated from chlorofluorocarbon inventories. *Deep-Sea Res. I*, 48:189-215, doi: 10.1016/S0967-0637(00)00048-0.

Spall, M. A., and R. S. Pickart, 2001: Where does dense water sink? A subpolar gyre example. *J. Phys. Oceanogr.*, 31:810-826.

Speer, K., 1997: A note on average cross-isopycnal mixing in the North Atlantic Ocean. *Deep-Sea Res. I*, 44:1981-1990.

Speer, K., and E. Tziperman, 1992: Rates of water mass formation in the North Atlantic Ocean. *J. Phys. Oceanogr.*, 22:93-104.

Speer, K., S. R. Rintoul, B. Sloyan, 2000: The diabatic Deacon cell. *J. Phys. Oceanogr.*, 30:3212-3222.

Sproson, D. A. J., I. A. Renfrew, and K. J. Heywood, 2010: A parameterization of Greenland's tip jets suitable for ocean or coupled climate models. *J. Geophys. Res.*, 115, C08022, doi: 10.1029/2009JC006002.

Stommel, H., 1979: Determination of water mass properties of water pumped down from the Ekman layer to the geostrophic flow below. *Proc. Natl. Acad. Sci.*, U.S.A., 76:3051-55.

Stouffer, R. J., and Coauthors, 2006: Investigating the causes of the response of the thermohaline circulation to past and future climate changes. *J. Clim.*, 19:1365-1387.

Straneo, F., 2006: On the connection between dense water formation, overturning, and poleward heat transport in a convective basin. *J. Phys. Oceanogr.*, 36:1822-1840.

Sutherland, D. A., and R. S. Pickart, 2008: The East Greenland Coastal Current: Structure, variability, and forcing. *Prog. Oceanogr.*, 78:58-77.

Sutton, R. T., and D. L. R. Hodson, 2005: Atlantic Ocean forcing of North American and European summer climate. *Science*, 309(5731):115-118.

Talley, L. D., 1999: Mode waters in the subpolar North Atlantic in historical data and during the WOCE period, *WOCE Newsl.*, 37:3-6.

Talley, L. D., 2008: Freshwater transport estimates and the global overturning circulation: Shallow, deep and throughflow components. *Prog. Oceanogr.*, 78:257-303,
doi: 10.1016/j.pocean.2008.05.001.

Thompson, D. W. J., and J. M. Wallace, 1998: The Arctic Oscillation signature in the wintertime geopotential height an temperature fields. *Geophys. Res. Lett.*, 25(9):1297-1300.

Tomczak, M., 1999: Some historical, theoretical and applied aspects of quantitative water mass analysis. *J. Mar. Res.*, 57:275-303.

Tomczak, M., 2000: An Introduction to online physical oceanography. *Oceanography*, 13:104-105.

Trenberth, K. E., and J. M. Caron, 2001: Estimates of meridional atmosphere and ocean heat transports. *J. Clim.*, 14:3433-3443.

van Aken, H. M., F. de Jong, I. Yashayaev, 2011: Decadal and multi-decadal variability of Labrador Sea Water in the north-western North Atlantic Ocean derived from tracer distributions: Heat budget, ventilation, and advection. *Deep-Sea Res. I*, 58:505-523, doi: 10.1016/j.dsr.2011.02.008.

Vellinga, M., and R. A. Wood, 2002: Global climatic impacts of a collapse of the Atlantic thermohaline circulation. *Climatic Change*, 54:251-267.

Visbeck, M., E. Chassignet, R. Curry, T. Delworth, B. Dickson, and G. Krahmann, 2003: The Ocean's Response to North Atlantic Oscillation Variability. In The North Atlantic Oscillation, J. W. Hurrell, Y. Kushnir, G. Ottersen, and M. Visbeck (Eds), Geophysical Monograph Series, 134, 113-146.

Våge K., R. S. Pickart, M. A. Spall, H. Valdimarsson, S. Jónsson, D. J. Torres, S. Østerhus, and T. Eldevik, 2011: Significant role of the North Icelandic Jet in the formation of Denmark Strait Overflow Water. *Nat. Geosci.*, doi: 10.1038/NGEO1234.

Walin, G., 1982: On the relation between sea-surface heat flow and thermal circulation in the ocean. *Tellus*, 34:187-195.

Wallace, J. M., and D. S. Gutzler, 1981: Teleconnections in the Geophysical Height Field during Northern Hemisphere winter. *Mon. Wea. Rev.*, 109:784-812.

Warren, B. A., 1981: Deep circulation of the World Ocean. In Evolution of Physical Oceanography, MIT Press, 6-41.

Willebrand, J., and Coauthors, 2001: Circulation characteristics in three eddy-permitting models of the North Atlantic. *Prog. Oceanogr.*, 48:123-161.

Woollings, T., A. Hannachi, and B. Hoskins, 2010: Variability of the North Atlantic eddy-driven jet stream. *Q. J. R. Meteorol. Soc.*, 136:856-868.

Worthington, L. V., 1981: The water masses of the world ocean: some results of a fine-scale census. In Evolution of Physical Oceanography, MIT Press, 42-69.

Wunsch, C., 2002: What is the thermohaline circulation? *Science*, 298:1180-1181.

Xu X., W. J. Jr. Schmitz, H. E. Hurlburt, P. J. Hogan, E. P. Chassignet, 2010: Transport of Nordic Seas overflow water into and within the Irminger Sea: an eddy-resolving simulation and observations. *J. Geophys. Res.*, 115, C12048. doi: 10.1029/2010JC006351.

Yashayaev, I., 2007a: Hydrographic changes in the Labrador Sea, 1960-2005. *Prog. Oceanogr.*, 73:242-276, doi: 10.1016/j.pocean.2007.04.015.

Yashayaev, I., 2007b: Changing freshwater content: insights from the subpolar North Atlantic and new oceanographic challenges. *Prog. Oceanogr.*, 73:203-209.

Zhang, R., 2010: Latitudinal dependence of Atlantic meridional overturning circulation (AMOC) variations. *Geophys. Res. Lett.*, 37, L16703, doi: 10.1029/2010GL044474.

Chapter 3

Paper I. Water mass transformation and the North Atlantic Current in three multi-century climate model simulations

Water mass transformation and the North Atlantic Current in three multi-century climate model simulations

Helene R. Langehaug[1,2]*, Peter B. Rhines*[3]*, Tor Eldevik*[2,4]*, Juliette Mignot*[5]*, and Katja Lohmann*[6]

[1]*Nansen Environmental and Remote Sensing Center, Bergen, Norway.*
[2]*Bjerknes Centre for Climate Research, Bergen, Norway.*
[3]*School of Oceanography, University of Washington, Seattle, Washington, USA*
[4]*Geophysical Institute, University of Bergen, Bergen, Norway*
[5]*LOCEAN, Institute Pierre Simon Laplace, University Pierre and Marie Curie, Paris, France*
[6]*Max Planck Institute for Meteorology, Hamburg, Germany*

Abstract

The warm and saline Subtropical Water carried by the North Atlantic Current undergoes substantial transformation on its way to higher latitudes as heat is released from ocean to atmosphere. The geographical distribution of the surface-forced water mass transformation is assessed in multi-century climate simulations in three different climate models, with a particular focus on the eastern subpolar North Atlantic Ocean. The models of the study are BCM, IPSLCM4, and MPI-M ESM. The diagnosis, originally introduced by Walin (1982), estimates the transformation in water mass outcrop areas from heat and freshwater fluxes. The integrated heat flux in the eastern subpolar region has a larger contribution than the freshwater flux to the water mass transformation in all three models. While the pattern of the Atlantic Meridional Overturning Ciculation (AMOC) is similar in all models, the fluxes are very different. The different pathways of the North Atlantic Current, and upper ocean low salinity water, as well as sea ice cover have strong influence on the water mass transformation. The water mass transformation in the eastern subpolar region shows pronounced variability on decadal time scale in all models, and is found to reflect the variability in the overturning circulation in two of the models with a time lag of 7-8 years.

Keywords: Water mass transformation, Subpolar Mode Water, North Atlantic Current, climate model intercomparison, decadal ocean variability.

1. Introduction

The Subtropical Water is cooled and freshened on its way northward, thereby releasing large amounts of heat to the atmosphere in the northern North Atlantic. This heat loss contributes to the relative warm European climate, both in the mean and seasonally (Rahmstorf 2002; Rhines et al. 2008). It is therefore of crucial importance to simulate the *water mass transformation* (hereafter denoted WMT) in the North Atlantic Ocean properly in climate models.

The warm and saline Subtropical Water carried by the North Atlantic Current undergoes substantial transformation in properties on its way northward from intense air-sea exchanges (Fig. 3.1; Pérez-Brunius et al. 2004; Brambilla et al. 2008). Areas of large WMT are associated with deep mixed layers and formation of Subpolar Mode Water, which is the dominant water mass above the permanent pycnocline in the northeastern North Atlantic Ocean (Fig. 3.2; McCartney and Talley, 1982; Brambilla and Talley, 2008). The Subpolar Mode Water is carried downstream from its formation region in the northeastern North Atlantic Ocean, splitting into recirculation in the western subpolar region and poleward flow into the Nordic Seas. The relative fraction of these two main branches of the North Atlantic Current is important in determining the water mass composition of the dense return flow in the North Atlantic Ocean; the Deep Western Boundary Current (Smethie and Fine 2001; Lumpkin and Speer 2003; Medhaug et al. 2011). The dense southward flow and its pathway have been very much studied (e.g., Dengler et al. 2006; Bower et al. 2009; Rhein et al. 2011).

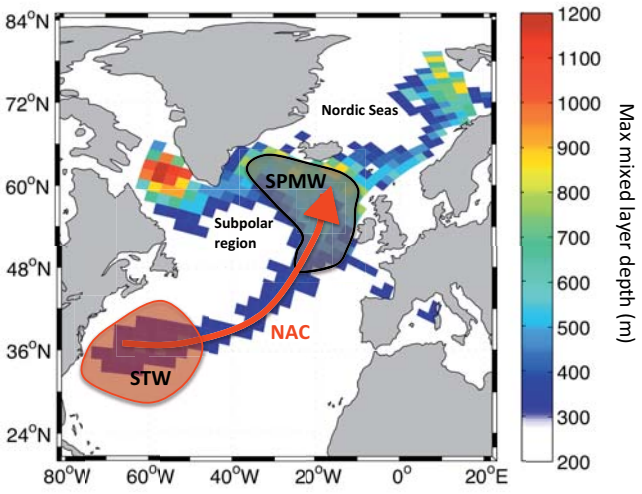

Figure 3.1: Schematics of the transformation of Subtropical Water (STW) to Subpolar Mode Water (SPMW) along the pathway of the North Atlantic Current (NAC). The mixed layer depth is deepest in March (obtained from the Bergen Climate Model).

The first objective of the present study is to investigate the magnitude and geographical distribution of the WMT in the eastern subpolar region in three different multi-century climate model simulations. The location and the typical densities of water masses involved in this WMT can be very model-dependent. Particularly the pathway of the models' North Atlantic Current defines regions of strong WMT associated with heat loss. The continuation of the North Atlantic Current into the western subpolar region and Nordic Seas, and the subsequent dense water formation and returning southward flow, have been investigated in several model studies (e.g., Mauritzen and Häkkinen 1999; Bailey et al. 2005; Medhaug et al. 2011; Langehaug et al., in revision).

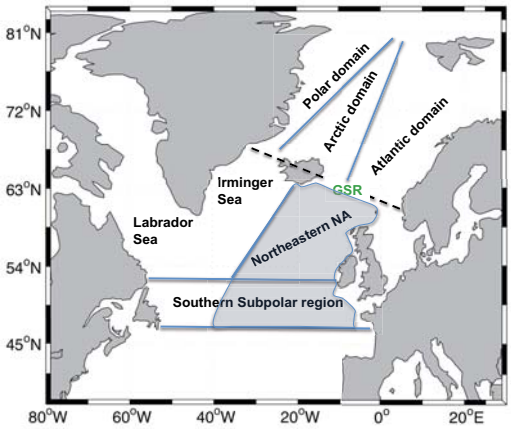

Figure 3.2: Map of the Subpolar North Atlantic (NA) and the Nordic Seas with names of geographical regions that are referred to in the text. The eastern subpolar region is indicated by the blue shaded area, and the rest as the western subpolar region. The Nordic Seas is divided into three domains after Swift (1986). The location of the Greenland-Scotland Ridge (GSR) is indicated with the dashed black line.

The North Atlantic Current forms the upper branch of the Atlantic Meridional Overturning Circulation (AMOC). The AMOC is the streamfunction of the meridional circulation in the Atlantic Ocean, with northward flow aloft and southward flow at depth (Manabe and Stouffer 1988). The variability in strength of this circulation has been investigated in a range of numerical studies, due to its climate relevance in the North Atlantic region (Bentsen et al. 2004; Jungclaus et al. 2005). The AMOC is traditionally quantified in latitude-depth space (hereafter denoted AMOCz). In the present study, where we analyze WMT, the AMOC in latitude-density space (hereafter denoted AMOCσ) is more appropriate. AMOCσ shows the density distribution associated with the overturning circulation (Mauritzen and Häkkinen 1999; Bailey et al. 2005). Particularly in the subpolar region, AMOCσ differs greatly from AMOCz, due to strong zonal density gradients (Willebrandt et al. 2001; Zhang 2010). The second objective of this study is to investigate the decadal relationship between WMT in the eastern subpolar region and AMOCσ.

In order to improve the understanding of the variability in the large-scale ocean circulation, several studies have investigated the relation between the WMT and the AMOC at high northern latitudes (Marsh 2000; Isachsen et al. 2007; Grist et al. 2009; Josey et al. 2009). Josey et al. (2009) found that the WMT due to air-sea exchanges has a significant relationship with the strength of AMOC at latitudes between 35°N and 65°N. The other source for WMT is interior mixing. Mixing plays an important role in the WMT of the Nordic Seas overflow as it descends the Greenland-Scotland Ridge and in the subsequent rising of deep water masses in the tropics (Munk and Wunsch 1998). Without interior mixing, the world ocean would gradually be filled with denser water. There are also mixing processes in the upper ocean related to the seasonal cycle of the mixed layer depth and lateral mixing of density within the mixed layer (Nurser et al. 1999).

In this study we consider the WMT due to surface forcing only; a main focus is the WMT associated with the North Atlantic Current in the upper ocean. Previous studies have shown that WMT at high northern latitudes is dominated by air-sea exchanges (Nurser et al. 1999; Tandon and Zhao 2004). Similar results were found in an observation-based study by Lumpkin and Speer (2003), who investigated WMT in the North Atlantic Ocean. However, they point out that the air-sea exchanges dominate *south* of the overflow region, i.e., south of the southern flank of the Greenland-Scotland Ridge. Pérez-Brunius et al. (2004) distinguish between the WMT of Subtropical Water in the western and eastern subpolar region, and found that water entering the Labrador Sea is mainly transformed by mixing between Subtropical Water and fresh and cold subpolar waters. In the eastern subpolar region, the focus region in this study, they found that the main factors in transforming Subtropical Water are air-sea exchanges and the entrainment of saline water from the northeastern subtropical gyre. The latter is not explicitly investigated in this study. However, the entrainment of saline water influences the surface density, and thus implicitly contribute to the WMT assessed herein.

The paper is organized as follows. The three climate models and the methods used are presented in Section 2. In Section 3, the long-term mean horizontal and vertical circulation in the North Atlantic Ocean are compared among the three different models. The models' long-term mean heat- and freshwater fluxes are compared with observation-based estimates. The geographical distribution of the WMT is estimated for each model, and compared with observation-based estimates in Section 4. The decadal variability of WMT in the eastern subpolar region is also estimated and related to the strength of AMOCσ. A summary and concluding remarks follows in Section 5.

2. Data and Method

2.1 Model descriptions

The control simulations from three different climate models are compared in the present study: the Bergen Climate Model (BCM; Furevik et al. 2003; Otterå et al. 2009), the Institute Pierre Simon Laplace Coupled Model (IPSLCM4; Marti et al. 2010; Servonnat et al. 2010), and the Max Planck Institute for Meteorology Earth System Model (MPI-M ESM; Jungclaus et al. 2010). We use multi-century simulations from the EU project THOR (Thermohaline Overturning - at Risk?), where we investigate the first 500 years after the spin-up phase of each integration. All models are run without any form of flux adjustments and are thus free to evolve following their own climates.

BCM has an atmosphere model that is run with a truncation at wave number 63 (T_L63) with 31 vertical levels. The ocean model is MICOM (Miami Isopycnic Coordinate Ocean Model; Bleck et al. 1992), and has a stack of 34 isopycnic layers in the vertical. The potential densities range from σ_2=1031.514 to σ_2=1037.800 kg m^{-3}, and a non-isopycnic surface mixed layer on top provides the linkage between the atmospheric forcing and the ocean interior. The ocean grid is almost regular with a horizontal grid spacing of approximately 2.4° x 2.4° in the North Atlantic, i.e., a resolution ranging from 150 to 200 km. The data is taken from a 700-year control integration based on pre-industrial climate and has previously been used in several climate studies (Otterå et al. 2009; Medhaug et al. 2011).

IPSLCM4 has an atmosphere model with the horizontal resolution 3.75° x 2.535° (lon x lat) and 19 vertical levels. The ocean model is OPA8 (Océan PArallélisé; Madec et al. 1997). The ocean grid has 31 vertical depth levels with 2° nominal horizontal resolution in the North Atlantic, i.e., a resolution ranging from 100 to 200 km. Note that the resolution is enhanced in the tropics and the northern North Atlantic. The data is taken from a 1000-year control integration based on pre-industrial climate and has been used in several climate studies (Servonnat et al. 2010; Gastineau and Frankignoul 2011). Note that as a result of excessive freshwater flux in the Labrador Sea, deep convection in this model only takes place in the Nordic Seas and south of Iceland (Marti et al. 2010).

MPI-M ESM has an atmosphere model that is run with T31 resolution with 19 vertical levels. The ocean model is Max Planck Institute Ocean Model (MPI-OM; Marsland et al., 2003) and has 40 vertical depth levels. The ocean grid has 40 vertical depth levels with 3° x 3° horizontal resolution. Due to the location of the grid's North Pole over Greenland, the horizontal resolution in the North Atlantic ranges from 50 to 200 km. The data is taken from a 3000-year long control integration based on pre-industrial climate (Jungclaus et al. 2010).

The freshwater fluxes for the three models are implemented in different ways: The freshwater flux (F_{flx}) for BCM is calculated from the virtual salt flux (VS_{flx}) and salinity (S) as $F_{flx} = -VS_{flx}/(SC)$, where C is the constant 1*10^{-3} g kg^{-1} to convert to the units of kg

m^{-2} s^{-1}. The virtual salt flux includes all freshwater sources: evaporation (E), precipitation (P), and contributions from river runoff (R) and sea ice melting/freezing. The freshwater flux for IPSLCM4 also includes all sources, and the free surface formulation of Roullet and Madec (2000) is applied in this model. MPI-M ESM uses a semi-implicit free surface scheme (Marsland et al. 2003). For the MPI-M ESM integration presented in this study, the surface fresh water flux output contains only the atmospheric part (i.e., P-E+R). The salt flux into the ocean due to sea ice melting and freezing is taken into account during the model integration, but cannot be diagnosed afterwards, since the freezing and melting of sea ice is implemented in the ocean component of the model (no external sea ice model is used for MPI-M ESM; personnel communication Helmuth Haak). The fresh water flux from MPI-M ESM is provided in units of m s^{-1}, and to convert this flux to the units of kg m^{-2} s^{-1} it has been multiplied by the density of fresh water (1000 kg m^{-3}).

2.2 Observation-based surface fluxes

The heat- and freshwater fluxes from the models are compared with observation-based data. We have used heat flux from the National Oceanography Centre, Southampton datasets (NOC1.1a; Grist and Josey 2003; Josey et al. 1999). This dataset is based on ship data from the period 1980 to 1993, and the ocean heat budget is closed to -5 W m^{-2} using inverse analysis. The data set is distributed as a monthly climatology. Note that the NOC1 climatology was previously referred to as the Southampton Oceanography Centre (SOC) flux climatology. The observation-based freshwater flux is obtained from NCEP atmospheric reanalysis (Kalnay et al. 1996). The NCEP reanalysis is using numerical models to perform data assimilation with past data from 1948 to the present. The annual mean freshwater flux is calculated from precipitation, evaporation, and water runoff on monthly time scale for the period 1948-2010. It is important to note that these observation-based surface fluxes can contain large uncertainties. This is particularly the case for freshwater flux from NCEP. In this study we only use the long-term annual mean of the observation-based heat- and freshwater fluxes.

2.3 Water mass transformation diagnosed from surface buoyancy fluxes

The estimation of the WMT is done following the method that was introduced by Walin (1982) and further developed by Speer and Tziperman (1992). The approach is based on the fact that surface heat and freshwater fluxes modify the temperature and salinity at the ocean's surface and thereby convert water from one density class to another - assuming the temperature and salinity changes are not density-compensated. Walin (1982) and Speer and Tziperman (1992) showed that the WMT of surface waters in an outcrop region due to air-sea exchanges is equivalent to the volume transport across the outcropping isopycnal. In this study we only consider the surface-forced WMT. This means that density changes due to cooling/heating of the ocean surface, evaporation, precipitation, and contributions from river runoff and ice melting/freezing are taken into account. Density changes due to interior mixing between different water masses

are neglected. The model data applied in this analysis are monthly mean fields, while AMOCz and AMOCσ are calculated from annual means.

The surface density flux D (kg m^{-2} s^{-1}) is the key factor in the calculation of the WMT. The density flux is computed from the buoyancy flux B (kg m^{-1} s^{-3}), which includes surface heat flux Q (W m^{-2}) and freshwater flux F_{flx} (kg m^{-2} s^{-1}) into the ocean, as well as surface salinity S (dimensionless). The density flux has one thermal (F_T) and one haline (F_S) component:

$$D = B/g = F_T + F_S \tag{3.1}$$

$$F_T = \alpha c_w^{-1} Q \tag{3.2}$$

$$F_S = -\beta S F_{flx} \tag{3.3}$$

where c_w is specific heat of water (3996 J kg^{-1} K^{-1}), g is gravitational acceleration (9.81 m s^{-2}), and α and β is the thermal expansion coefficient and haline contraction coefficient, respectively. We have here used the UNESCO formulas (McDougall 1987) to calculate α and β.

The complete water mass transformation G can be expressed as the sum of the surface-forced water mass transformation F and the derivative of the diffusive density flux D_{diff} across a given σ-isopycnal (Garrett et al. 1995; Nurser et al. 1999). The annual mean F is equal to a volume transport across the given isopycnal (i.e., diapycnal transport), and is found by integrating the surface density flux over the outcrop region for surface densities between σ and $\sigma + \Delta\sigma$ (Fig. 3.3a; Speer and Tziperman 1992):

$$G(\sigma) = F(\sigma) - \frac{\partial D_{diff}(\sigma)}{\partial \sigma} \tag{3.4}$$

$$F(\sigma) = \frac{1}{T}\int_0^T (\lim_{\Delta\sigma \to 0} \frac{1}{\Delta\sigma}\int_\sigma^{\sigma+\Delta\sigma} D dA) dt \tag{3.5}$$

where A is the area of the outcrop region and T is one year. The annual mean F is given in units of Sv (1 Sv = 10^6 m^3 s-1). In this study D_{diff} is neglected and G becomes F (Eq. 4).

In practice, to obtain geographical maps of the annual mean WMT across a given σ-isopycnal from monthly means we calculate for each grid cell the surface density flux between σ and $\sigma + \Delta\sigma$ and average over one year:

$$F_i(\sigma) = \frac{1}{N_T \Delta\sigma}\sum_{n=1}^{12} D_{n,i} dA_i, n = 1, 2, 3...12 \tag{3.6}$$

where N_T is the 12 months. Note that this F is not exact the same as the F in Equation (3.5). The F in the latter is the integrated F over the outcrop region, whereas the F in Equation (3.6) is the F in one grid cell (denoted with the index i).

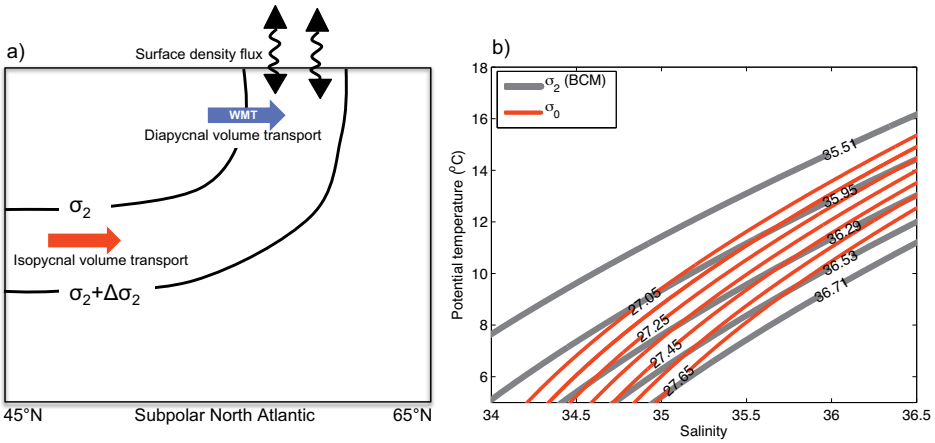

Figure 3.3: a) Schematics to describe surface-forced water mass transformation (WMT). WMT of surface water from one density class to another class due to surface density fluxes is equivalent to diapycnal volume transport (adapted from Brambilla et al. 2008). b) The typical density range of Subpolar Mode Water from observational studies is shown in red curves (in σ_0), and the density range used to capture the models' Subpolar Mode Water is illustrated by grey curves (in σ_2).

Based on previous studies the WMT from monthly data tend to overestimate the actual WMT (Tandon and Zhao 2004; Cerovecki and Marshall 2008). Eddies in the upper ocean and mixing associated with deepening of the mixed layer have been shown to contribute to the WMT with an opposite effect than the surface forcing (Tandon and Zhao 2004; Cerovecki and Marshall 2008). In this study we use climate models that are non-eddy resolving. This means that higher temporal resolution of the model data, if they were available, would not better resolve the eddy-induced bias of the WMT estimation.

Another aspect of the calculation of the WMT is the outcrop region. The summer outcrop for a given density can be located far away from the winter outcrop for the same density. For instance, cold melt water in the vicinity of the Arctic sea ice edge during summer could have similar densities as Subpolar Mode Water during winter. This means that when integrating the WMT over a year and a specific region, the water masses with the same density do not necessarily communicate with each other over a year. This will however not be an issue in the geographical distribution of the annual mean WMT.

We have used density with reference pressure of 2000 dbar (σ_2), for consistency with the vertical coordinate of the ocean model in BCM. The WMT is calculated for σ_2-densities in the

interval 34.95-36.85 kg m^{-3}. These densities correspond to the isopycnals that outcrop in the eastern subpolar region. The σ_2-densities are compared with the typical observed density range of Subpolar Mode Water in Fig. 3.3b (Brambilla and Talley 2008; Brambilla et al. 2008). $\Delta\sigma$ in Equation (3.6) is the density difference between the σ_2-densities investigated here (in kg m^{-3}), illustrated by the density difference between the grey lines in Fig. 3.3b.

To estimate the amount of new water masses that are produced due surface-forced WMT, the surface-forced formation must be calculated. The surface-forced formation is the difference in WMT across two neighboring density layers. If there is convergence, water will subduct in the densest layer of the two, i.e., accumulation of water in the densest layer, and vice versa in case of divergence, i.e., removal of water in the densest layer. Hence, this surface-forced formation expresses changes in the isopycnal transport (Fig. 3.3a). If there is no difference in the WMT across the two neighboring density layers, there is no formation of new water masses and no change in the isopycnal transport. The AMOCσ is the actual isopycnal transport derived from the models, integrated zonally and in density space. The surface-forced formation in the subpolar region is therefore compared with changes in the isopycnal transport within the subpolar region obtained from the AMOCσ in section 3.4.

2.4 Statistical methods

To filter out high-frequency variability, all time series have been low-pass filtered using an 11-year running Bartlett window. The time series are linearly detrended prior to correlation/regression analysis. For significance testing a Student's *t*-test is used together with the method of Chelton (1983) to estimate the effective number of degrees of freedom. All correlations given in the text are significant above the 95% confidence level.

3. Model climatologies in the northern North Atlantic

In this section the annual mean surface density with the barotropic streamfunction is first presented for the different models. Then sources to changes in the surface density, namely heat- and freshwater fluxes, are presented and compared with observation-based estimates. The thermal (F_T) and haline (F_S) components are calculated to compare the relative contributions of the heat- and freshwater fluxes to the surface density flux within each model. The thermal component (i.e., heat flux) dominates the haline component in the eastern subpolar region in all models. Finally, the annual mean meridional overturning streamfunction in both latitude-depth space and latitude-density space are compared among the models.

The surface density for the different models is shown in Fig. 3.4. All models have high densities in the subpolar region and in the Nordic Seas, with the densest water surfacing in the latter. The lowest densities are found in the North Sea and along the western rim of the North Atlantic, i.e., in the area of Baffin Bay, Davis Strait and Hudson Strait. These low densities

are particularly evident in IPSLCM4 and MPI-M ESM (Fig. 3.4). The annual mean barotropic streamfunction is placed on top of the surface density (contours in Fig. 3.4). The models' Subpolar Gyre and Subtropical Gyre are illustrated by their cyclonic (negative) and anti-cyclonic (positive) circulations, respectively. To emphasize the position of the North Atlantic Current, the contours at the interface between the Subpolar Gyre and the Subtropical Gyre are marked with thicker lines than the other contours. In BCM and IPSLCM4 the North Atlantic Current has a similar northeastward pathway, but the strength of the circulation is weaker in IPSLCM4 than in BCM. In MPI-M ESM the North Atlantic Current has a more zonal direction, crossing the North Atlantic Basin before flowing northward along the eastern rim of the North Atlantic Basin. There are substantial differences among the models' Subpolar Gyre shape and intensity. In all three cases, nevertheless, the North Atlantic Current crosses the North Atlantic Basin too far south compared to observational estimates (Krauss 1986; Pérez-Brunius et al. 2004).

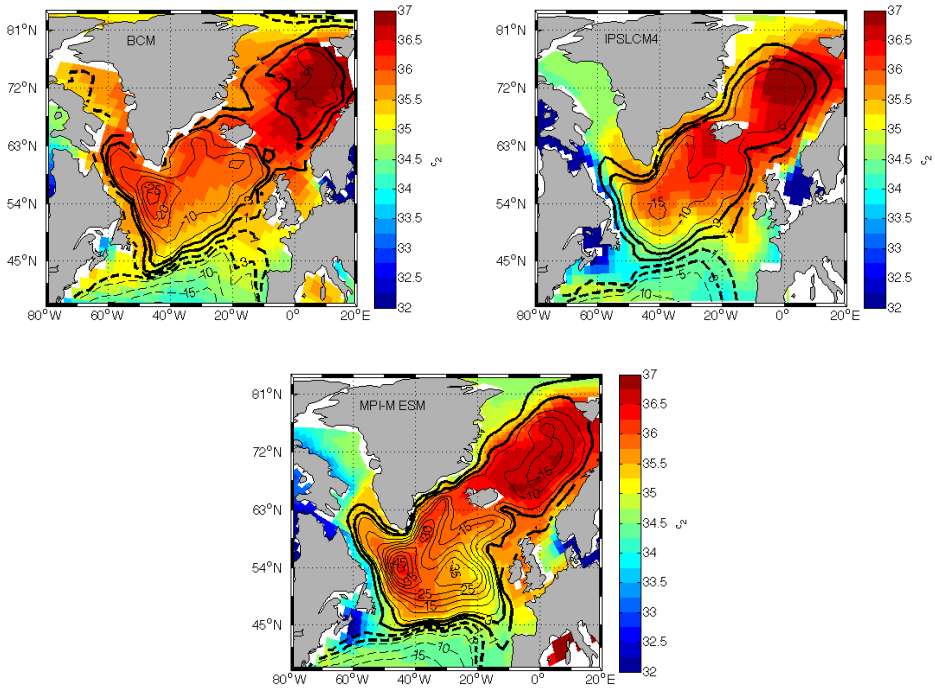

Figure 3.4: Surface density (in σ_2) for all models. Model names are indicated in the upper left corner of the figures. The barotropic streamfunction is shown in black contours (numbers are given in Sv), where negative (positive) streamfunction indicate the Subpolar (Subtropical) Gyre. Thin contours are shown with intervals of 5 Sv. Thick contours are shown for ± 1 Sv and ± 3 Sv, to emphasize the position of the North Atlantic Current at the border between the Subpolar and Subtropical gyres.

3.1 Thermal and haline contribution to the annual mean density flux

Two features dominate the comparison between the heat- and freshwater fluxes from the models and the observation-based estimates (Fig. 3.5). The first feature is the positive heat flux in NOC1.1a along the pathway of the North Atlantic Current and in the Labrador Sea. This is relatively well reproduced in BCM, except that the pathway of the North Atlantic Current is shifted eastward compared to NOC1.1a. On the contrary, in the two other models there is weak heat loss in the southern subpolar region. The reason for the weak heat loss in IPSLCM4 is that the North Atlantic Current subducts beneath the unrealistic fresh surface layer in this region (Mignot and Frankignoul 2010). In IPSLCM4 and MPI-M ESM the long-term mean heat loss is positive mainly in the vicinity of the Greenland-Scotland Ridge and in the eastern part of the Nordic Seas. The second feature is the excessive freshwater input close to Newfoundland in IPSLCM4 and MPI-M ESM compared to NCEP and BCM. The source for this excessive freshwater input points both to stronger precipitation and weaker evaporation compared to NCEP. Possible explanation for these model differences is discussed in the following comparison of the thermal and haline components, that is the heat and freshwater fluxes expressed in terms of buoyancy, and comparison of the sea ice extents.

The thermal and haline contribution to the annual mean density flux determine the magnitude of the WMT (Equation 3.1 and 3.5). We therefore compare the haline and thermal contributions to the density flux, to better understand differences in the WMT at northern high latitudes among the models (Fig. 3.6). Positive values of the thermal contribution mean that heat is lost from the ocean to the atmosphere, thereby contributing to denser surface water. Negative values of the haline contribution mean freshwater input to the ocean, as a result of net precipitation, river runoff, or sea ice melting. Overall the northward flowing water becomes denser as a result of buoyancy forcing, although changes in the haline and thermal contribution can regionally produce lighter surface water. Geographically, the haline contribution dominates or is comparable to the thermal contribution in the westernmost half of the Nordic Seas (the Polar/Arctic domain in Fig. 3.2), while the thermal contribution dominates in the eastern part of the Nordic Seas (the Atlantic domain in Fig. 3.2). In the eastern subpolar region the thermal contribution dominates the surface density flux, except in IPSLCM4 where the thermal and haline contribution are comparable (Table 3.1). In the western subpolar region the three model simulations differ: In BCM the thermal contribution dominates, in IPSLCM4 the haline contribution dominates, and in MPI-M ESM the two are of comparable size (Table 3.1).

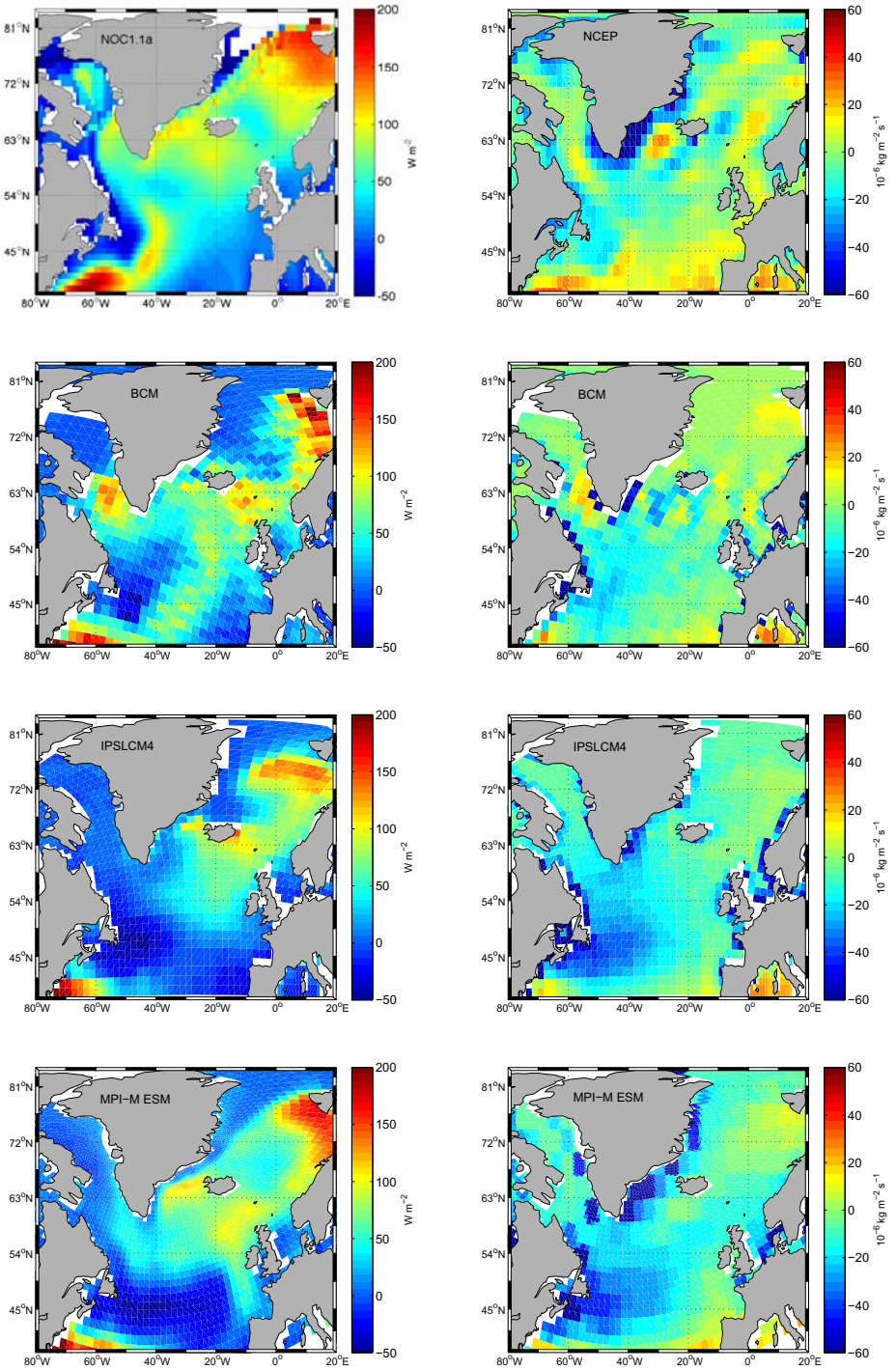

Figure 3.5: The annual mean net heat loss from ocean (left; W m^{-2}) and net freshwater loss from ocean (right; quantified as virtual salt flux, kg m^{-2} s^{-1}) from the different models and observation-based estimates (upper panel). The freshwater flux is calculated from: Precipitation - Evaporation + Runoff. Model names and source for observational based data are indicated in the upper left corner of the figures.

The haline contribution in the Nordic Seas has a similar structure in BCM and IPSLCM4, with a broad band of negative density flux in the Polar/Arctic domain. This haline contribution is located between the maximum and minimum sea ice extent in September throughout the 500 years of each simulation (Fig. 3.6), suggesting that the haline contribution is dominated by sea ice melting. Similar haline contribution in the Nordic Seas is not evident in MPI-M ESM. This is most likely related to absent contribution from ice melting/freezing in the freshwater field from MPI-M ESM. In the western subpolar region, the haline parts in both MPI-M ESM and IPSLCM4 contribute to a negative density flux covering a broad region. The maximum and minimum sea ice extent in March is illustrated in grey contours in Fig. 3.6. Both in IPSLCM4 and MPI-M ESM the sea ice extent in March can reach south of Newfoundland and eastward to about 40°W. In BCM the sea ice extent in March is only reaching the northern part of the Labrador Sea.

The excessive sea ice extent in the Labrador Sea in IPSLCM4 and MPI-M ESM, compared to observations (Johannessen et al. 2004), could be related to the pathway of the North Atlantic Current. In IPSLCM4 the barotropic circulation is generally weaker than in the other two models (Fig. 3.4), and in the western subpolar region the heat flux is weak (Fig. 3.5). The distance between the Labrador Sea and the pathway of the North Atlantic Current in MPI-M ESM is larger than in the other two models (Fig. 3.4), and the heat loss is weak in the Labrador Sea (Fig. 3.5). Both IPSLCM4 and MPI-M-ESM have been found to have a cold bias in the western subpolar region (Jungclaus et al. 2006; Marti et al. 2010). Weak advection of heat and salt into the Labrador Sea accommodates an extensive sea ice cover in this region. In addition, fresher water requires less cooling to form sea ice. The excessive sea ice extent in the Labrador Sea can also be related to the anomalous positive net precipitation close to Newfoundland in IPSLCM4 and MPI-M ESM relative to NCEP (Fig. 3.5). The weaker evaporation close to Newfoundland is most likely linked to absence of the North Atlantic Current at surface in this region.

Regarding the thermal contribution to the mean density flux, the structure and magnitude in BCM are quite different from those of the other two models. This is particularly the case in the southern subpolar region and in the Labrador Sea, where BCM has a strong positive density flux (Fig. 3.6). These model differences are related to the differing pathway of the North Atlantic Current and the excessive freshwater input close to Newfoundland in IPSLCM4 and MPI-M ESM, as discussed above. In IPSLCM4 and MPI-M ESM there are low values of the thermal contribution in the southeastern part of the subpolar region, whereas there is a negative thermal contribution close to Newfoundland, where water becomes more buoyant. The latter is the model representation of the warming of the Labrador Current in summer time. There is also a similar contribution in the BCM in the summer months (not shown), but the annual mean is nevertheless slightly positive. Generally, the thermal contribution in BCM is larger than that in IPSLCM4 and MPI-M ESM (Table 3.1). All models agree on a dominant thermal contribution in the vicinity of the Greenland-Scotland Ridge and in the northeastern Nordic Seas.

One standard deviation of interannual variability of the thermal and haline component is calculated, to give an estimate of the magnitude of temporal variations (Fig. 3.6). The thermal contribution has largest variability along the pathway of the models' North Atlantic Current. In BCM there is also large variability in the Labrador Sea, while variability is low in this region in the other two models. In BCM the thermal variability in the Atlantic domain of the Nordic Seas (Fig. 3.2) is of similar magnitude to the variable heat loss associated with the North Atlantic Current. This is also the case for MPI-M ESM in the northern Atlantic domain. In BCM and IPSLCM4 the haline contribution has largest variability in the Irminger Sea/Denmark Strait and the Polar/Arctic domain of the Nordic Seas. The haline contribution has low variability in MPI-M ESM.

Table 3.1

Mean thermal (F_T) and haline (F_S) contribution (in 10^{-6} kg m^{-2} s^{-1}) to the surface density flux in the Nordic Seas (63-79°N, 40°W-20°E) and the eastern (E) and western (W) subpolar region (47-63°N, 60°W-10°E). The eastern and western region is separated at 35°W. Note that ice melting/freezing is not taken into account in the F_S for MPI-M ESM.

	BCM		**IPSLCM4**		**MPI-M ESM**	
Region	F_T	F_S	F_T	F_S	F_T	F_S
E subpolar	2.72	-0.35	1.25	-0.47	2.22	-0.41
W subpolar	1.18	-0.55	-0.02	-1.00	0.72	-0.77
Nordic Seas	2.20	-0.59	1.13	-1.07	1.50	-0.86

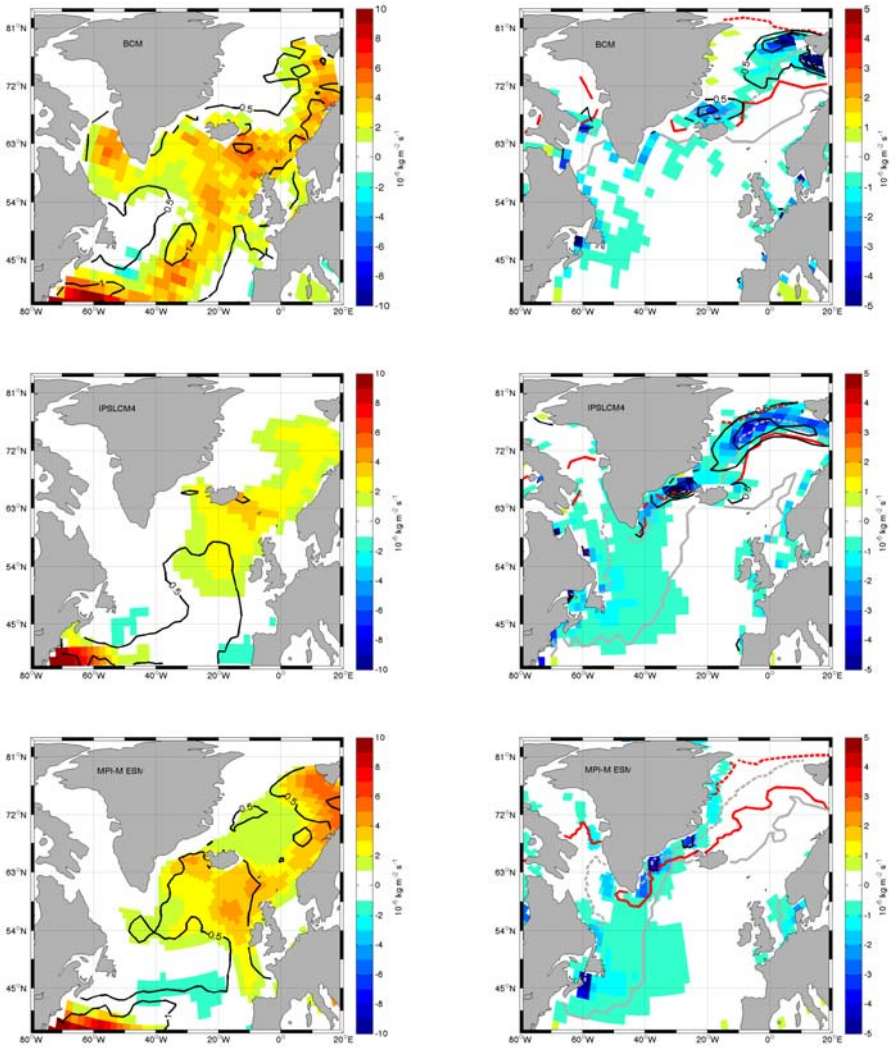

Figure 3.6: The thermal (left; F_T) and haline (right; F_S) contribution to the annual mean density flux into the ocean for the different models, given in 10^{-6}*kg m^{-2} s^{-1}. Positive values indicate densification. Model names are indicated in the upper left corner of the figures. Note the different scales on the colorbars between F_T and F_S, and that ice melting/freezing is not taken into account in the F_S for MPI-M ESM. One standard deviation of the interannual variability of F_T and F_S are shown by black contours with intervals of 0.5. The red solid (dashed) lines indicate maximum (minimum) sea ice extent in September. Likewise for the grey lines, but for March.

3.2 AMOCz versus AMOCσ

The strength and structure of the overturning circulation in latitude-depth space, i.e., AMOCz is shown in Fig. 3.7 (left panel). The BCM and MPI-M ESM have comparable maximum value of the AMOCz (17.9 Sv and 15.2 Sv, respectively, at 35.5°N), while the maximum value for IPSLCM4 is about half of that (9.6 Sv at 44°N). The maximum values of the AMOCz are located at 1000 m, 1020 m, and 1406 m in BCM, MPI-M ESM, and IPSLCM4 respectively.

To emphasize the gradual densification of the Subtropical Water, AMOCσ (Fig. 3.7, right panel) is presented for the same region as AMOCz. The density bins chosen for the computation of AMOCσ in IPSLCM4 and MPI-M ESM are consistent with the isopycnal discretization of the ocean model in BCM. The WMT from lighter to denser water masses of the poleward flowing water is evident in all models considered here, although their strengths and pattern differ. The WMT in BCM occurs over a broad density range compared to that in IPSLCM4 and MPI-M ESM. North of 50°N, the isolines of the overturning streamfunction incline from low to high densities in the density range of Subpolar Mode Water. The density of the surface flow increases also south of 50°N in BCM, whereas there is less densification (i.e., less sloping) in IPSLCM4 and MPI-M ESM in this region.

Assessing the overturning circulation in latitude-density space captures the densification with the essentially horizontal Subpolar Gyre circulation (Fig. 3.4). This leads to a stronger AMOCσ than AMOCz in the subpolar region, and in general an overturning circulation cell that extends further north. The maximum value of AMOCσ is still much lower for IPSLCM4 (9.4 Sv at 53°N) than in the two other models (18.3 Sv at 58°N and 51°N for BCM and MPI-M ESM, respectively). The maximum AMOCσ is located in a slightly less dense layer for MPI-M ESM (σ_2=36.29) compared to that of the two other models (σ_2=36.71).

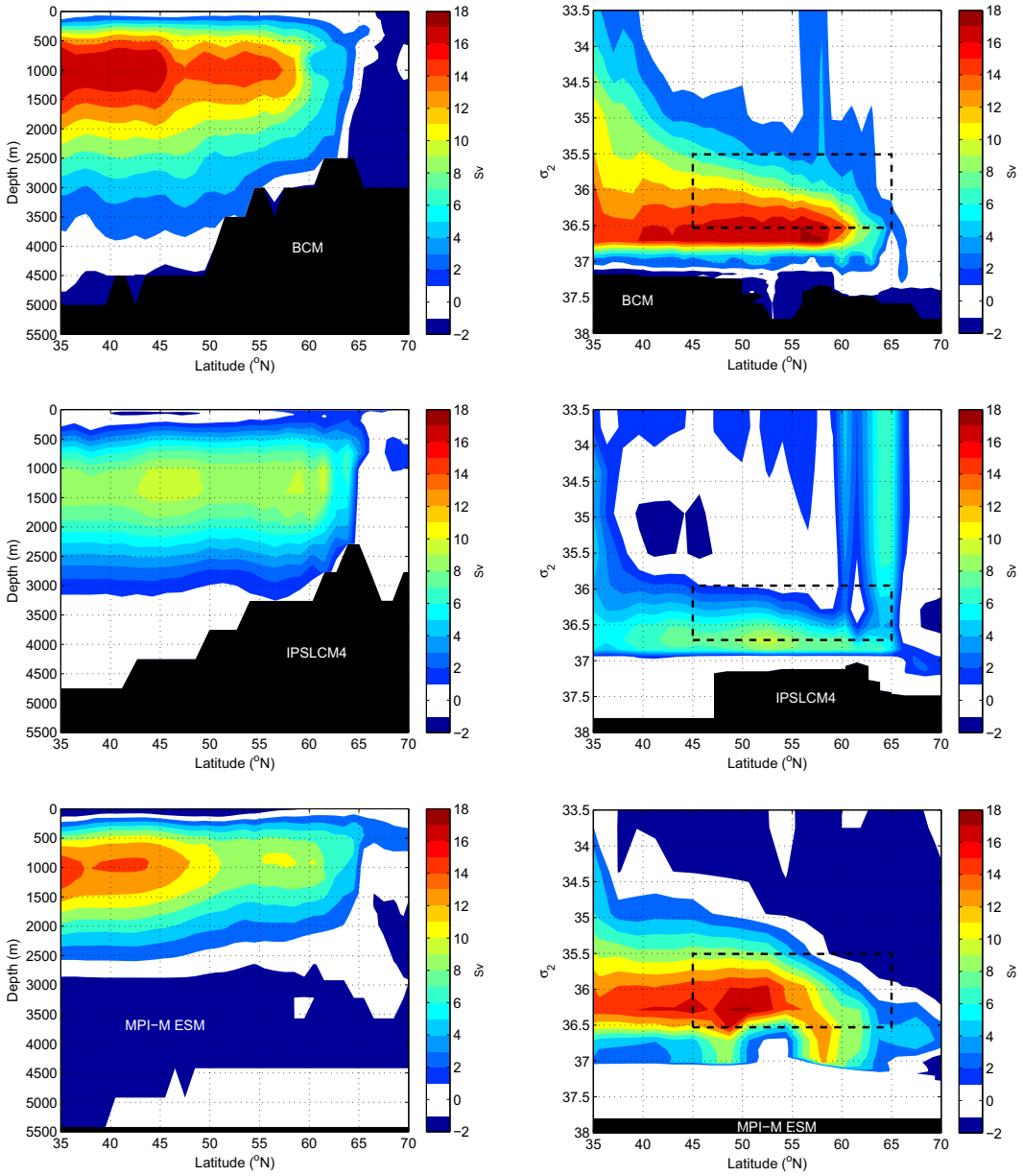

Figure 3.7: Meridional overturning streamfunction in latitude-depth space (AMOCz; left) and latitude-density space (AMOCσ; right) for the different models. Model names are indicated in the figures. The dashed rectangles illustrate the approximate density range of the model's Subpolar Mode Water in the latitude band from 45°N to 65°N.

3.3 Surface-forced water mass transformation in the eastern subpolar North Atlantic

While AMOCσ quantifies zonally averaged WMT from the actual isopycnal transports, the approach of Walin (1982) estimates the geographical distribution of WMT from the surface density fluxes and hydrography in outcrop regions (Fig. 3.3a; cf. 2.3). The density range investigated for each model is defined by the isopycnals that outcrop in the eastern subpolar region (Fig. 3.3b).

Brambilla et al. (2008) have done an extensive observation-based analysis on the WMT of Subtropical Water and subsequent formation of Subpolar Mode Water in the northeastern North Atlantic (Fig. 3.8). We have applied the same methodology as Brambilla et al. (2008), and their observation-based WMT therefore provides a benchmark for assessing model performance in this particular region. The WMT of the models and the observation-based WMT are intercompared according to two criteria: WMT structure and density range. The magnitude of the WMT cannot be compared, since the horizontal resolution of the models and the observation-based data differs, but our focus is on WMT structure. To further look at the quantitative WMT of the models, the magnitude of the *integrated* WMT in the eastern subpolar region is compared at the end of this section.

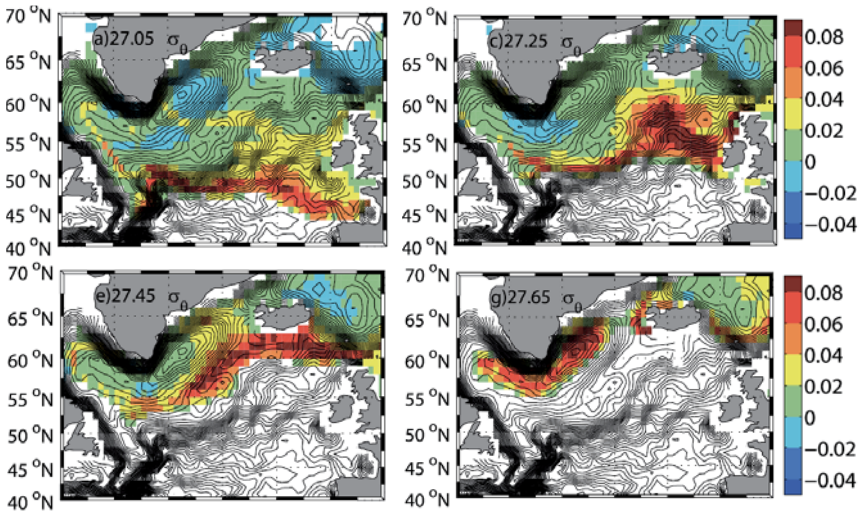

Figure 3.8: Observation-based annual mean surface forced water mass transformation (Sv) is shown in color. The corresponding density is noted in the figures. Positive values denote densification. Values are plotted on a regular 1° x 1° grid. The black lines are the surface flow streamlines. Figure 4 in Brambilla et al. (2008).

In BCM the structure of the WMT for four different densities (Fig. 3.9) are in qualitative agreement to those obtained from the observation-based study. Several branches of strong WMT with distinct densities are associated with different classes of Subpolar Mode Water. The BCM has strong WMT from Cape Cod and towards the northeastern North Atlantic. This is in accor-

dance with the observation-based WMT. However, the position of the North Atlantic Current differs between BCM and the observation-based estimates (Fig. 3.8; see also Krauss 1986; Pérez-Brunius et al. 2004), thereby giving somewhat different regions of strong WMT. The BCM is nevertheless more similar to the observation-based WMT in this aspect than the other two models. The North Atlantic Current is observed to curve around Newfoundland before it turns northeastward in the "Northwest Corner" (e.g., Arhan 1990). In BCM on the other hand, the North Atlantic Current turns northeastward already south of Newfoundland (cf. Fig. 3.4; see also Langehaug et al., in revision, for more details). In BCM, the WMT occurs for densities comparable to the observation-based WMT (Fig. 3.9), but for slightly lighter water masses. The densities of BCM's Subpolar Mode Water are captured by the four lightest densities shown in Fig. 3.3b, which is probably due to a warm bias of the ocean surface in the North Atlantic region compared to observations (Otterå et al. 2009).

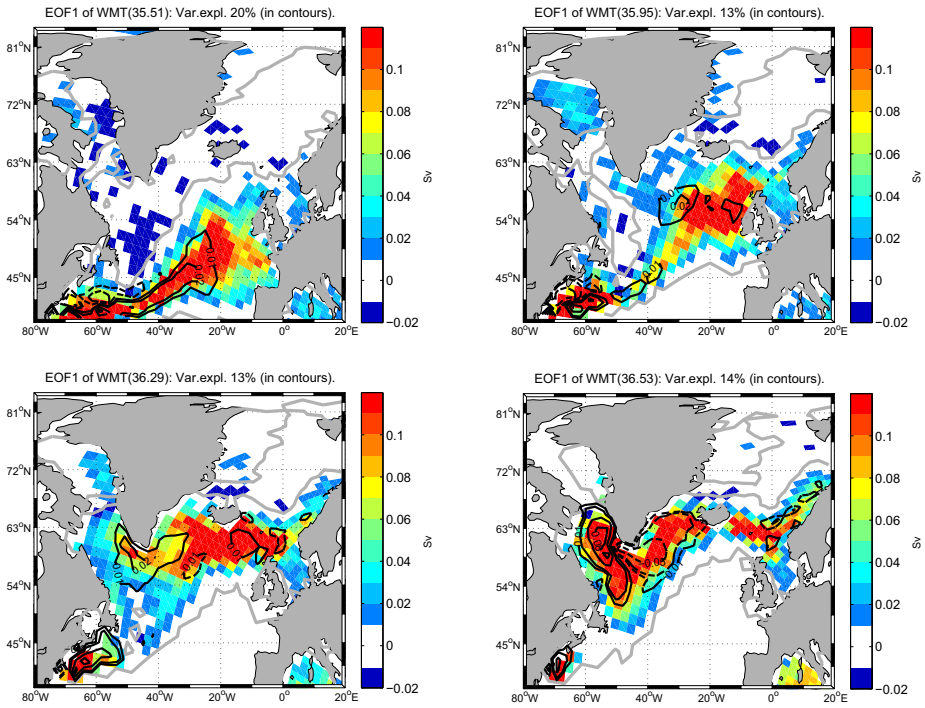

Figure 3.9: BCM's annual mean surface-forced water mass transformation (WMT) is shown in color. The corresponding σ_2-density is noted in the title of the figures. Positive values denote densification. The grey line indicate the zero line for the annual mean WMT. EOF1 of the WMT is shown in contours with intervals of 0.03 Sv, starting from $\pm$0.02 Sv. Contours for $\pm$0.01 Sv are also shown. Solid (dashed) lines indicate positive (negative) values. The variance explained by EOF1 of the total variability in the WMT is given in the title of the figures.

In IPSLCM4, the WMT shows a different structure than both BCM and the observation-based WMT (Fig. 3.10). IPSLCM4 shows strong WMT just south of Newfoundland, but between

this region and the northeastern North Atlantic the WMT is weak with values lower than 0.01 Sv. In the southern subpolar region the weak WMT could be due to the excessive amount of freshwater in this region mentioned above (see the negative surface density flux in Fig. 3.6), preventing outcropping of the same isopycnals that outcrop in the northeastern North Atlantic. In the vicinity of the Greenland-Scotland Ridge the structure of the WMT in IPSLCM4 is more similar to BCM and the observation-based WMT, where distinct densities are related to different branches of strong WMT. In IPSLCM4 the WMT occurs for densities comparable to the observation-based WMT, but for slightly denser water masses than in BCM. This might be due to a cold bias of the IPSLCM4 at middle to high latitudes (Marti et al. 2010).

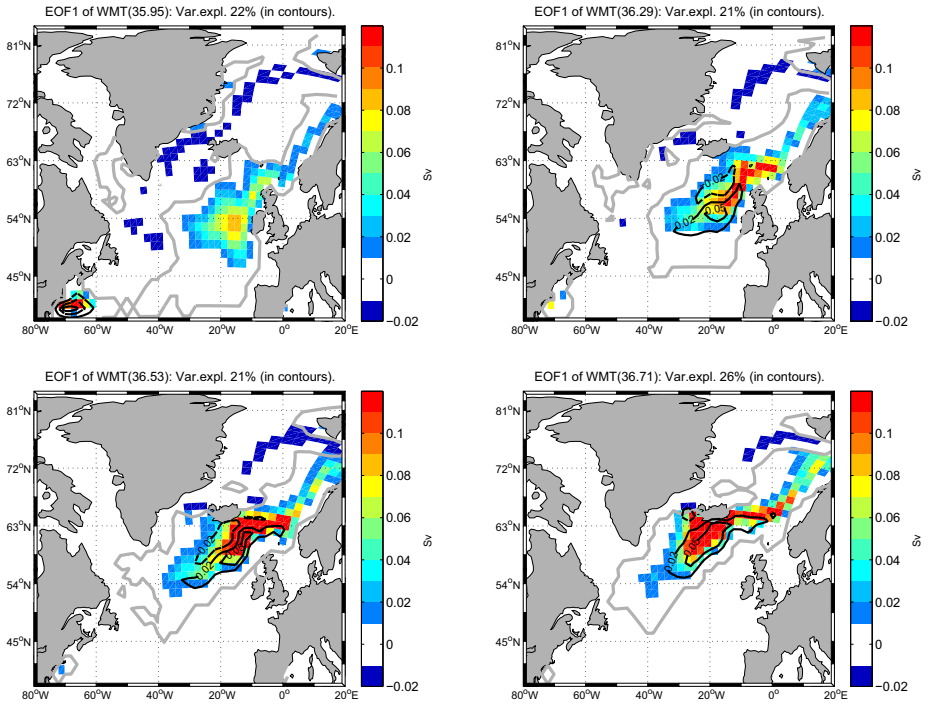

Figure 3.10: IPSLCM4's annual mean surface-forced water mass transformation (WMT) is shown in color. The corresponding σ_2-density is noted in the title of the figures. Positive values denote densification. The grey line indicate the zero line for the annual mean WMT. EOF1 of the WMT is shown in contours with intervals of 0.03 Sv, starting from $\pm$0.02 Sv. Solid (dashed) lines indicate positive (negative) values. The variance explained by EOF1 of the total variability in the WMT is given in the title of the figures.

The MPI-M ESM displays a different WMT structure than both the other two models and the observation-based estimate (Fig. 3.11). Here WMT mainly occurs along the eastern boundary of the North Atlantic Basin and the Nordic Seas. This is consistent with the very zonal North Atlantic Current in MPI-M ESM, crossing the entire basin before continuing north (Fig. 3.4). Similar to IPSLCM4, MPI-M ESM has strong WMT just south of Newfoundland and weak

WMT in the southern subpolar region. The WMT for the lightest density becomes negative east of Newfoundland (upper left panel in Fig. 3.11). This means that the surface water becomes less dense here, which is consistent with the negative contribution to the annual mean density flux both from the thermal and haline component in this region (Fig. 3.6). This is also the case in IPSLCM4 (upper left panel in Fig. 3.10). In MPI-M ESM the WMT occurs for the same densities as in BCM.

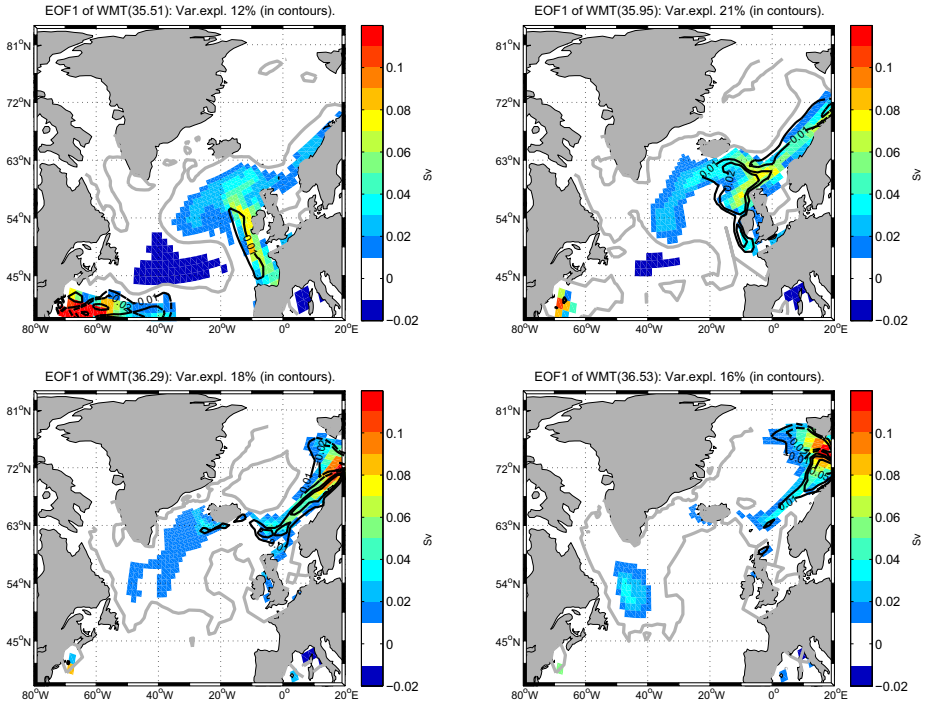

Figure 3.11: MPI-M ESM's annual mean surface-forced water mass transformation (WMT) is shown in color. The corresponding σ_2-density is noted in the title of the figures. Positive values denote densification. The grey line indicate the zero line for the annual mean WMT. EOF1 of the WMT is shown in contours with intervals of 0.03 Sv, starting from $\pm$0.02 Sv. Contours for $\pm$0.01 Sv are also shown. Solid (dashed) lines indicate positive (negative) values. The variance explained by EOF1 of the total variability in the WMT is given in the title of the figures.

To locate where most of the WMT occurs and to allow for quantitative comparison of the magnitude of the WMT among the models, the integrated WMT of the entire subpolar North Atlantic and the eastern subpolar region (48-62°N and east of 35°W) are shown for the whole density range (Fig. 3.12). For IPSLCM4 and MPI-M ESM, nearly all of the WMT in the subpolar region occurs in the eastern part, east of 35°W. This is also the case for BCM for $\sigma_2 \leq 35.95$, but the WMT in the western part contributes with a substantial amount of the denser WMT (cf. Fig. 3.9).

This graphic also shows that the integrated WMT in the subpolar region is generally stronger in BCM than in the other two models (Fig. 3.12). The maximum integrated WMT in the subpolar region in BCM (12.7 Sv) is 72% of the northward flow at the entrance to the subpolar region (Table 3.2). This means that the surface water in the subpolar region is not transformed at the same rate as the incoming transport of Subtropical Water. In IPSLCM4 and MPI-M ESM the fraction of transformed surface water in the subpolar region is even less, and is at maximum 57% and 40%, respectively, of the incoming transport of Subtropical Water (Table 3.2). However, the isopycnals that outcrop in the subpolar region also outcrop in neighboring seas, such as the Nordic Seas (see Fig. 3.9, 3.10, and 3.11). Hence, part of the "missing" transformation takes place in neighboring seas. Particularly MPI-M ESM has large WMT close to Svalbard.

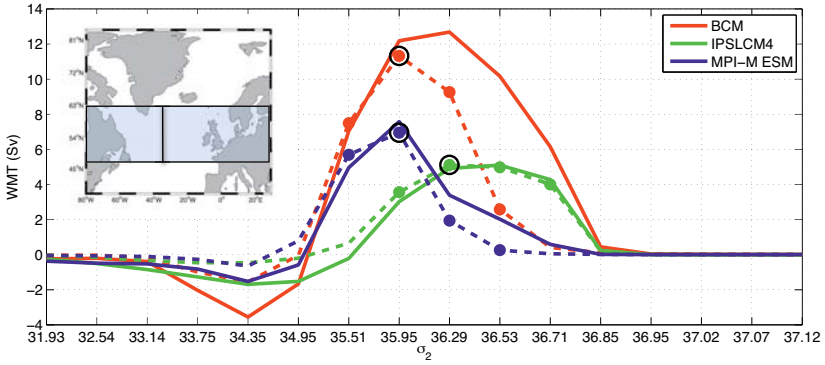

Figure 3.12: Annual mean surface-forced water mass transformation (WMT) as a function of density, integrated over the entire subpolar region (48°N-62°N as indicated in the inset; solid lines) and over the eastern subpolar region (east of 35°W; dashed lines). Filled circles indicate the integrated WMT for the densities shown in Fig. 3.9, 3.10, and 3.11. The density associated with the strongest WMT is indicated with a black circle, and the time series of this WMT is shown in Fig. 3.14 for the different models.

Table 3.2

Northward volume transport (in Sv) obtained from AMOCσ at the southern (48°N) and northern (60-64°N) boundary of the subpolar region.

	BCM	IPSLCM4	MPI-M ESM
Southern	17.6	8.9	18.9
Northern	9.9	6.8	8.7

3.4 Comparing isopycnal transport and surface-forced water mass formation

To investigate how the surface-forced WMT according to the approach of Walin (1982) represents the actual WMT in the models, we compare the estimated surface-forced formation (cf. Section 2.3) and isopycnal transports obtained from AMOCσ (Fig. 3.7, right panel). The surface-forced formation is calculated for all isopycnals that outcrop in the region between 48°-62°N. The surface-forced forced formation has a similar structure in all models, i.e., removal of water with lighter densities and accumulation of water with denser densities (Fig. 3.13). The difference in the isopycnal transport between the northern (48°N) and southern (62°N) boundary of the subpolar region corresponds well with the estimated surface-forced formation in IPSLCM4 and MPI-M ESM, but less well for BCM (Fig. 3.13).

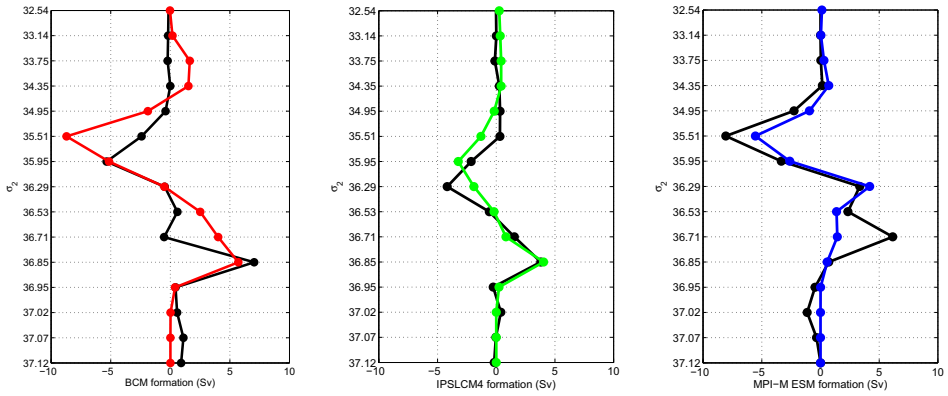

Figure 3.13: Annual mean surface-forced water mass *formation* integrated over the subpolar region (colored lines; derivatives with respect to density of the solid curves in Fig. 3.12). The region is indicated in the inset in Fig. 3.12. The net isopycnal volume transport through the subpolar region (black lines) is found by subtracting the transport profile in density bins at 48°N from the transport profile in density bins at 62°N.

One reason for the difference between the surface-forced formation and net isopycnal transport through the subpolar region in BCM is the model parameterization of deep convection: whenever the water column is unstable, such as for instance in the Labrador and Irminger seas, there is an instantaneous re-stratification of the water column and thickening of the denser layers (Medhaug et al. 2011). Due to this instantaneous re-stratification at each time step in the model simulation, there is no outcropping in our diagnosis associated with this process. This means that parts of the water that are accumulated in the isopycnal layers with densities σ_2 = 36.53 and σ_2 = 36.71 (red curve in Fig. 3.13) are in BCM placed in denser layers by deep convection (black curve in Fig. 3.13).

An additional contribution is mixing. It should therefore not be a perfect match between the surface-forced formation and the net isopycnal transport through the subpolar region. For in-

stance, the surface-forced formation in MPI-M ESM cannot explain the positive isopycnal flow with density σ_2 = 36.71 (black curve in Fig. 3.13). In BCM, the separate mixed layer makes the dynamics of the upper ocean in BCM different from the other two models. For instance, vertical mixing is implicit to the model formulation, for the model mixed layer to be vertical homogenous at all times (Eldevik 2002). Nurser et al. (1999) used an isopycnal model to investigate the contribution from mixing on the total WMT in the North Atlantic Ocean. Mixing was found to reduce the effect of the surface-forced WMT. In the upper layers of BCM the magnitude of the estimated surface-forced formation is larger than the net isopycnal transport through the subpolar region (Fig. 3.13). This may therefore be attributed to the fact that we have not included mixing as a source for WMT in our analysis.

4. Decadal variability

Several model studies have shown that decadal climate variations are linked to variations of AMOC (Eden and Willebrandt 2001; Bentsen et al. 2004; Deshayes and Frankignoul 2008). In this section, we thus investigate the variability of the WMT and its link with decadal variability of the AMOCσ.

4.1 Surface-forced water mass transformation in the eastern subpolar North Atlantic

The dominant patterns of WMT variability are included in Fig. 3.9, 3.10, and 3.11. In BCM the dominant Empirical Orthogonal Function (EOF) pattern for the two lighter densities show strongest variability along the pathway of the North Atlantic Current from Cape Hatteras to Ireland, whereas the dominant pattern for the two denser densities show strongest variability mainly in the Labrador and Irminger seas (Fig. 3.9). The densest density is associated with a dipole pattern with anomalous strong WMT in the Labrador Sea and anomalous weak WMT in the Irminger Sea. The leading mode and associated magnitude shown in Fig. 3.9 is generally less than the annual mean WMT. Since the annual mean WMT is mostly positive in the regions with pronounced variability, the northward flowing water becomes generally denser in these regions. The principal components of the dominant modes for three lighter densities are largely fluctuating in phase. On the other hand, the principal components for the lightest and densest density have significant, but low, positive correlation. This implies that the variability of WMT in the eastern subpolar region, associated with the inflow of Subtropical Water, differs from the variability of the WMT in the Labrador and Irminger seas (lower right panel in Fig. 3.9).

In IPSLCM4 the strongest WMT variability is mainly confined between Iceland and the British Isles, and extends into the Nordic Seas (Fig. 3.10). The leading mode and associated magnitude shown in Fig. 3.10 is generally less than the annual mean WMT similarly to BCM, reflecting that the northward flowing surface water becomes denser in the northeastern North Atlantic. The dominant modes for σ_2 = 36.29 and σ_2 = 36.53 constitute a zonal dipole pattern. The principal components of the dominant modes are largely fluctuating in phase, except for the principal component for the lightest density. This principal component has no significant correlation with

the other principal components, due to its relatively less variability in the northeastern North Atlantic (upper left panel in Fig. 3.10).

In MPI-M ESM the strongest WMT variability is found between Iceland and the British Isles and along the eastern rim of the Nordic Seas (Fig. 3.11). Similar to IPSLCM4, the variability of the WMT for the lightest density is low. The dominant modes for the two denser densities are characterized by a meridional dipole pattern; when there is anomalous strong WMT in the Norwegian Sea, there is anomalous weak WMT close to Svalbard (lower panels in Fig. 3.11). Similarly to the other two models, the leading mode and associated magnitude shown in Fig. 3.11 is generally less than the annual mean WMT. The principal components of the dominant modes have high lagged correlation, except for the principal component for the lightest density. For instance, the dominant mode with increased WMT (for σ_2 = 35.95) to the north of the British Isles leads the dominant mode with increased WMT (for σ_2 = 36.53) close to Svalbard with a time lag of about two years.

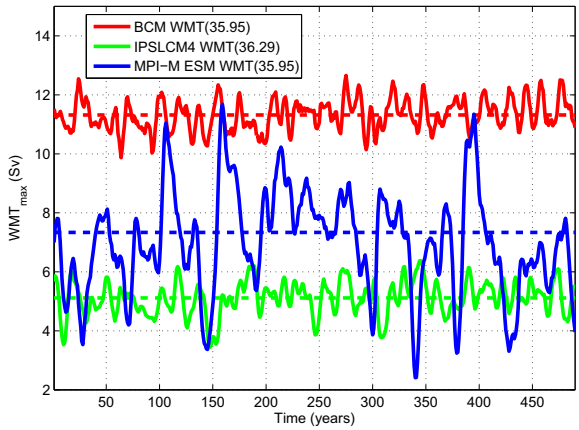

Figure 3.14: Surface-forced water mass transformation integrated over the eastern subpolar region (48^{o}N-62^{o}N, east of 35^{o}W, as indicated in the inset in Fig. 3.12) for the σ_2-densities indicated in the legend for the different models. These densities correspond to the maximum WMT for the different models (shown in Fig. 3.12). The time series are filtered using a 11-year low-pass filter. The dashed lines illustrate the mean integrated WMT for each model.

There is no common pattern in the variability of the WMT among the models, according to the EOF analysis above, except that the strongest variability is found in the regions with largest annual mean WMT. In Section 3.3 we demonstrated that the geographical distribution of the annual mean WMT differ among the models. However, all models agreed on positive WMT in the northeastern North Atlantic. In the following, the maximum WMT (WMTmax) in the eastern subpolar region (indicated by black circles in Fig. 3.12) is used to represent the decadal variability of the WMT associated with Subpolar Mode Water (Fig. 3.14). In IPSLCM4 and

MPI-M ESM the correlation is high between WMTmax and the principal components of the dominants mode shown in Fig. 3.10 and 3.11 (Table 3.3). In BCM the correlation is significant, but low. The dominants modes for IPSLCM4 and MPI-M ESM are mainly confined to the northeastern North Atlantic, whereas those for BCM cover a broader region. This partly explains the lower correlation in BCM.

Table 3.3

Peak correlations (r) within time lags of -5 and +5 years between the maximum WMT in the eastern subpolar region (WMT_{max}, shown in Fig. 15) and the first principal components (PC1) of the WMT across the different σ_2-isopycnals ($\sigma1$-$\sigma4$). WMT_{max} leads for positive lags. Time series are filtered using a 11-year low-pass filter.

	BCM WMT_{max}		**IPSLCM4** WMT_{max}		**MPI-M ESM** WMT_{max}	
	r	lag	r	lag	r	lag
PC1 of WMT($\sigma1$)	0.24	1	-	-	0.49	1
PC1 of WMT($\sigma2$)	0.31	1	0.83	2	0.97	1
PC1 of WMT($\sigma3$)	0.30	0	0.79	3	0.92	3
PC1 of WMT($\sigma4$)	0.44	-1	0.72	3	0.86	3

4.2 Relationship between AMOCσ and surface-forced water mass transformation variability in the eastern subpolar North Atlantic

The dominant patterns of AMOCσ variability for each model are shown in Fig. 3.15 (left panel). In BCM and MPI-M ESM the dominant mode shows mainly a strengthening of the southward flow in the dense layers and a slightly weakening of the mass flux in lighter layers. Unlike AMOCz, variability in AMOCσ can also be related to changes in thickness of the isopycnal layers. For instance, if the thickness of a dense layer increases, the thickness of lighter layers decreases. In other words, a reorganization of the water masses in the water column, which could be caused by deep convection. This reorganization does not necessary give a larger net southward volume flux. The dominant mode of AMOCσ indicates that there is strong variability in the dense layers, either due to changes in layer thickness, or a combination of changes in thickness and velocity. Therefore, there can be a strengthening of the deep flow without an immediate strengthening of the surface flow.

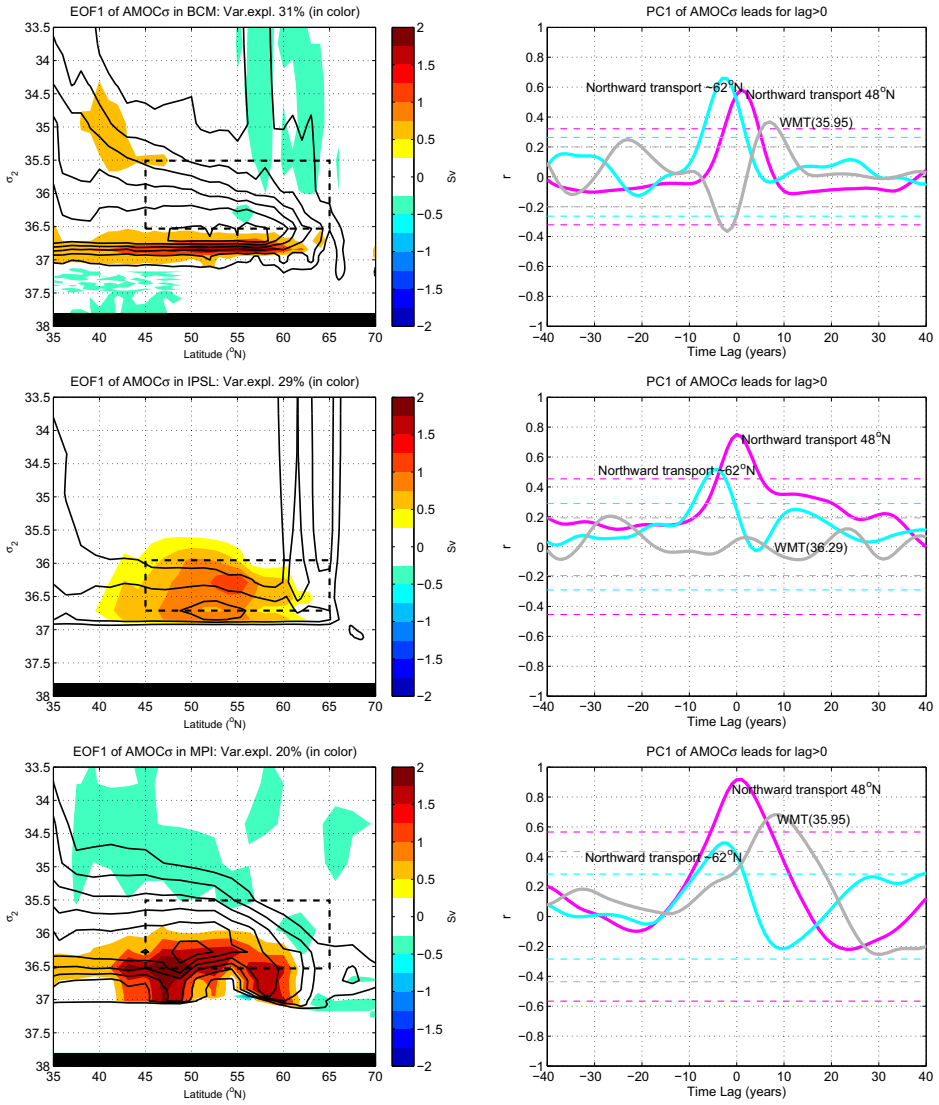

Figure 3.15: Left panel: EOF1 of AMOCσ is shown in color for the different models. Model names and the variance explained by EOF1 of the total variability in AMOCσ is indicated in the title of the figures. Mean AMOCσ is shown in contours with intervals of 3 Sv. The dashed rectangles illustrate the approximate density range of the model's Subpolar Mode Water in the latitude band from 45°N to 65°N. Right panel: Cross-correlation (r) between PC1 of AMOCσ and 1) net northward volume transport at 48°N, 2) mean net northward transport between 60-64°N, and 3) surface-forced water mass transformation (WMT) integrated over the eastern subpolar region for the σ_2-densities indicated in the figures. These densities correspond to the maximum WMT for the different models (shown in Fig. 3.12). PC1 of AMOCσ leads for positive time lags, as indicated in the title of the figures. The time series are filtered using a 11-year low-pass filter.

The northward flow at 48°N is found to increase one year after the southward flow in the dense layers strengthens (Table 3.4 and magenta curves in Fig. 3.15). Similar results have been shown by Grist et al. (2009), although in a somewhat different way. They investigated the total surface-forced WMT north of 48°N. Their WMT therefore includes the formation of the densest water masses in the Nordic Seas and Labrador and Irminger seas, and is thus possibly more related to the variability of the dense southward flow. This corresponds to our dominant mode of AMOCσ (Fig. 3.15). A main finding from Grist et al. (2009) is that increased formation of dense water masses at northern high latitudes leads to lagged increase in the northward flow at 48°N (i.e., an increase in the maximum AMOCz at 48°N). In IPSLCM4 the dominant mode shows a strengthening of the entire AMOCσ, where the northward flow at 48°N increases at zero time lag (Table 3.4 and Fig. 3.15).

Table 3.4

Peak correlations (r) and corresponding time lag (in years) between the first EOF of AMOCσ and the northward volume transport at the southern (48°N) and northern (60-64°N) boundary of the subpolar region, and the maximum WMT in the eastern subpolar region (WMT_{max}, shown in Fig. 15). AMOCσ leads for positive lags. Time series are filtered using a 11-year low-pass filter.

	BCM AMOCσ		**IPSLCM4** AMOCσ		**MPI-M ESM** AMOCσ	
	r	lag	r	lag	r	lag
Northern	0.66	-3	0.52	-4	0.49	-3
Southern	0.58	1	0.75	0	0.92	1
WMT_{max}	-0.37/0.37	-2/7	-	-	0.68	8

To investigate the decadal relationship between WMT associated with Subpolar Mode Water and AMOCσ, the WMTmax (shown in Fig. 3.14) has been correlated with the first principal component of AMOCσ. In BCM and MPI-M ESM the two have a significant correlation, where the WMTmax is found to lag AMOCσ (Table 3.4 and grey curves in Fig. 3.15). This means that 7-8 years after an increase in the southward flow of dense water masses in the North Atlantic Basin there is an increase in the WMT, and hence, the heat loss in the eastern subpolar region. Gastineau and Frankignoul (2011) used the same model simulations as presented in this study, among others, and found that an intensification of AMOCz was followed by low sea level pressure anomalies over the North Atlantic, with a time lag of 1-10 years. They found that this atmospheric response was caused by increased northward oceanic heat transport, resulting in increased heat release along the pathway of the North Atlantic Current. These results are consistent with the results from BCM and MPI-W ESM in this study.

In IPSLCM4 there is no significant correlation between the WMTmax and AMOCσ (Table 3.4 and Fig. 3.15), although the mechanism discussed above is also found in IPSLCM4 in the study by Gastineau and Frankignoul (2011). The reason is that the latter study focuses on a broader region, and therefore captures the increased heat loss in the subtropical region. In this study we only investigate changes in the eastern subpolar region, where there is no significant increase in the heat loss. This is consistent with Gastineau and Frankignoul (2011). The reason for this difference in IPSLCM4 compared to the other models could be related to the anomalously cold and fresh surface layer in the southern subpolar region (Fig. 3.5). The North Atlantic Current subducts beneath this layer, where its positive sea surface temperature anomalies could be eroded, before it enters the eastern subpolar region. In MPI-M ESM there is also a cold and fresh surface layer in the southern subpolar region (Fig. 3.5). However, the North Atlantic Current has a more zonal pathway in this model (Fig. 3.4), omitting the cold and fresh surface layer spreading eastward from Newfoundland.

If we move further north and investigate the relationship between the northward transport at 60-64°N and the first principal component of AMOCσ, a strengthening of the former is found to lead an increase in AMOCσ (Table 3.4 and blue curves in Fig. 3.15). The northward transport at 60-64°N represents mainly the inflow into the Nordic Seas. This suggests a key role for the light-to-dense water transformation in the Nordic Seas in the strengthening of the southward dense flow in the North Atlantic Basin. The northward transport both at 48°N and 60°-64°N is shown in Fig. 3.16. The variability of the northward transport at 60-64°N in MPI-M ESM (one standard deviation is 1.8 Sv) is about two times larger than for the other two models (0.5 Sv). The mean ratio of the northward transport at 60°-64°N to the northward transport at 48°N is 57%, 76%, and 47% for BMC, IPSLCM4, and MPI-M ESM, respectively. In BCM and MPI-M ESM, about half of the northward flow at 48°N re-circulate in the western subpolar region, while about a quarter re-circulates in IPSLCM4. The bifurcation of the North Atlantic Current continuing into the Nordic Seas and the Labrador Sea is an important factor in setting the regions of dense water formation, and hence the composition of the North Atlantic Deep Water. In IPSLCM4 there is WMT in the Nordic Seas but weak and slightly negative WMT in the Labrador Sea (Fig. 3.10), whereas in MPI-M ESM there is positive WMT in the vicinity of the Labrador and Irminger seas, although not as strong as in the Nordic Seas. In BCM there is WMT in both the Nordic Seas and the Labrador and Irminger seas, with particularly strong WMT in the Labrador Sea.

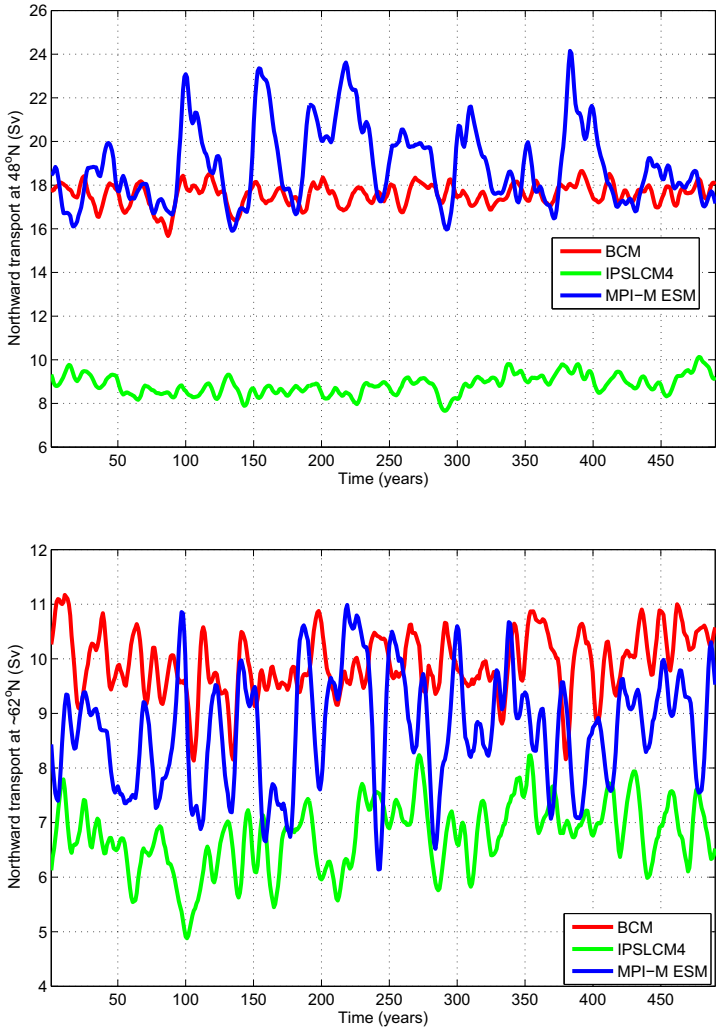

Figure 3.16: Northward transport at 48°N (upper) and 60-64°N (lower). The northward transports are the integrated positive volume transport in density space. The time series are filtered using a 11-year low-pass filter.

5. Summary and Concluding remarks

In this study we have analyzed three 500-year long climate model simulations of a pre-industrial climate. The focus has been on the mean state and decadal variability of the North Atlantic Current and WMT associated with Subpolar Mode Water. The model intercomparison reveals both similarities and differences in the geographical distribution of WMT. One similarity is that heat loss dominates WMT in the eastern subpolar region, considering both the mean state and variability (Fig. 3.6). The dominance of the thermal contribution over the haline contribution in the subpolar region is also found in a study using both a high- and coarse resolution ocean model forced with ERA15 reanalysis data (Gulev et al. 2007). In addition, all models show that the main part of the WMT in the subpolar region occurs in the eastern part (east of 35°W; Fig. 3.12).

Among the three models, the mean WMT in BCM is most comparable to the observation-based mean WMT (Fig. 3.8 and 3.9; Brambilla et al. 2008), since it appears to have the more realistic structure of the North Atlantic Current. The other two models differ from the observation-based WMT in the southern subpolar region and in the Labrador Sea (Fig. 3.10 and 3.11). In IPSLCM4 the barotropic circulation is weaker than in the two other models (Fig. 3.4), the North Atlantic Current subducts in the southern subpolar region, and a quarter of northward flow at 48°N is estimated to re-circulate in the western subpolar region. The pathway and strength of the North Atlantic Current in IPSLCM4 could be related to the excessive sea ice extent in the Labrador Sea (Fig. 3.6). In MPI-M ESM, the North Atlantic Current crosses the entire North Atlantic Basin before continuing north (Fig. 3.4). Even though about half of the model's northward flow at 48°N is estimated to re-circulate in the western subpolar region, the heat carried by the current is not sufficient to keep the sea ice from advancing south (Fig. 3.6). Hence, similarly to IPSLCM4, the excessive sea ice extent could be related to the pathway of the North Atlantic Current.

Since the WMT is weak in the southern subpolar region and the Labrador Sea in IPSLCM4 and MPI-M ESM, the magnitude of the integrated WMT in the subpolar region is larger in BCM than in the two other models. In addition, the magnitude of the WMT in the eastern subpolar region is large in BCM compared to the other two. This is both due to stronger heat loss and less freshwater input than in IPSLCM4 and MPI-M ESM in this region (Table 3.1). The magnitude of the spatially integrated WMT varies with respect to density in all models (Fig. 3.12). The maximum WMT in the eastern subpolar region for BCM, IPSLCM4, and MPI-M ESM is 11 Sv, 7 Sv, and 5 Sv, respectively.

An important result from this study is that the pathway of the North Atlantic Current, and hence the northern WMT, can be quite different between two models despite of a similar AMOCz. The structure of the AMOCz in BCM and MPI-M ESM are comparable, and they have a similar maximum strength of about 18 Sv (Fig. 3.7). However, the above discussion demonstrates that there are several important differences between these two models in the northern North Atlantic. It is thus necessary to apply additional analysis complimentary to the frequently used

AMOCz. One way of assessing the *zonally* averaged WMT is to use AMOCσ. For instance, the weak WMT in the southern subpolar region in IPSLCM4 and MPI-M ESM compared to BCM is also evident from comparing AMOCσ from the models (Fig. 3.7). The maximum AMOCσ for the different models are similar to the values obtained from AMOCz, although the maxima are shifted towards the subpolar region. On the other hand, AMOCσ does not provide information on the pathway of the North Atlantic Current. For instance, in IPSLCM4 the WMT is weak due to subduction of the North Atlantic Current, and hence, there is little heat loss in this region (Fig. 3.5). In MPI-M ESM the WMT is weak in the subpolar region due to a balance of buoyancy gain in the western part and buoyancy loss (heat loss) in the easternmost part (Fig. 3.6). Thus, the models appear to be similar, but are similar for the wrong reasons. It therefore seems important to investigate the geographical distribution of WMT. The method introduced by Walin (1982) provides a simple and useful way of assessing WMT in climate models. However, the most accurate description of WMT associated with the overturning circulation in climate models would be from two-dimensional fields of diapycnal mixing and diapycnal velocity for each isopycnal layer. Unfortunately, these fields are not available model output from the model simulations used herein.

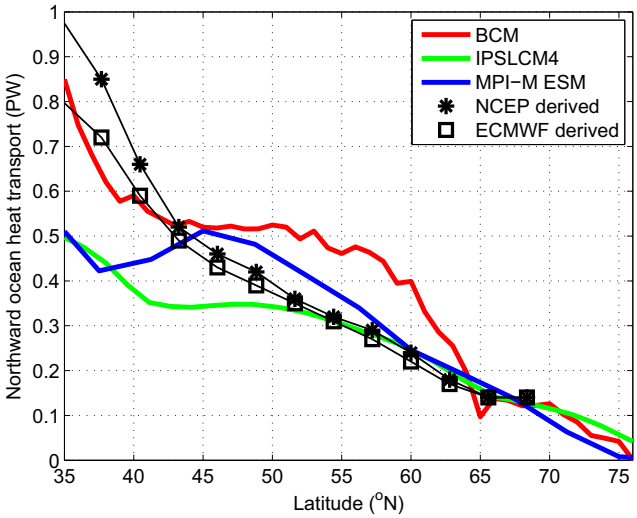

Figure 3.17: Net northward ocean heat transport in the subpolar North Atlantic for the three models. The black squares and stars denote the ocean heat transport based upon surface fluxes for 1985 to 1989 for NCEP and ECMWF reanalysis (Trenberth and Caron 2001).

WMT at northern high latitudes, particularly in the eastern subpolar region and the Nordic Seas, is highly related to ocean heat loss (Table 3.1). It is therefore useful to investigate the northward ocean heat transport in climate models, since divergence in the merdional ocean heat transport denotes regions with heat loss. The northward ocean heat transport is shown for all three mod-

els in Fig. 3.17, and is compared with observation-based estimates. It is important to note that the observation-based data contain large uncertainties. The ECMWF and NCEP derived data compare relatively well in the northern North Atlantic, but the difference between these two estimates is larger at low latitudes (Rhines et al. 2008). The divergence of ocean heat transport in BCM is particularly large between 35°-40°N and 60°-65°N, consistent with large heat loss in these regions (Fig. 3.5). Between these regions the North Atlantic Current is generally aligned with the front between subpolar and subtropical waters (Fig. 3.4), i.e., weaker heat loss occurs in this region. Also the other two models have large divergence just north of 35°N, due to large heat loss close to Cape Cod. On the other hand, between 38°-45°N there is convergence of ocean heat transport in MPI-M ESM. This is consistent with warming of the ocean surface close to Newfoundland (Fig. 3.5). In IPSLCM4 there are almost no meridional changes in the ocean heat transport between 43°-50°N, since the heat loss in the eastern subpolar region is similar to the heat gain in the western subpolar region (Fig. 3.5). It is evident that the model comparison of northward ocean heat transport highlights several differences in the location and strength of heat loss. The northward ocean heat transport has a significant impact on the North Atlantic climate (Gregory et al. 2005; Rhines et al. 2008). The impact of these model differences on their North Atlantic Climate should therefore be investigated.

In the previous section we described a mechanism where AMOCσ decadal scale variability is reflected in the variability of air-sea exchanges in the eastern subpolar region in two of the models; an increase in the southward dense flow in the North Atlantic Basin is associated with a lagged increase in the WMT in the eastern subpolar region. In BCM the dense layers in the North Atlantic Basin are filled up by overflow water from the Nordic Seas or dense water formed in the Labrador and Irminger seas. The decadal variability of Labrador Sea Water and Nordic Seas overflow are related to the first and third dominant mode of atmospheric variability, respectively, namely the North Atlantic Oscillation and the Scandinavian Pattern. The dense water formation in BCM and its link to the overturning and gyre circulations have been investigated in detail in Medhaug et al. 2011 and Langehaug et al. (in revision).

A strengthening of the overturning circulation (i.e., first EOF of AMOCz) three years after a positive phase of NAO is found in all three models but IPSLCM4 (Gastineau and Frankignoul 2011). The delayed oceanic response to positive NAO forcing has previously been investigated in BCM (Langehaug et al., in revision). Three years after high positive NAO periods there are evident changes in the northern North Atlantic, with indication of a northward shift in the North Atlantic Current, and positive temperature and salinity anomalies along the intensified path of the North Atlantic Current. The pattern of temperature anomalies resembles the WMT pattern for σ_2=35.51 (Fig. 3.9). This oceanic response to high positive NAO forcing is similar to what is found in both observation-based and model studies (Curry and McCartney 2001; Cooper and Gordon 2002; Lohmann et al. 2009).

Several recent studies investigate temperature and salinity anomalies on decadal scale in the northeastern North Atlantic (e.g., Johnson and Gruber 2007; Thierry et al. 2008; Häkkinen et

al. 2011). The mechanisms in these studies are different from the above mentioned associated with the overturning circulation. Häkkinen et al. (2011) suggest that wind-induced changes in the Subtropical and Subpolar gyres are responsible for the temperature and salinity anomalies observed in the northeastern North Atlantic. For instance, the observed recent relaxation of the gyres' circulation leads to a contraction of the Subpolar Gyre and an expansion of the Subtropical Gyre. This change in the surface circulation forms a gateway for warm and saline anomalies to propagate from the Subtropical region to the Subpolar region (see Fig. 13 in Häkkinen et al. 2011). However, the wind-driven horizontal gyres and the overturning circulation are highly interconnected. It is therefore not straightforward to understand the relationship between the overturning circulation and sea surface temperature anomalies in the northern North Atlantic. This is demonstrated in an intercomparison of all climate model simulations from IPCC AR4 (Medhaug and Furevik 2011). The study shows that the models strongly differ in their relationship between AMOCz and sea surface temperature in the North Atlantic, and hence, no consistent mechanism was found to operate in all of the models.

Although the subpolar North Atlantic Ocean is one of the most studied ocean regions, there are still challenges in understanding the variability on decadal time scale both in nature and climate model simulations. In this study all models show similar mechanisms regarding the strength of AMOCσ and northward transport at the northern and southern boundary of the subpolar region (Fig. 3.15). Two of the models show similar mechanism regarding the strength of AMOCσ and WMT in the eastern subpolar region, as discussed above. Thus, an intriguing aspect of the present study is that even if the climate models are diverging in their representation of the northern North Atlantic mean climate, they appear to an extent to show similar mechanisms on decadal time scale.

Acknowledgments

The project has been supported by the Research Council of Norway through the BIAC (HRL and TE). The research leading to these results has also received funding from the European Community's 7th framework programme (FP7/2007-2013) under grant agreement No. GA212643 (THOR: "Thermohaline Overturning - at Risk", 2008-2012; HRL, TE, JM, and KL). This publication is no. XXXX from the Bjerknes Centre for Climate Research. We thank Cecilia M. Bitz for assistance in using the water mass transformation methodology on climate model data. We also thank Iselin Medhaug, Helge Drange, and Odd Helge Otterå for comments helping to improve the manuscript.

References

Arhan, M. (1990), The North Atlantic Current and Subarctic Intermediate Water, J. Mar. Res., 48, 109-144.

Bailey, D. A., P. B. Rhines, and S. Häkkinen (2005), Formation and pathways of North Atlantic Deep Water in a coupled ice-ocean model of the Arctic-North Atlantic Oceans, Clim. Dyn., 25, 497-516.

Bentsen, M., H. Drange, T. Furevik, and T. Zhou (2004), Simulated variability of the Atlantic meridional overturning circulation. Clim. Dyn., 22, 701-720. doi:10.1007/s00382-004-0397-x.

Bleck R., C. Rooth, D. Hu, and L. T. Smith (1992), Salinity-driven thermocline transients in a wind- and thermohaline-forced isopycnic coordinate model of the North Atlantic, J. Phys. Oceanogr., 22, 1486-1505.

Bower, A. S., M. S. Lozier, S. F. Gary, and C. W. Bö ning (2009), Interior pathways of the North Atlantic Meridional Overturning Circulation, Nature, 459, 243-247.

Brambilla, E., and L. D. Talley (2008), Subpolar mode water in the northeastern Atlantic: 1. Averaged properties and mean circulation, J. Geophys. Res., 113, C04025, doi:10.1029/2006JC004062.

Brambilla, E., L. D. Talley, and P. E. Robbins (2008), Subpolar Mode Water in the northeastern Atlantic: 2. Origin and transformation, J. Geophys. Res., 113, C04026, doi:10.1029/2006JC004063.

Cerovecki, I., and J. Marshall (2008), Eddy modulation of air-sea interaction and convection, J. Phys. Oceanogr., 38, 65-83.

Chelton, D. B. (1983), Effects of sampling errors in statistical estimation, Deep-Sea Res., 30, 1083-1101.

Cooper, C., and C. Gordon (2002), North Atlantic oceanic decadal variability in the Hadley Centre coupled model, J. Clim., 15, 45-72.

Curry, R. G., and M. S. McCartney (2001), Ocean gyre circulation changes associated with the North Atlantic oscillation, J. Phys. Oceanogr., 31(12), 3374-3400.

Dengler, M., J. Fischer, F. A. Schott, and R. Zantopp (2006), Deep Labrador Current and its variability in 1996-2005, Geophys. Res. Lett., 33, L21S06, doi:10.1029/2006GL026702.

Deshayes, J., C. Frankignoul (2008), Simulated variability of the circulation of the North Atlantic from 1953 to 2003, J. Clim., 21, 4919-4933, doi:11.1175/2008JCLI1882.1.

Eden, C., and J. Willebrand (2001), Mechanisms of interannual to decadal variability of the North Atlantic circulation, J. Clim., 14, 2266-2280.

Eldevik, T. (2002), On frontal dynamics in two model oceans, J. Phys. Oceanogr., 32, 2915-2925.

Furevik, T., M. Bentsen, H. Drange, I. K. T. Kindem, N. G. Kvamstø , and A. Sorteberg (2003), Description and validation of the Bergen Climate Model: ARPEGE coupled with MICOM, Clim. Dyn., 21, 27-51, doi:10.1007/s00382-003-0317-5.

Garrett, C., K. Speer, and E. Tragou (1995), The relationship between water mass formation and surface buoyancy flux, with application to Phillips' Red Sea model, J. Phys. Oceanogr., 25, 1696-1705.

Gastineau, G., and C. Frankignoul (2011), Cold-season atmospheric response to the natural variability in the Atlantic merdional overturning circulation, Clim. Dyn., doi:10.1007/s00382-011-1109-y.

Gregory, J. M., and Coauthors (2005), A model intercomparison of changes in the Atlantic thermohaline circulation in response to increasing atmospheric CO2 concentration, Geophys. Res. Lett., 32, L12703, doi:10.1029/ 2005GL023209.

Grist, J. P., R. Marsh, and S. A. Josey (2009), On the Relationship between the North Atlantic Meridional Overturning Circulation and the Surface-Forced Overturning Streamfunction, J. Clim., 22, 4989-5002, doi:10.1175/2009JCLI2574.1.

Grist, J. P., and S. A. Josey (2003), Inverse analysis adjustment of the SOC air-sea flux climatology using ocean heat transport constraints, J. Clim., 20, 3274-3295, doi: 10.1175/1520-0442(2003)016%3C3274:IAAOTS%3E2.0.CO;2.

Gulev, S. K., B. Barnier, J.-M. Molines, T. Penduff, and J. Chanut (2007), Impact of spatial resolution of simulated surface water mass transformation in the Atlantic, Ocean Modell., 19, 138-160, doi:10.1016/j.ocemod.2007.07.004.

Häkkinen, S., P. B. Rhines, and D. L. Worthen (2011), Warm and saline events embedded in the meridional circulation of the northern North Atlantic, J. Geophys. Res., 116, C03006, doi: 10.1029/2010JC006275.

Isachsen, P. E., C. Mauritzen, and H. Svendsen (2007), Dense water formation in the Nordic Seas diagnosed from sea surface buoyancy fluxes, Deep-Sea Res. I, 54, 22-41.

Johannessen, O. M., and Coauthors, 2004: Arctic climate change: observed and modelled temperature and sea-ice variability, Tellus, 56A, 328-341

Johnson, G. C., and N. Gruber (2007), Decadal water mass variations along 20W in the northeastern Atlantic Ocean, Prog. Oceanogr., 73, doi:10.1016/j.pocean.2006.03.022.

Josey, S. A., E. C. Kent, and P. K. Taylor (1999), New insights into the ocean heat budget closure problem from analysis of the SOC air-sea flux climatology, J. Clim., 12(9), 2856-2880.

Josey, S. A., J. P. Grist, and R. Marsh (2009), Estimates of meridional overturning circulation variability in the North Atlantic from surface density flux fields, J. Geophys. Res., 114, C09022, doi:10.1029/2008JC005230.

Jungclaus, J. H., H. Haak, M. Latif, and U. Mikolajewicz (2005), Arctic-North Atlantic interactions and multidecadal variability of the meridional overturning circulation, J. Clim., 18(19), 4013-4031.

Jungclaus, J. H., and Coauthors (2006), Ocean circulation and tropical variability in the coupled model ECHAM5/MPI-OM, J. Clim., 19(16), 3952-3972.

Jungclaus, J. H., and Coauthors (2010), Climate and carbon-cycle variability over the last millennium, Climate of the Past, 6, 723-737.

Kalnay, E., and co-authors (1996), The NCEP/NCAR 40-year reanalysis project, Bull. Amer. Meteor. Soc., 77, 437-471.

Krauss, W. (1986), The North Atlantic Current, J. Geophys. Res., 91, 5061-5074.

Langehaug, H. R., I. Medhaug, T. Eldevik, and O. H. Otterå (2011), Arctic/Atlantic exchanges via the Subpolar Gyre, J. Clim., in revision.

Lohmann, K., H. Drange, and M. Bentsen (2009), Response of the North Atlantic subpolar gyre to persistent North Atlantic Oscillation like forcing, Climate Dyn., 32, 273-285, doi: 10.1007/s00382-008-0467-6.

Lumpkin, R., and K. Speer (2003), Large-scale vertical and horizontal circulation in the North Atlantic Ocean, J. Phys. Oceanogr., 33, 1902-1920.

Madec, G., P. Delecluse, M. Imbard, C. Levy (1997), OPA version 8.1 Ocean general circulation model reference manual, 3. LODYC, Technical Report, 91 pp.

Manabe, S., and R. J. Stouffer (1988), Two stable equilibria of a coupled ocean-atmosphere

model, J. Clim., 1(9), 841-866.

Marsh, R. (2000), Recent variability of the North Atlantic thermohaline circulation inferred from surface heat and freshwater fluxes, J. Clim., 13, 3239-3260.

Marsland, S., H. Haak, J. H. Jungclaus, M. Latif and F. Röske (2003), The Max Planck Institute global ocean / sea ice model with orthogonal curvilinear coordinates. Ocean Modelling, 5, 91-127.

Marti, O., and Coauthors (2010), Key features of the IPSL ocean atmosphere model and its sensitivity to atmospheric resolution, Clim. Dyn., 34, 1-26.

Mauritzen, C., S. Häkkinen (1999), On the relationship between dense water formation and the "Meridional Overturning Cell" in the North Atlantic Ocean, Deep-Sea Res. I, 46, 877-894.

McCartney, M. S., and L. D. Talley (1982), The Subpolar Mode Water of the North Atlantic, J. Phys. Oceanogr., 12, 1169-1188.

McDougall, T. J. (1987), Neutral Surfaces, J. Phys. Oceanogr., 17, 1950-1964.

Medhaug, I., T. Furevik (2011), North Atlantic 20th century multidecadal variability in coupled climate models: sea surface temperature and ocean overturning circulation. Ocean Sci., 7, 389-404. doi:10.5194/os-7-398-2011.

Medhaug, I., H. R. Langehaug, T. Eldevik, T. Furevik, and M. Bentsen (2011), Mechanisms for decadal scale variability in a simulated Atlantic meridional overturning circulation, Clim. Dyn., doi:10.1007/s00382-011-1124-z.

Mignot, J., and C. Frankignoul (2010), Local and remote impacts of a tropical Atlantic salinity anomaly, Clim. Dyn., 35 (7-8), 1133-1147.

Munk, W., and C. Wunsch (1998), Abyssal recipes II: Energetics of tidal and wind mixing, Deep-Sea Res., Part I, 45, 1977-2010.

Nurser, A. J. G., R. Marsh, and R. G. Williams (1999), Diagnosing water mass formation from air-sea fluxes and surface mixing. J. Phys. Oceanogr., 29, 1468-1487.

Otterå, O. H., M. Bentsen, I. Bethke, and N. G. Kvamstø (2009), Simulated pre-industrial climate in Bergen Climate Model (version 2): model description and large-scale circulation features, Geosci. Model Dev., 2, 507-549.

Pérez-Brunius, P., T. Rossby, and D. R. Watts (2004), Transformation of the warm waters of the

North Atlantic from a geostrophic streamfunction perspective, J. Phys. Oceanogr., 34, 2238-2256.

Rahmstorf, S. (2002), Ocean circulation and climate during the past 120,000 years, Nature, 419, 207-214.

Rhein, M., and Coauthors (2011), Deep water formation, the subpolar gyre, and the meridional overturning circulation in the subpolar North Atlantic, Deep-Sea Res. II, doi:10.1016/j.dsr2.2010.10.061.

Rhines, P., S. Häkkinen, and S. A. Josey (2008), Is oceanic heat transport significant in the climate system? In Arctic-Subarctic Ocean Fluxes: Defining the role of the Northern Seas in Climate, Dickson, B., Meincke, J., and Rhines, P., editors, 87-109, Springer Verlag.

Roullet, G., and G. Madec (2000), Salt conservation, free surface, and varying levels: a new formulation for ocean general circulation models, J. Geophys. Res. (Oceans), 105(10), 23927-23942.

Servonnat J., P. Yiou, M. Khodri, D. Swingedouw, and S. Denvil (2010), Influence of solar variability, CO2 and orbital forcing during the last millennium in the IPSLCM4 model. Climate of the Past, 6, 445-460.

Smethie W. M., and R. A. Fine (2001), Rates of North Atlantic Deep Water formation calculated from chlorofluorocarbon inventories, Deep-Sea Res. I, 48, 189-215, doi:10.1016/S0967-0637(00)00048-0.

Speer, K., and E. Tziperman (1992), Rates of water mass formation in the North Atlantic Ocean, J. Phys. Oceanogr., 22, 93-104.

Swift, J. H. (1986), The Arctic waters, in The Nordic Seas, edited by B. G. Hurdle, pp. 129-153, Springer-Verlag, New York.

Tandon, A., and L. Zhao (2004), Mixed layer transformation for the North Atlantic for 1990-2000, J. Geophys. Res., 109(C05018), 1-9, doi:10.1029/2003JC002059.

Thierry, V., E. de Boisséson, and H. Mercier (2008), Interannual variability of the Subpolar Mode Water properties over the Reykjanes Ridge during 1990-2006, J. Geophys. Res., 113, C04016, doi:10.1029/2007JC004443.

Trenberth, K. E., and J. M. Caron (2001), Estimates of meridional atmosphere and ocean heat transports, J. Clim., 14, 3433-3443.

Walin, G. (1982), On the relation between sea-surface heat flow and thermal circulation in the ocean, Tellus, 34, 187-195.

Willebrand, J., and Coauthors (2001), Circulation characteristics in three eddy-permitting models of the North Atlantic, Prog. Oceanogr., 48, 123-161.

Zhang, R. (2010), Latitudinal dependence of Atlantic meridional overturning circulation (AMOC) variations, Geophys. Res. Lett., 37, L16703, doi:10.1029/2010GL044474.